Biophysical Investigation of the Ligand-induced

Assembling of the human Type I Interferon Receptor

Dissertation

zur Erlangung des Doktorgrades

der Naturwissenschaften

vorgelegt beim Fachbereich

Chemische und Pharmazeutische Wissenschaften

der Johann Wolfgang Goethe-Universität in Frankfurt am Main

von

Peter Lamken

aus Kelsterbach am Main

Frankfurt, 2005

vom Fachbereich Chemische und Pharmazeutische Wissenschaften der

Johann Wolfgang Goethe-Universität als Dissertation angenommen.

Dekan:

1. Gutachter: Dr. Jacob Piehler

2. Gutachter: Prof. Dr. Robert Tampé

Datum der Disputation:

Index

1 Deutsche Zusammenfassung

Die biochemischen und zellbiologischen Mechanismen der interzellulären Kommunikation über Zellbotenstoffe, die Zytokine, spielen eine bedeutende Rolle sowohl in der grundlagenorientierten als auch in der biomedizinischen Forschung. Eine Gruppe der Zytokine, die Typ I Interferone (IFN), stellt aufgrund ihrer antiviralen, antiproliferativen, immunmodulatorischen und antiinflammatorischen Aktivitäten eine wichtige Komponente des angeborenen Immunsystems dar. Von besonderer Bedeutung ist ihre Rolle bei der frühzeitigen Abwehr von Viren, in der sie die erste Antwort in einer Reihe von antiviralen Mechanismen bilden. Bisher sind 16 humane Typ I Interferone bekannt (13 IFNα, β, ϵ und ω). Abhängig vom Zell- und Gewebetyp kann ein Interferon zu unterschiedlichen zellulären Aktivitäten führen, was als pleiotroper Effekt bezeichnet wird.

Zentrales Element der Interferon-vermittelten Signaltransduktion ist der IFN Rezeptor ifnar, welcher sich aus den beiden Transmembranproteinen ifnar1 und ifnar2 zusammensetzt und zur Familie der Klasse II Zytokin Rezeptoren gehört. Dieser Rezeptor fungiert als Verbindungselement zwischen extrazellulärem Milieu und dem Zytoplasma. Alle bekannten IFN rekrutieren ifnar, jedoch führen sie in Abhängigkeit vom jeweiligen Interferon und vom zellulären Kontext zu unterschiedlicher Akzentuierung der aktivierten Signalwege, was als differentielle Signalaktivierung bezeichnet wird. Dies lässt vermuten, dass die differentielle Signalaktivierung in der Erkennung der IFN durch den Rezeptor codiert ist.

Ziel dieser Arbeit war es, die Ligand-induzierte Rezeptorassemblierung biophysikalisch zu untersuchen und damit die molekularen Prinzipien der differentiellen Signalaktivierung *in vitro* zu erforschen. Als Modellsystem dienten die extrazellulären Domänen ifnar1-EC und ifnar2-EC, welche für die Ligandenbindung verantwortlich sind. Die hochaffine Interaktion zwischen ifnar2-EC und IFNα2 ist detailliert *in vitro* untersucht worden, jedoch war nur wenig über ifnar1 bekannt. Da vermutet wird, dass die niedrigaffine Komponente ifnar1 für die differentielle Signalaktivierung verantwortlich ist, steht die extrazelluläre Domäne ifnar1-EC im Fokus dieser Arbeit. Die folgenden Aspekte lagen dabei im Zentrum des Interesses:

 ➢ Thermodynamik, Kinetik und Stöchiometrie der Einzelinteraktionen zwischen allen involvierten Proteinen: ifnar1-EC, ifnar2-EC und Interferon

 ➢ Charakterisierung der Bindungsstelle für verschiedene Liganden auf ifnar1-EC

 ➢ Stabilität, Dynamik und Stöchiometrie des Signalkomplexes hinsichtlich verschiedener Liganden

 ➢ Strukturelle Organisation von ifnar1-EC im Signalkomplex

Ifnar1-EC musste zunächst in quantitativen Mengen hergestellt werden, um die Etablierung eines Bindungsassays zu ermöglichen. Die heterologe, periplasmatische Expression in *E. coli* führte nur zu geringen Ausbeuten (50 µg/l), und auch andere Expressionsstrategien lieferten keine nachweisbaren Mengen an monomerem Protein. Aus diesem Grund wurde die Expression in *Sf*9 Insektenzellen eingesetzt. Mittels homologer Rekombination wurde das Gen ifnar1-EC mit einem C-terminalen Deca-Histidin-*tag* in das Genom des Baculovirus integriert. Von diesen Viren infizierte *Sf*9 Zellen exprimierten ifnar1-EC und sezernierten es in das Medium, was zugleich den ersten Reinigungsschritt darstellte. Durch Metall-Affinitätschromatographie wurde ifnar1-EC aus dem Medium extrahiert und von anderen Proteinen abgetrennt. Im abschließenden Reinigungsschritt, der Gelfiltration, wurden dann Aggregate und niedermolekulare Kontaminationen entfernt und gleichzeitig sichergestellt, dass ifnar1-EC als Monomer vorliegt. Die Ausbeute für lag bei ca. 10 mg pro Liter Zellkultur. Es zeigte sich, dass ifnar1-EC glykosyliert war, was durch Deglykosylierungsexperimente mittels *PNGase*F bestätigt werden konnte. Die Glykosylierung erwies sich als protein-stabilisierender Faktor, der die Handhabung und Lagerung wesentlich erleichterte. Ebenso konnte die Ausbildung von Disulfidbrücken, welche bei Stabilität und Funktion eine wichtige Rolle spielen, nachgewiesen werden.

Um Stöchiometrie und Kinetik der Rezeptor-Ligand-Interaktionen mittels Reflektometrischer Interferenzspektroskopie (RIfS) zu untersuchen, wurden ifnar1-EC und ifnar2-EC mit Hilfe des Deca-Histidin-*tags* gerichtet und funktional auf Oberflächen immobilisiert. Die Immobilisierung wurde wie bei der Reinigung über eine Metall-Chelator Interaktion gewährleistet. Dazu wurden multivalente Chelatoren auf einer modifizierten Glasoberfläche kovalent gebunden und Ni^{2+} über 4 Koordinationsstellen komplexiert. Der Deca-Histidin-*tag* konnte darauf über die freien Koordinationsstellen des Ni^{2+} binden und so das Protein stabil auf der Oberfläche verankert werden.

Zur Untersuchung der Einzelinteraktionen wurde stets eine Untereinheit immobilisiert und anschließend der Assoziations- und Dissoziationsprozess für IFNα2 und IFNβ untersucht. Alle Interaktionen zwischen ifnar1-EC bzw. ifnar2-EC und IFNα2/β wiesen eine 1:1 Stöchiometrie auf. Es zeigten sich jedoch sowohl zwischen den Interferonen als auch zwischen den Rezeptoren große Unterschiede in der Affinität. Für ifnar2-EC wurde eine Dissoziationskonstante von 3 nM für IFNα2 bestimmt, wohingegen IFNβ erheblich stärker bindet (K_D < 0.1 nM). Ifnar1-EC bindet sowohl IFNα2 (K_D = 5 ± 2 µM) als auch IFNβ (K_D = 50 ± 30 nM) etwa drei Größenordnungen schwächer als ifnar2-EC. Im Falle von IFNα2 wurde eine transiente Interaktion mit einer Lebensdauer ~ 1 s gemessen. Eine kooperative Bindung in Anwesenheit von ifnar2-EC ohne His-*tag* konnte weder für IFNα2 noch für IFNβ gezeigt werden. Dieses Ergebnis wurde durch die Beobachtung gestützt, dass keinerlei Interaktion

zwischen den beiden Rezeptoren nachgewiesen werden konnte. Eine Interaktion zwischen ifnar1-EC und ifnar2-EC konnte somit ausgeschlossen werden.

Um die Bindungsstelle(n) für IFNα2 und IFNβ genauer zu charakterisieren, wurden verschiedene Konstrukte von ifnar1-EC hergestellt, die eine unterschiedliche Anzahl an Immunglobulin-ähnlichen Sub-domänen (SD) beinhalteten. Da ifnar1-EC vier solcher Domänen mit einer Größe von je ~100 Aminosäuren enthält (SD1234), wurden die folgenden Sub-Fragmente anhand der Domänenanordnung und Stellung des His-tags benannt: H10-SD12, SD34-H10, SD123-H10, H10-SD123 und SD234-H10. Alle Sub-Fragmente ließen sich in vergleichbaren Ausbeuten wie der Wildtyp exprimieren und reinigen. Zudem wurde ein ifnar1-EC-Konstrukt mit N- und C-terminalem His-*tag* (SD1234-DT) hergestellt, welches eine doppelte Verankerung mit der Membran simulieren sollte. Um sicherzustellen, dass alle Konstrukte korrekt gefaltet waren, wurde die Sekundärstruktur mittels CD-Spektroskopie untersucht. Wie erwartet wiesen alle Proteine einen hohen Anteil an β-Faltblättern auf (~ 80 %), was ein typisches Strukturmerkmal aller extrazellulären Domänen von Klasse I Zytokinrezeptoren darstellt. Bei der biochemischen Charakterisierung mittels analytischer Gelfiltration und SDS-PAGE fiel auf, dass H10-SD123 und SD234-H10 trotz etwa gleichem Molekulargewichts ein unterschiedliches Laufverhalten aufwiesen, wobei H10-SD123 zu einem höheren Molekulargewicht verschoben wurde. Diese auch nach Deglykosylierung reproduzierbare Verschiebung indiziert eine eher gestreckte Anordnung der drei N-terminalen gegenüber den drei C-terminalen Domänen und damit einen nicht symmetrischen Aufbau von ifnar1-EC. In Bindungsexperimenten zeigte sich, dass nur SD123-H10 und H10-SD123 Bindungsaktivität für IFNα2 und IFNβ aufwiesen, alle anderen Sub-Fragmente zeigten keinerlei Bindung im detektierbaren Konzentrationsbereich. Auch eine Rekonstruktion der Bindungsstelle durch Co-Immobilisierung von H10-SD12 und SD34-H10 konnte nicht erreicht werden. Hieraus lässt sich folgern, dass für die Liganden-Bindung alle drei N-terminalen Domänen in einem Polypeptidstrang vorliegen müssen. Hinsichtlich der Bindungsaffinität waren keine signifikanten Unterschiede zwischen ifnar1-EC, SD1234-DT und H10-SD123 nachweisbar. Um mögliche Unterschiede in der Bindungsregion auf ifnar1-EC bzw. SD123 für IFNα2 und IFNβ nachzuweisen, wurden Kompetitionsexperimente mit Fluoreszenz-markiertem IFNα2 durchgeführt. Hierbei zeigte sich, dass IFNα2 und IFNβ, wie bei ifnar2-EC, um die gleiche Bindungsregion auf ifnar1-EC konkurrieren und damit auch in dieser Hinsicht kein Unterschied zwischen diesen beiden Interferonen in der Rekrutierung von ifnar1-EC besteht.

Zur genaueren Charakterisierung der Liganden-Bindungsstelle wurden mehrere Mutationen auf allen 4 Sub-Domänen auf ifnar1-EC eingeführt. Diese Mutanten, von denen sich der größte Teil wie der Wildtyp exprimieren und reinigen ließ, wurden hinsichtlich ihrer

Bindung an IFNα2 und IFNβ untersucht. Anstelle von IFNα2wt wurde eine höher affine Mutante (IFNα2-HEQ) verwendet, die ähnliche Bindungseigenschaften wie IFNβ aufwies, jedoch leichter zu handhaben war. Es wurden mehrere Reste identifiziert, die die Bindungsaffinität sowohl für IFNα2-HEQ als auch für IFNβ um eine Größenordnung oder mehr reduzierten. Auf SD1 wurde eine Aminosäure (Y70), auf SD2 vier (E111, K113, W129 und F136) und auf SD3 auch eine Aminosäure (K251) identifiziert. Auf SD4 konnte keine Mutation erzeugt werden, welche die Bindungsaffinität reduziert. Diese Ergebnisse untermauerten die Beobachtungen mit den Sub-Fragmenten und stärkten die Vermutung, dass die 3 N-terminalen Domänen für die Ligandenbindung und SD4 für die Komplexbildung verantwortlich sind.

Um die Bildung des Signalkomplexes durch IFN Zugabe zu untersuchen, wurden ifnar1-EC und ifnar2-EC auf einer Chelator-Lipid-Oberfläche co-immobilisiert. Die Verwendung einer Lipid-Doppelschicht ermöglichte laterale Mobilität. Dies wurde durch entsprechende FRAP-Messungen mit Fluoreszenz-markiertem ifnar2 bestätigt. Nach Zugabe von IFNα2 bildete sich ein stabiler Komplex mit einer 1:1:1 Stöchiometrie. Diese Stöchiometrie konnte in Lösung mittels Gelfiltration bestätigt werden. Durch Verwendung von IFNα2- und ifnar2-EC-Mutanten mit niedrigerer Affinität wurde gezeigt, dass die Stabilität der IFNα2-ifnar2-EC Interaktion durch ifnar1-EC um den Faktor 200 gesteigert wurde. Kontrollexperimente auf Glasoberflächen zeigten, dass die Mobilität der Rezeptorkomponenten, wie sie in Lipid-Doppelschichten vorliegt, für die Bildung eines solchen stabilen Komplexes essentiell ist. Es stellte sich nun die Frage, ob der ternäre Komplex statisch oder dynamisch stabilisiert wurde. Um diese Frage zu beantworten, wurde die Oberflächenkonzentration von ifnar1-EC und ifnar2-EC reduziert und die Bindung von Fluoreszenz-markiertem IFNα2 S136C mittels TIRFS (Totalinterne Reflektions-Fluoreszenz-Spektroskopie) aufgrund erheblich höherer Sensitivität gegenüber RIfS detektiert. Hierbei zeigte sich mit abnehmender Rezeptor-Oberflächenkonzentration eine zunehmende Dissoziationsratenkonstante, was einen ersten Hinweis auf eine dynamische Stabilisierung darstellte. Diese Vermutung wurde durch Austauschexperimente mit unmarkiertem IFNα2 bestätigt. Zudem wurde durch Injektion von löslichem ifnar2-EC gezeigt, dass die Stabilität des ternären Komplexes kein Diffusions-basiertes Rückbindungsphänomen aufgrund von Diffusionen an Grenzflächen ist.

Diese Ergebnisse lassen sich durch ein zweistufiges Bindungsmodell erklären. Zunächst wird der Ligand an die hochaffine Rezeptorkomponente ifnar2 gebunden und bildet damit einen binären Komplex (beschrieben durch K_1). Im zweiten Schritt, welcher in der Membranebene stattfindet (beschrieben durch K_2), führt die Bindung von ifnar1 über die direkte Interaktion mit IFN zur Bildung des ternären Komplexes. Die Komplexbildung und die

Dissoziation lassen sich durch die 2-dimensionale Assoziationsratenkonstante (k_2) bzw. die Dissoziationsratenkonstante (k_{-2}) der IFN/ifnar1-EC-Interaktion auf der Membran beschreiben. Da unterschiedliche Affinitäten für IFNα2 und IFNβ bestimmt wurden, wird klar, dass die Stabilität des Komplexes und damit die Effizienz der Signalaktivierung von der Dissoziationsratenkonstante der IFN/ifnar1-EC-Interaktion abhängen. Die differentielle Signalaktivierung durch verschiedene Interferone ließe sich somit durch die unterschiedlichen Dissoziationsratenkonstanten erklären. Ebenso wird klar, dass die Komplexbildung und damit k_2 zum einen von der Rezeptoroberflächenkonzentration, zum anderen von der Affinität von ifnar1 mit dem binären Komplex abhängen. Unterschiedliche Rezeptoroberflächenkonzentrationen auf verschiedenen Zelltypen könnten erklären, warum verschiedene Zelltypen unterschiedlich auf das gleiche IFN reagieren (pleitroper Effekt).

Um diesen Prozess der Komplexbildung genauer zu untersuchen, wurde die Rezeptorassemblierung mit verschiedenen ifnar1-Varianten auf Lipid-Doppelschichten untersucht. SD123-H10, H10-SD123 und SD1234-DT waren bei hohen Oberflächenkonzentrationen in der Lage, einen stabilen ternären Komplex zu bilden. Bei niedrigeren Rezeptor-Oberflächenkonzentrationen jedoch waren deutliche Unterschiede in der Komplexstabilität zu beobachten. C-terminal und doppelt verankerter ifnar1-EC zeigten keinen Unterschied, jedoch wies SD123 unabhängig von der Position des His-*tags* eine deutlich gesteigerte Dissoziation auf. Offensichtlich erhöht SD4 die Wahrscheinlichkeit einer erfolgreichen Komplexbildung, was die reduzierte Komplexstabilität bei Entfernung dieser Domäne erklären könnte. Diese Vermutung wurde durch Bindungsexperimente auf Zellen bestätigt, in denen ausschließlich ifnar1-EC zu messbarer Bindung führte. Um den Einfluss der Orientierung von SD4 auf die Komplexbildung genauer zu untersuchen, wurden weitere Konstrukte hergestellt. Zum einen wurde ifnar1-EC mit einem N-terminalen His-*tag* ausgestattet (H10-SD1234), zum anderen wurde SD4 von ifnar1 durch SD2 des IFNλ-Rezeptors (SD123-LRD2-H10) bzw. des IL-10 Rezeptors (SD123-IL-10R2D2) ersetzt. Sowohl die N-terminale Verankerung als auch der Austausch von SD4 zeigte gegenüber der C-terminalen Immobilisierung eine reduzierte Komplexstabilität ähnlich wie SD123. Hieraus lässt sich der Schluss ziehen, dass SD4 offensichtlich für die optimale Orientierung der Ligandenbindungsstelle von ifnar1 verantwortlich ist und damit eine essentielle Rolle bei der Assemblierung des ternären Komlexes spielt.

2 Summary

Type I interferons (IFNs) elicit antiviral, antiproliferative and immunmodulatory responses through binding to a shared receptor consisting of the transmembrane proteins ifnar1 and ifnar2. Differential signaling by different interferons suggests different modes of receptor engagement. In this work the ligand-induced receptor assembly of the extracellular domains (EC) of ifnar1 and 2 was investigated in terms of thermodynamics, kinetics, stoichiometry and structural organization. An efficient expression and purification strategy for ifnar1-EC using Sf9 insect cells was established. Using reflectance interference spectroscopy (RIfS) the interactions between IFNα2/β and ifnar1-EC and ifnar2-EC were studied in order to understand the individual contributions within the ternary complex. Low affinity for the IFNα2/ifnar1-EC interaction (K_D ~ 5 µM) in comparison to high affinity for IFNα2/ifnar2-EC (K_D ~ 3 nM) was observed. Substantially tighter binding of IFNβ to both ifnar2-EC and ifnar1-EC compared to IFNα2 was observed. For neither IFNα2 nor IFNβ any cooperative effect of ifnar2-EC on IFN-ifnar1-EC interaction was detected. Thus stem-stem interactions between the extracellular domains do not seem to play a role for ternary complex formation. Based on this analysis a two-step binding mechanism was suggested. In order to identify differences between different IFNs in ligand recognition, ifnar1-EC was dissected into sub-fragments containing different potential Ig-like domains. Appropriate folding of these proteins was confirmed by CD-spectroscopy. Surprisingly, only fragments containing all three N-terminal Ig-like domains were active in terms of ligand binding. Additionally it was demonstrated that IFNα2 and IFNβ compete for the same binding site and mainly the same residues. To investigate the mechanism of complex formation, ligand-induced cross-talk between ifnar1-EC and ifnar2-EC being tethered onto solid-supported, fluid lipid bilayers was investigated by RIfS and total internal reflection fluorescence spectroscopy. A very stable binding of IFNα2 at high receptor surface concentrations was observed. The apparent k_d value was approximately 200-times lower than for ifnar2-EC alone. A strong dependency of this apparent k_d on the receptor surface concentration suggested kinetic rather than static stabilization, which was corroborated by dynamic exchange experiments. Cellular binding assays as well as different ifnar1-EC fragments in $vitro$ highlighted the key role of the membrane-proximal Ig-like domain for the formation of an in $situ$ IFN-receptor complex and the ensuing signal activation. All these results suggested a two-step binding model: After ifnar2 recruitment by IFN, ifnar1 binding mediates ternary complex formation. The complex is stabilized by the transient interaction of ifnar1 with the ifnar2-bound ligand, which is several orders of magnitude more efficient for IFNβ than for IFNα2. Thus differential signaling is proposed to be encoded by the efficiency of signaling complex formation depending on the affinity of ifnar1-EC toward IFNs as well as on the receptor surface concentration.

3 Introduction

3.1 Cytokines and cytokine receptors

3.1.1 Overview of cytokines and cytokine receptors

Cytokines are soluble proteins and glycoproteins mediating intercellular communication in a variety of physiological processes. Based on the structure three classes of cytokines are distinguished. Class I cytokines have a 4 short α-helix motif (each helix ~15 residues), whereas cytokines of class II share a structural core of 4 long α-helices (each helix ~25 residues). In contrast to class I and II, members of class III (TNFα/β) show no helical structure motifs but a set of β-sheets. It depends on the literature source if class III cytokines belong to the cytokines in the classical manner.

Cytokines play a key role in regulating the immune system as a central element of innate immunity. A special characteristic of cytokines is the pleiotrophic effect, which means one cytokine is able to activate different activities in different cells. Different cytokines are also able to cause the same effect leading to accumulated cellular responses, which is termed cytokine redundancy. Cytokines are known to be involved in proliferation, differentiation, cell activation, embryogenesis, tissue repair and apoptosis. A short overview of cytokines and their functions is shown in Table 1.

Cytokine receptors are classified by the structural arrangement of their extracellular domains. Characteristic sequences of domains, such as cysteine-rich domains, fibronectin type III-like domains and immunoglobulin-like domains vary in different receptor types. Another variable classification parameter is the subunit structure of different cytokine receptors. Some receptors form homodimers, other receptors have two or more subunits leading to a hetero-oligomeric structure. All subunits are proteins with one single transmembrane domain, an extracellular located N-terminal domain and an intracellular C-terminal domain.

Type I cytokine receptors (hematopoietin receptor family) consist of one or two polypeptide chains responsible for cytokine binding and an additional chain for signal transduction. The erythropoietin receptor, the growth hormone receptor and the G-CSF receptor belong to this receptor family. The IFNα/β receptor and IFNγ receptor represent the family of type II cytokine receptors (Interferon receptor family). Depending on the literature source the TNF receptor family belongs to the type III cytokine receptors with huge structural differences compared to the first two classes.

Table 1   *Overview of cytokine function*

Cytokine	Producing cells	Target Cell	Function
Class I Cytokines			
GM-CSF	Th cells	progenitor cells	growth and differentiation of monocytes and dentritic cells
IL-1	monocytes	Th cells	co-stimulation
	macrophages	B cells	maturation and proliferation
	B cells	NK cells	activation
	DC	various	inflammation, acute phase response, fever
IL-2	Th1 cells	activated T and B cells, NK cells	growth, proliferation, activation
IL-3	Th cells	stem cells	growth and differentiation
	NK cells	mast cells	growth and histamine release
IL-4	Th2 cells	activated B cells	proliferation and differentiation
			IgG1 and IgE synthesis
		macrophages	MHC Class II expression
		T cells	proliferation
IL-5	Th2 cells	activated B cells	proliferation and differentiation
			IgA synthesis
IL-7	marrow stroma, thymus stroma	stem cells	differentiation into progenitor B and T cells
IL-8	macrophages endothelial cells	neutrophils	chemotaxis
IL-12	macrophages	activated Tc cells	differentiation into CTL
	B cells	NK cells	activation

Cytokine	Producing cells	Target Cell	Function
Class I Cytokines			
IFNγ	Th1 cells,	various	viral replication inhibition
	Tc cells, NK cells	macrophages	MHC expression
			pathogen elimination
		activated B cells	Ig class switch to IgG2a
		Th2 cells	proliferation
Class II Cytokines			
EPO	kidney cells		differentiation and proliferation of erythrocytes
G-CSF	monocytes, macrophages, neutrophiles	progenitor cells	proliferation and differentiation of hematopoietic progenitor cells
IL-6	monocytes	activated B cells	differentiation into plasma cells
	macrophages	plasma cells	antibody secretion
	Th2 cells	stem cells	differentiation
	stromal cells	various	acute phase response
IL-10	Th2 cells	macrophages	cytokine production
		B cells	activation
IL-28/29 (IFNλ)	various	various	Antiviral, but not antiproliferative effects
IFNα	leukocytes	various	viral replication inhibition
			MHC I expression
IFNβ	fibroblasts	various	viral replication inhibition
			MHC I expression

One of the key questions of cytokine receptor signaling is: How is the signal propagated over the membrane? Since no structure of a complete cytokine receptor including transmembrane- and cytosolic domains has been published yet, the structural and dynamical determinants of signal activation are not understood. However, interactions of the extracellular domains of several receptors provided some evidences, that signal activation is propagated by ligand induced cross-linking of the receptor subunits. Thus, ligand recognition plays a key role in receptor cross-linking and has been studied for several receptors.

3.1.2 Extracellular structure of type I cytokine receptors

A hallmark for understanding cytokine-receptor structure and mechanism was the determination of the crystal structure of the growth hormone receptor complex [1-3]. This receptor consists of two identical subunits, each subunits contains two seven-stranded fibronectin III-like domains. Interestingly two ligand binding sites were identified on each subunit, mainly localized on the N-terminal fibronectin III-like domain. These two different binding sites mediate the cross linking of two single receptor molecules induced by one ligand (Figure 1A). Another interesting observation was the difference in affinity of the two binding sites, indicating a two-step binding mechanism. In the first step GH binds to the high affinity binding site of one subunit, in the second step, which takes place in plane of the membrane, the signaling complex is formed. That model is also supported by the contact area formed by the two C-terminal fibronectin III-like domains (Figure 1A). Thus ligand induced receptor cross-linking of the receptor subunits is proposed to initiate intracellular signaling.

Another cytokine receptor forming a receptor homodimer together with one ligand molecule is the erythropoietin receptor (EPOR) [4]. As for GHR, ligand binding sites of the EPOR are mainly located on the N-terminal fibronectin III domain and the linker region (Figure 1B). In contrast to the GHR, for EPOR no receptor-receptor contacts were observed in the crystal structure, indicating different ways of receptor orientation for signal activation.
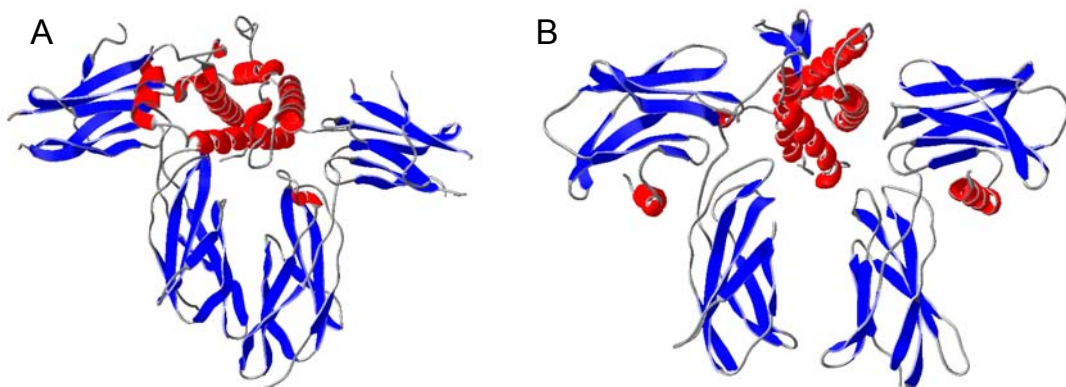

Figure 1   A, B: Crystal structure of the GHR (A) and the EPOR (B) complexes.

In contrast to GHR and EPOR, IL-4 recruits a heterodimeric receptor complex involving IL-4, IL-4R and a subunit called gamma chain (γC). The structure of IL-4/IL-4R was solved by crystallization [5] and in the binary complex two independent binding sites on IL-4R have been identified via mutagenesis [6]. These data indicate a stoichiometry of 1:1:1, but currently no ternary complex structure including γC has been determined.

A 2:2 stoichiometry was found for the G-CSF:G-CSFR complex. In the 2:2 complex neither interactions between the G-CSF molecules nor interactions between the two receptor molecules could be observed. This complex was reported to be formed by two binary complexes of G-CSF:G-CSFR, again via a second ligand binding site. The first binding site, which is responsible for the formation of the 1:1 complex, is localized at the C-terminal domain in proximity to the linker region (Figure 2). This contradicts to the observations on other cytokine receptors, where the high affinity binding site is mainly localized at the N-terminal domain. In this case, the region on G-CSF, which corresponds to the high affinity binding site on GH, mediates the formation of the 2:2 complex. In other studies higher stoichiometries up to 4:4 are proposed for this complex [7]. However the exact stoichiometry of the signaling complex remains to be elucidated.
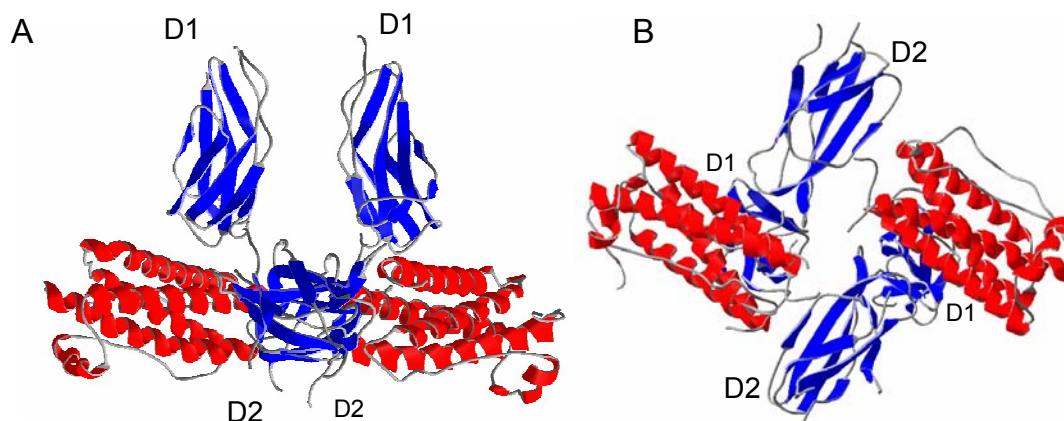
Figure 2   A, B: Structure of the G-CSFR:G-CSF 2:2 complex, side view (A) and upview (B). The receptors are drawn in blue, the ligands in red.

Also receptor-ligand complexes with a higher stoichiometry were investigated, for example the IL-6 receptor. This complex is arranged in a 2:2:2 stoichiometry of IL-6:IL-6R and gp130. The crystal structure of IL-6:gp130 was determined by using a viral homolog to human IL-6 (vIL-6), which has a comparable structure and function. In contrast to human IL-6, vIL-6 is able to activate signaling without forming a binary complex with IL-6R. The vIL-6:gp130 complex shows a two-fold symmetric ring structure with a bridge between the receptors formed by the ligands [8] (Figure 3). This arrangement is mediated by two different ligand binding sites on gp130. One binding site is localized on the N-terminal domain D1, the

other binding site which recruits the opposite vIL-6 is localized at domain D3. With human IL-6 a hexameric complex of IL-6:IL-6R/gp130 in a 2:2:2 stoichiometry was observed in single particle analysis [9] including the three C-terminal domains of gp130 (D4, D5 and D6).
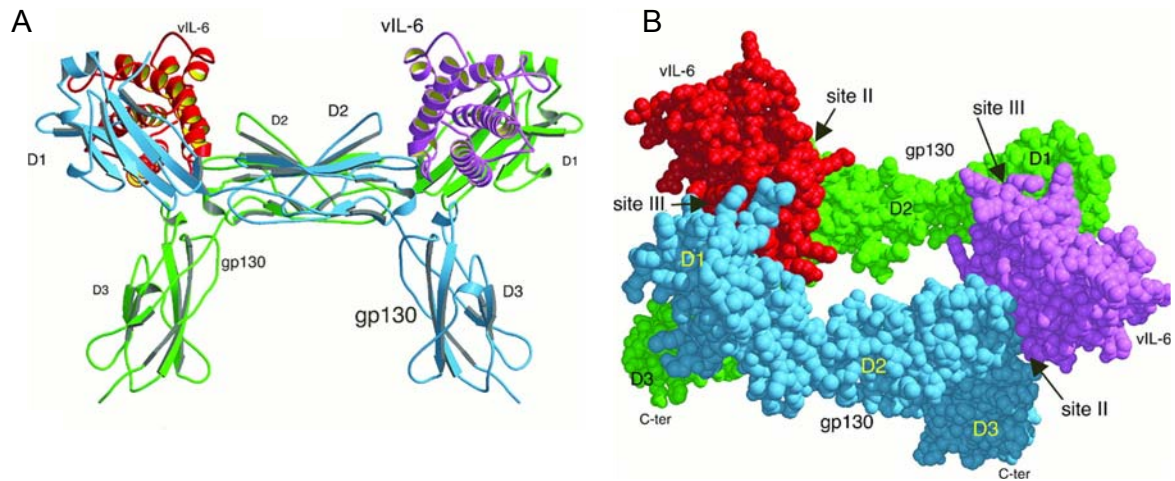
Figure 3   *Structure of the vIL-6-gp130 complex in 2:2 stoichiometry (as published in [8]). A: Ribbon scheme of the side view showing that each gp130 interacts with both vIL-6 molecules via different domains. B: Top view demonstrating the ring structure of the complex.*

3.1.3 Type II cytokine receptors

In contrast to some type I cytokine receptors, all type II cytokine receptors are heterodimers or multimers with a high and a low affinity component. Currently no complete complex structure of the extracellular domains of a type II cytokine receptor is available.

For the IFNγR complex a stoichiometry of 2:2:2 was proposed, the solved structure shows a 2:2 complex of IFNγ and IFNγR1 [10] (Figure 4). In contrast to type I cytokine receptors, where dimerization is mediated via two different interaction sites on the ligand, dimerization of the IFNγR complex is driven by a ligand dimer. IFNγ forms a dimer in solution, which binds two IFNγR1 with high affinity ($K_D \sim 0.1$ nM) at the identical binding site [10] (Figure 4). The membrane proximal domains of IFNγR1 receptors do not show a contact interface like GHR. The 2:2 complex binds two β-receptor chains (IFNγR2) that are specific to the type of responding cell [11]. The low affinity of IFNγR2 indicates a two-step binding mechanism.
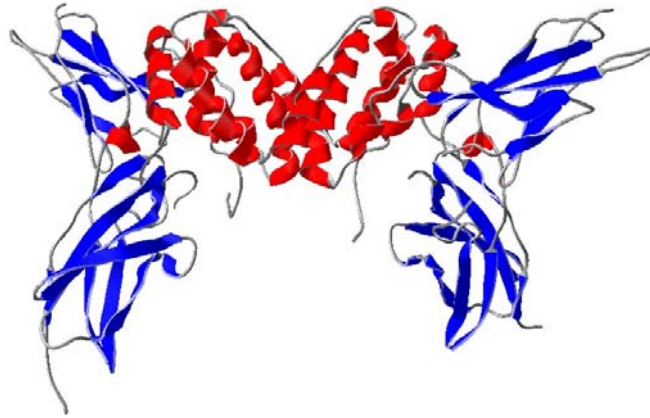
Figure 4   *Structure of IFNγ and IFNγRα in a 2:2 complex formation. This complex is recruited by two IFNγR chains to the signaling complex.*

Like IFNγ, IL-10 has 6 α-helices and forms also a dimer [12]. As shown for IFNγ the structure of the 2:2:2 complex has not been determined yet, but the structure of a IL-10:IL-10R1 complex has been solved by X-ray crystallography (reviewed in [13]). Based on this structure a model showing the 2:2:2 stoichiometry of IL-10:IL10R1:IL-10R2 was proposed (Figure 5). In this model two IL-10 dimers form a central ligand core. IL-10R1 and IL-10R2 are arranged in an anti-parallel manner on two sites. This prediction is based on crystallography results and measurements in solution, where two IL-10 dimers and four IL-10R1 molecules form a complex, which is not believed to be formed on the membrane.
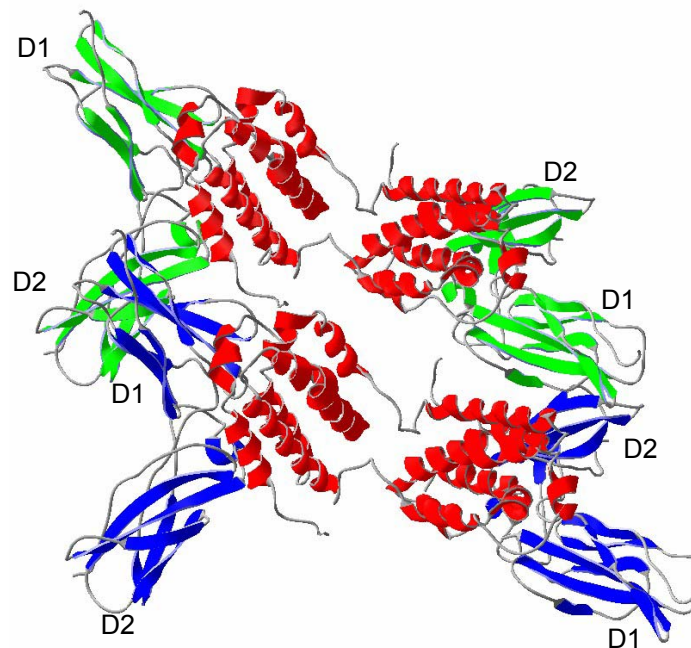
Figure 5   *Model of an IL-10/IL-10R1/IL-10R2 complex (kindly provided by Mark R. Walter). The localization of each Ig-like domain is labeled with D1 or D2 (green: IL-10R1, blue: IL-10R2). The model is based on the structure of IL-10/IL-10R1 determined by X-ray.*

3.1.4 Mechanisms of cytokine receptor signaling

As an initial step in cytokine signaling the ligand-induced assembly of the extracellular domains is suggested. This assembly is proposed to bring the intracellular domains into a closed proximity, which leads to cross- or autophosphorylation of receptor-associated kinases like JAK (Janus kinase). These activated kinases phosphorylate several tyrosine residues of the receptor cytoplasmic domains. In the next step STAT proteins (signal transducer and activator of transcription) dock to receptor subunits and become also phosphorylated by the associated kinases. The activated STATs are able to form homo- as well as heterodimers translocating to the nucleus. There they act as transcription factors and control the expression of response genes.

Currently it is still under debate, how kinase activation is mediated by cytokine binding. One model is the ligand-induced cross-linking which is responsible for bringing the cytoplasmic domains into proximity leading to signal propagation. Based on different binding affinities of the subunits a two-step assembling was proposed. In this model it is possible to control responsiveness by varying the surface receptor concentration. For some cytokine receptors pre-assembly of receptors in an inactive state is proposed. Thus ligand binding leads to a conformational change of the pre-assembled subunits and not to a ligand-induced assembly.

3.1.5 Type I cytokine receptor signaling

The formation of a $GH:GHR_2$ complex at the cell surface leads to an activation (by trans-phosphorylation) of the tyrosine kinase JAK2, which associates with the cytoplasmic domain after ligand binding (reviewed in [14]). The activated JAK2 phosphorylates GHR and STAT proteins activating a variety of cellular responses. Each domain has a high and a low affinity ligand binding site suggesting a sequential assembly. In the first step the high affinity binding site of GH binds to one GH receptor subunit. The second step, which takes place in plane of the membrane, is mediated by low affinity interactions [15, 16]. The interaction interface between two receptor domains was investigated in detail by mutagenesis [15, 17-20]. On sub-domain 2 several residues were mutated leading to reduced signaling activity. Interestingly dimerization was not affected in these mutants. These results indicated that not only dimerization is required for signaling, but subtle structural changes can influence signaling activity. Still many other aspects like interactions between the transmembrane domains or the formation of intermolecular disulfide bonds have not been investigated yet.

Another receptor system, which is studied in detail, is the erythropoietin receptor. Like GH also EPO is proposed to dimerize two receptor molecules sequentially in the membrane with one high affinity ($K_D \sim 1$ nM) and one low affinity ($K_D \sim 1$ µM) interaction [21] forming a $EPO:EPOR_2$ complex. Studies with cross-linked EPOR dimers either covalently by

introduction of additional cysteines [22] or non-covalently by EPO-mimetic peptides [23] demonstrate, that a close proximity of receptors is necessary for activation. Either life-time or orientation of the receptor complex have strong influences on activity, demonstrated by different EPO-mimetic peptides [24, 25]. In contrast to the two-step assembly mechanism the existence of pre-associated, inactive EPOR dimers was proposed [26]. In this self-associated dimer the intracellular domains are suggested to be kept apart preventing background phosphorylation by associated JAK2 [27]. If EPO binds, structural changes of the extracellular domains promote a closer and correct proximity of the intracellular domains, which permits self-phosphorylation of JAK2 and thus initiates signaling (Figure 6, [4]). The model of a pre-assembled receptor based on crystallization data [26] was supported by an in vivo complementation assay [28]. Interestingly, also the transmembrane domains were also proposed to play a role in receptor pre-assembly [29]. However, a pre-assembly in an "off-state" may promote a tight regulation of EPOR signaling. Similar pre-association of homodimeric complexes has been proposed for IL-1R [30] and IL-2R [31].
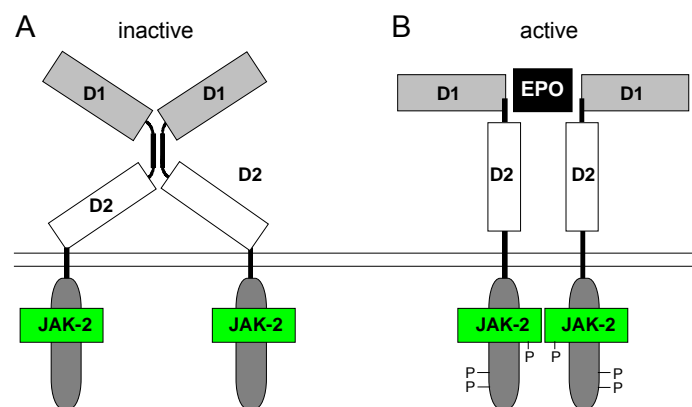
Figure 6   *Schematic of the EPO receptor complex [4]. A: Inactive "off-state" of the dimer with distantly arranged cytosolic domains. B: Liganded active receptor configuration. The cytosolic domains are in closed proximity and right orientation to each other, which enables JAK-2 mediated phosphorylation and signal cascade initiation.*

In contrast to EPOR and GHR several receptors forming heterodimers are described, e.g. the IL-4R. In the first step IL-4 binds specifically to IL-4αR, then to a so called γ-chain. This second protein is also involved in IL-2, IL-7 and IL-9 signaling [32], indicating broader intersections of different signaling pathways. Structurally the high affinity binding site of IL-4αR corresponds to the low affinity site on GH or EPO [5].

The protein gp130 is a shared signal-transducing receptor, involved in the signaling of IL-6, IL-11 and several other cytokines [33]. In the first step of IL-6 signaling, IL-6 binds specifically to the receptor IL-6R forming a binary complex. This complex is recognized by gp130 for the assembly of a trimolecular complex, which is not competent for signaling. Two ligand/receptor complexes then form a 2:2:2 complex in a manner that the N-terminus of

gp130 binds the opposite IL-6 (Figure 7, [8]). Interestingly, the intracellular domains of IL-6R seem not to be required for signal activation. This was demonstrated by experiments with a soluble complex of the extracellular domain of IL-6R and IL-6, which also leads to gp130 mediated signal activation. Here, the formation of a binary complex of IL-6/IL-6R is required for gp130 binding, indicating a cooperative interaction of IL-6 and IL-6R with gp130. Thus, soluble splicing variants of gp130 (sgp130) and IL-6R (sIL-6R) are proposed to play a role in regulating IL-6 signaling. Soluble IL-6R was shown to increase IL-6 activity, whereas sgp130 acts as a natural inhibitor of IL-6 signaling [34]. Interestingly the three membrane proximal domains of gp130 are proposed to keep the complex in a certain distance to the membrane [9]. This arrangement was suggested to enable a closed proximity of the C-terminal domains (D6) mediating signal activation.
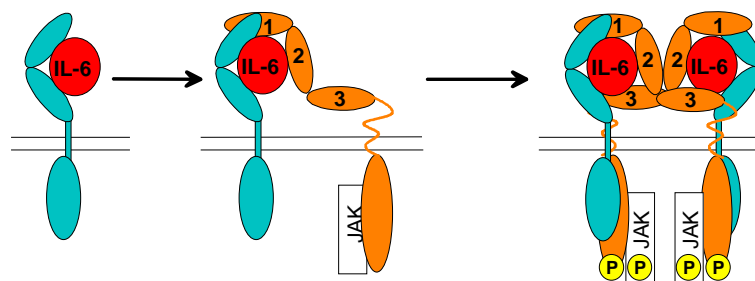
Figure 7   Cartoon of IL-6 signaling. In the first step one ternary complex of IL-6/IL-6R and gp130 is formed. Subsequently two ternary complexes dimerize to a 2:2:2 complex, which activates intracellular signal transduction.

3.1.6 Type II cytokine receptor signaling

IFNγR consisting of IFNγR1 and IFNγR2 was proposed to be pre-assembled in an inactive state. In fluorescence transfer experiments it was obseved that ligand binding led to a decrease in FRET efficiency [35]. It was concluded, that this decay is due to a conformational change of a pre-assembled receptor (Figure 8). Probably an increase in receptor flexibility induced by ligand binding activates the receptor. Since IFNγ is a dimer, it binds two IFNγR1 but does not directly bind to IFNγR2 in the absence of IFNγR1. In contrast to a pre-formation, the observation of a high and a low affinity component also suggested a two-step binding mechanism with IFNγR1 as a binding protein and IFNγR2 as the activator of signal transduction.
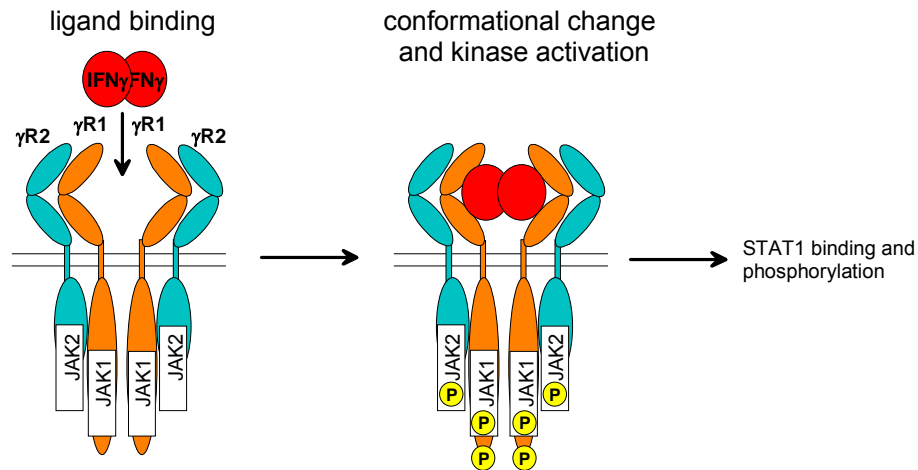
Figure 8   Cartoon of IFNγR signal activation. Ligand induced conformational changes in the pre-associated complex generate kinase activity.

3.2 Type I interferons

Interferons mediate the antiviral activity as a first defense line and furthermore prevent secondary viral infections [36]. Three types of human interferons are classified by their receptors: type I, type II and type III. 13 non allelic IFNα sub-types, IFNβ, IFNε, IFNκ and IFNω belong to the type I interferons. IFNγ is the only known type II interferon. Additionally four IFN-like cytokines, defined as type III interferons, have been reported recently: IFNλ1 (IL-29), IFNλ2 (IL-28A) and IFNλ3 (IL-28B) are found in humans and other mammals (reviewed in [37]). Here, only type I IFNs will be discussed in more detail.

Exposure of cells to viruses or double stranded RNA (dsRNA) induces the production of IFNαs, IFNβ and IFNω. The level of each expressed IFN depends on the tissue of origin and the nature of viral challenge. Signaling induced by type I interferons plays a key role in host innate immunity by eliciting a pleiotrophic response including antiviral, antiproliferative, immunmodulatory and anti-inflammatory activities. These activities make type I IFNs to attractive candidates for a variety of clinical applications [38].

IFNs affect certain levels of viral infection like transcription, translation, RNA stability, virus maturation and replication. The spectrum of cellular effects depends on IFN-stimulated cell type or tissue. Hundreds of genes were identified by DNA arrays to respond to IFN stimulation [39], but the whole network of IFN mediated signaling pathways has not been understood yet. Several signaling pathways propagating antiviral response were investigated in detail [40, 41]. The best characterized IFN-induced protein is the dsRNA dependent protein kinase R (PKR) [42]. It was predicted, that PKR specifically binds viral dsRNA and turns after autophosphorylation into the activated state by the exposition of the catalytic C-terminal domain [43]. No sequence specificity has been identified yet. However, cellular

dsRNA (tRNA, rRNA) does not affect PKR activity. Once PKR is activated, it phosphorylates the eukaryotic initiation factor eIF-2 α-subunit resulting in the inhibition of translation initiation. This effect decreases host as well as virus protein synthesis and supports the propagation of an antiviral state. PKR is also known to phosphorylate histones inhibiting DNA synthesis, which drives antiproliferation. Other IFN-induced key enzymes are 2´,5´-oligoadenylate-synthases (2-5A-sythases) producing short polymers of 2´,5´-oligoadenylate. This polymer activates RNAse F leading to extensive ssRNA digestion [44]. 2-5A binds inactive monomeric RNAse L and induces reversible formation of an active dimer [45]. Additionally 2-5A-sythases modify the Cap-structure of mRNA inhibiting the binding to the ribosome. Thus also translation level is affected by this enzyme.

PKR and 2-5A-synthase act effectively during the antiviral response. Additionally several secondary effects supporting the efficiency of this primary response are known. Mx proteins belong to the GTPases in the dynamin superfamily and are also induced by IFNs. They interfere with viral growth and replication at the transcriptional and translational level [46, 47]. Fas is an apoptosis-propagating receptor protein inducing cell death after binding Fas ligand.

Also elements of the adaptive immune system are known to be stimulated by IFNs. The increased level of antigen-MHC-I at the cell surface activates cytotoxic T-lymphocytes (CD8$^+$) eliminating infected cells, so viruses lose their replication hosts. Also the expressions of TAP, proteasome components and chemokines are influenced by IFNs. Proteasomes and TAP propagate the antigen pathway by cleavage of virus proteins to peptides and their loading to MHC-I via the TAP complex. Thus IFNs are elements of innate immunity, which furthermore initiate responses by the adaptive immune system.

Interferons have been used in clinical applications for two decades for different diseases. Recombinant IFNα2 was the first IFN used as a drug for treatment of hairy cell leukemia and Kaposi´s sarcoma [48]. Today different preparations of IFNα2 (Pegasys$^®$, Roferon$^®$, IntronA$^®$) and IFNβ (Rebif$^®$, Avonex$^®$, Betaferon$^®$) are used in a variety of cancers and viral diseases. For example chromic myelogenous leukemia and metastatic malignant myeloma have been successfully treated with IFNα2 [49, 50]. Because of its antiviral activity IFNα2 has also been approved for the therapy of chronic hepatitis B [51] and C [52], liver diseases caused by HCV infection. The potent antiviral and immunmodulatory activity proved in cell culture propagate IFNα2 as a drug candidate for many other viral infections, e.g. HIV. However, only minor effects in the treatment of retroviral diseases were observed [53]. The anti-inflammatory character of IFNβ is used for the treatment of relapsing-remitting multiple sclerosis [54]. It is not able to eliminate the disease, but it is proposed that by migration inhibition of activated T-lymphocytes into the nervous system the velocity of neuron

degradation is reduced [55]. As for many other biotherapeutics, side effects often cause interruption or dosage limitation in IFN therapy. Also antibodies generated during the therapy can reduce the efficiency of IFN treatment dramatically [56]. Currently several modifications of IFNα2 (e.g. different PEGylations) are used in clinical trials for a variety of further applications, mainly cancer diseases [57].

3.3 The human type I interferon receptor ifnar

3.3.1 Overview

All human type I interferons exert activity through binding to the same receptor subunits, ifnar1 [58] and ifnar2 [59]. Ifnar1 and ifnar2 are transmembrane proteins with an extracellular domain (EC), a trans-membrane domain (TMD) and an intracellular domain (CP) associated with JAK1 (ifnar2) or Tyk2 (ifnar1) (Figure 9). Based on sequence alignment of the extracellular domains both receptor components belong to the type II cytokine receptor family [60]. Typically the extracellular domains of this receptor family are divided into two Ig-like domains (7 β-sheets with one disulfide bond) consisting of ~100 residues each and forming one cytokine binding module (CBM) [61]. Ifnar2-EC forms one CBM and the structure was solved by NMR [62]. Interestingly ifnar1-EC consists of ~400 residues, twice of the size of ifnar2-EC. This suggests two CBMs and a more complex stoichiometry than the 1:1:1 complex of ifnar1-EC, ifnar2-EC and IFNβ observed in solution [63]. In contrast to ifnar2-EC no structural data from NMR or crystallography are currently available for ifnar1-EC.
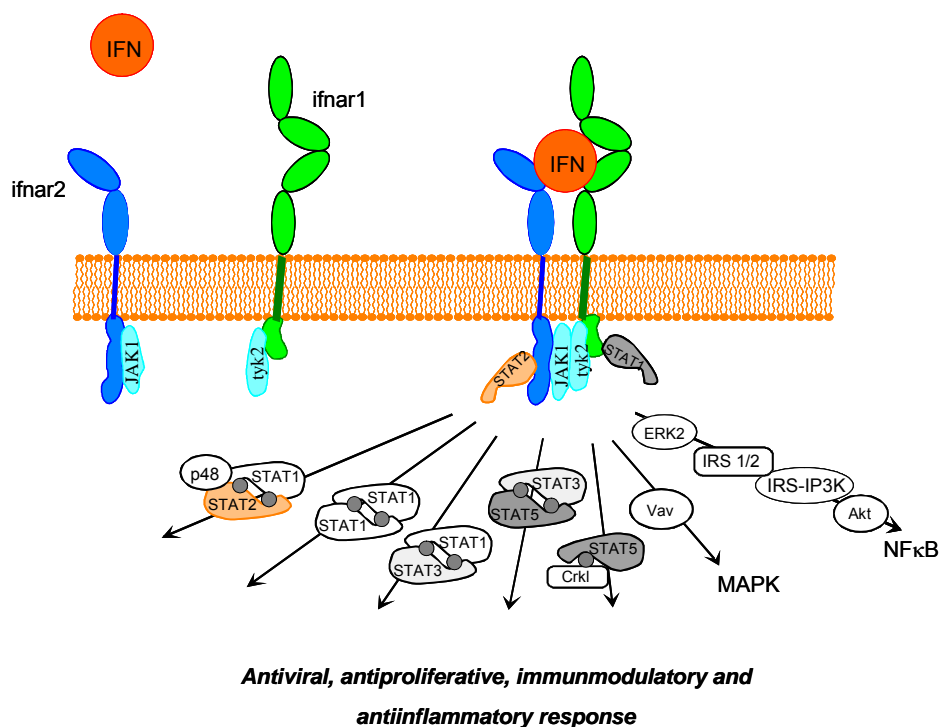

Figure 9   *Schematic of the human type I interferon complex and associated signaling pathways.*

3.3.2 Signal transduction induced by IFN mediated receptor assembly

For the type I IFN receptor a signaling complex formation by the ligand-induced assembly of the two receptor subunits ifnar1 and ifnar2 is suggested (Figure 9). In this signaling complex the tyrosine kinases JAK1 and Tyk2 associated with the cytoplasmic domains are activated by auto-phosphorylation, followed by phosphorylation of several tyrosine residues on the receptor and other effector molecules, which are mainly members of the STAT family. STAT1 and STAT2 play a central role in type I IFN signaling. After phosphorylation together with p48 a STAT1/STAT2 heterodimer forms the transcription factor ISGF3. This factor activates the transcription of interferon-stimulated genes (ISGs) genes in the cell nucleus by binding to interferon-stimulated regulatory elements (ISREs) [40, 41, 64]. But also other members of the STAT family (STAT3 and STAT5) were identified to form homo- or heterodimers after IFN stimulation leading to the activation of different signaling pathways.

Another pathway induced by IFN receptor assembly is the IRS/PI-3-K pathway [65]. The IRS (insulin receptor substrate) family consists of 6 proteins with several phosphorylation sites, which act as binding sites for SH2-domains. During receptor activation IRS-1 binds to the ifnar cytoplamic domain and is subsequently phosphorylated on different tyrosines. After dissociation from the receptor IRS-1 activates the PI-3-K (phosphatidyl-inositol-3-kinase) enzyme subunit p85 via SH2 interaction. The second subunit p110, were phophoinositol- and serinkinase activity are located, subsequently binds to p85 and the activated enzyme leads to a variety of signaling processes [41]. In addition, downstream effectors like the Ser/Thr kinase Akt activates the nuclear factor κB [66], which is involved in apoptosis and cell cycle arrest. Also P21(ras)/Raf-1/MAPK are activated by type I IFNs [37]. Also the tumor-suppressor p53 is reported to be induced by interferons [67]. These pathways are proposed to be responsible for the antiproliferative and pro-apoptotic character of type I interferons.

It appears that the function of the 15 known human type I interferons is not fully redundant, but that differential signaling by different IFNs can be observed [68-73]. In particular between IFNα subtypes and IFNβ, substantial differences have been observed on the level of receptor phosphorylation [68] and effector recruitment [74], as well as on the level of gene induction [75]. As no further receptor component has yet been identified, these differences have to be explained through the mode of interaction of IFNs with the extracellular domains of ifnar1 and ifnar2. Therefore, a comprehensive structural, biophysical and mechanistic picture of how the receptor domains are recruited in time and space is required for understanding the specificity of signal propagation though the membrane. The differences in affinity, binding kinetics, recognition and bindings modes, which have been so

far reported for the interaction of IFNα2 and IFNβ with ifnar2-EC are only minute [76, 77] and therefore can hardly explain the functional differences. The interaction between ifnar1 and IFN has been reported to be of much lower affinity and its contribution towards complex formation is less well characterized, because the properties of cell surface receptor such as affinity and competitiveness is dictated by the (high-affinity) interaction with ifnar2.

3.3.3 Structure-function relationships

The 3-dimensional structures of IFNα2 [78] and IFNβ [79] were determined by crystallography. Both interferons consist of 5 α-helices (A-E) which are connected via loops and short 3_{10}-helices (Figure 10). Helices A and B are ordered to each other in a parallel manner, to helices C, D and E they are oriented anti-parallel. While helix D is part of a loop connecting helices C and E, helices A, B, C and E form a 4 helix bundle (Figure 10A), a very compact and stable structure mediating type I IFNs´ temperature and pH resistance. Both IFNs obtain a disulfide-bond linking AB- and DE loop (IFNα2: C29-C139; IFNβ: C31-C141). IFNβ, which is glycosylated (N80), has an additional free cysteine (C17). IFNα2 subtypes have an additional disulfide-bond between C1 and C98, which is not essential for receptor binding.
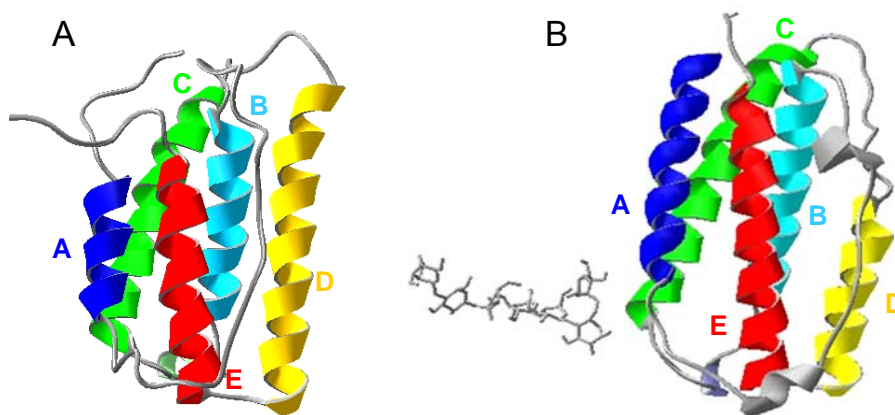
Figure 10   *A: Structure of IFNα2 determined by NMR. Helices A, B, C and E are arranged in a 4-helix bundle. B: Structure of IFNβ with glycosylation solved by X-ray analysis.*

The interaction between IFNα2 and the high affinity receptor component ifnar2 was well characterized by mutagenesis [76, 80]. The structure of the binary complex based on double mutant cycle analysis is shown in Figure 11. On IFNα2 a core binding site to ifnar2 is formed by 6 residues (L30, R33, R144, A145, M148 and R149). R144, A145, M148 and R149 are localized in the E-helix. L30, A145 and M148 form together with L26 and F27 a hydrophobic pocket. Ten additional amino acids on helices A and E are involved in ifnar2 binding mainly by electrostatic interactions. For binding IFNα2 and IFNβ the same residues on ifnar2 are involved, but these residues are differently accentuated [76]. For IFNα2 binding T46, I47 and M48 were determined to form a "hot spot", for binding of IFNβ another set of

residues (I47, H78, N100, W102) accentuates the interaction. The 3-D structure of ifnar2-EC was successfully solved by NMR studies [62] and modeled to IFNa2 based on double mutant cycle analysis data (Figure 12).

Figure 11   Model of ifnar2-EC with residues involved in binding of IFNα2 (A) and IFNβ (B). Color coding corresponds to the decrease in binding affinity (red: >10-fold, orange: >3-fold, yellow: <3-fold, blue: <50%, green: increase).

Figure 12   Structure of the ifnar2-EC-IFNα2 obtained by double mutant cycle analysis (same color coding as in Figure 10). The structure of ifnar2-EC was determined by NMR analysis.
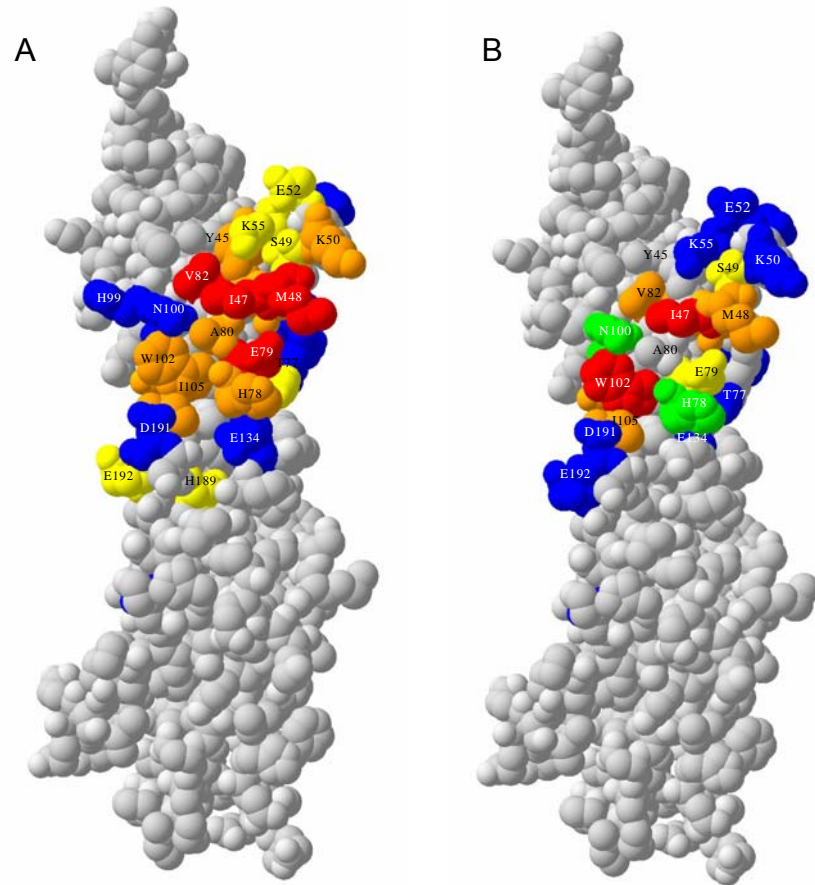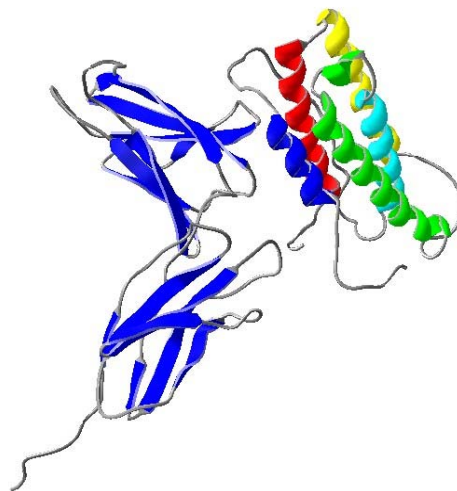
In contrast to ifnar2 much less is known about the interaction between type I IFNs and the low affinity component ifnar1 (with a K_D in the µM range). One method to investigate ifnar1 was monitoring its effect on the high affinity ifnar2-IFN interaction upon ternary complex formation, i.e. the activity of ifnar1 was indirectly detected. In such experiments different binding sites for IFNα and IFNβ on human ifnar1 were predicted by using neutralizing anti-ifnar1-antibodies [81]. Antibody binding of different epitopes inhibited specifically the transcription of IFNα or IFNβ target genes [82]. However, it was not shown that the epitopes for the antibodies correlate with the IFN binding sites. To identify those epitopes, direct interaction between ifnar1 and IFN was investigated. Because of the low affinity of ifnar1, bovine ifnar1, which has a much higher affinity for human IFNα2 (K_D ~ 10 nM), was used. Thus, specific binding of IFNα2 to cells transfected with bovine ifnar1 could be detected. By using human/bovine chimeras of ifnar1, SD2 and SD3 were identified to play an essential role in IFN binding [83]. SD1 and SD4 also appeared to be involved in ligand binding. These results were confirmed by site directed mutagenesis on bovine ifnar1 [84]. In this study the most identified residues were located on SD2 and SD3 while SD1 and SD4 play a minor but significant role in IFN binding. In order to map the ligand binding site on human ifnar1, several mutants were investigated by cellular binding assays [85]. The peptide ^{62}FSLKLNVY^{70} on SD1 and W129 were identified to be crucial for IFNα binding and biological activity. Interestingly ^{278}LRV on SD3 is not critical for binding but for biological activity. Based on this result a model was predicted, where SD1 and SD2 act as a lid of a closed signaling complex indicating the closing mechanism as the trigger for differential signaling.

The general limitation of these strategies, the direct detection with bovine ifnar1 as well as the indirect detection via ifnar2, is the dependency on cellular systems. In these experiments receptor surface expression has to be strictly controlled, because the binding efficiency is expected to depend strongly on the receptor surface concentration (absolute surface concentration) and on the ratio between ifnar1 and ifnar2 (relative concentration). Furthermore, stoichiometry or individual contributions of single ifnar1 sub-domains are very difficult to be quantitatively investigated on cells.

However, an effective expression and purification system for studying the interaction *in vitro* has not been established yet. Functional ifnar1-EC was successfully expressed in *P. pastoris*, but very low yields were obtained (personal communication with R. Arduini). A 1:1:1 complex of ifnar1-EC, ifnar2-EC and IFNβ (but not with IFNα2) was detected by size exclusion chromatography [63]. As no direct interaction between IFNβ and ifnar1-EC was shown under these conditions, this result indicated that cooperative interaction leads to stabilization of the ternary complex as shown for IL-6/IL6-R and gp130. These initial results could not explain differences between individual IFNs with respect to the role of signaling

complex stoichiometry, the dynamics or binding sites. To address these questions as well as to confirm cooperative effects an effective *in vitro* assay has to be established.
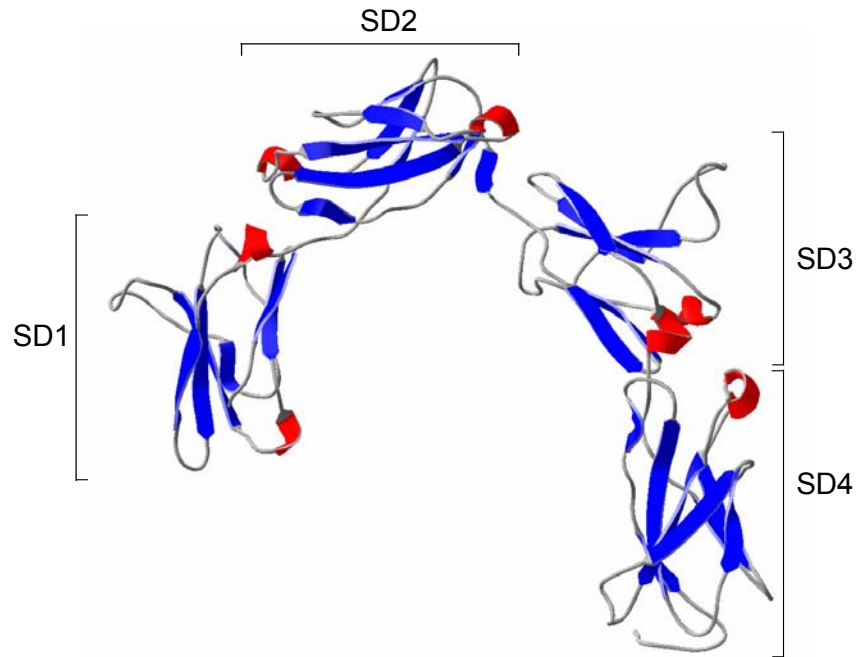

Figure 13   Model of ifnar1-EC based on the structure of ifnar2-EC (SD: sub-domain, red: α-helix, blue: β-sheet)

3.4 Objectives

All IFNs recruit only one receptor with the subunits ifnar1 and ifnar2. Thus differential signaling has to be encoded in the ligand recognition process of the extracellular domains of ifnar1 and ifnar2. Since ifnar1 appears to be responsible for mediating differential signaling, the goal of this work was to define the role of ifnar1-EC in the formation of the signaling complex. In this context also possible differences between individual IFNs had to be elucidated. In order to quantitatively investigate stoichiometry, thermodynamics, kinetics and the structural organisation of the ligand recognition process under controlled surface conditions, an effective *in vitro* approach was followed.

Thus, an efficient expression and purification strategy for ifnar1-EC had to be developed. To achieve quantitative amounts of protein, expression was tried in different compartments of *E. coli* as well as *Sf*9 insect cells. For the analysis of individual interactions governing complex assembly, receptor subunits had to be tethered functionally in an oriented manner onto a glass surface. Then Immobilized receptors could be used to probe stoichiometry, thermodynamics and kinetics of different IFNs solid phase detection. In order to identify possible differences between IFNα2 and IFNβ in terms of binding sites, different ifnar1-EC sub-fragments and mutants had to be generated. One major issue was the investigation of the whole signaling complex in an environment comparable to cell surface conditions. This objective was addressed by the co-immobilization of both receptor subunits on a solid-supported lipid bilayer mimicking the lateral mobility of the cell membrane. Immobilization had to be mediated by tethering the proteins via their his-tags onto a lipid which is covalently linked to a multivalent chelator head group. With this immobilization technique, in combination with surface-sensitive fluorescence detection, complex stoichiometry, dynamics and architecture were investigated. Thus this work should help to draw a detailed picture of complex assembly and should answer the question, how the determinants governing complex assembly are correlated with differential signaling.

3.5 Strategy

3.5.1 Ifnar1-EC expression in quantitative amounts

For the investigation of ligand-receptor interactions *in vitro* adequate amounts of all required proteins were necessary. The extracellular domain of ifnar2 and IFNα2 have been successfully expressed in *E. coli,* refolded and purified in amounts of 2-3 mg/l [86]. In contrast establishing an expression and purification strategy for ifnar1-EC was a challenge. The key problem of ifnar1-EC expression was the formation of 4 predicted disulfide bonds in the Ig-like domains [60]. Different expression systems in *E. coli* were tried to express properly folded ifnar1-EC. As described for ifnar2-EC [87] refolding from inclusion bodies (reviewed in [88]) was investigated, but without success. Ifnar1-EC was not monomeric and the cysteines were still reduced. Also fusing ifnar1-EC to the maltose binding protein (MBP) was tried. MBP was predicted to act as an intramolecular chaperone by mediating proper folding of the target protein and preventing aggregation [89]. MBP-Ifnar1-EC was expressed in the cytoplasm by using the expression vector pMAL-c2X, but only aggregated fusion protein was detected. In order to express ifnar1-EC in an oxidative environment the *E. coli* strain FA113 with an oxidizing cytoplasm was used for ifnar1-EC expression. This strain lacks reducing cytoplasmic enzymes and was used for successful expression of antibody Fab fragments [90]. For ifnar1-EC, however, no monodispers protein was detectable. As an alternative, periplasmic expression was tried using expression plasmids carrying a translocation sequence (pMAL-p2X and pASK-IBA2). For MBP-ifnar1-EC no secretion into the periplasm was detectable, but ifnar1-EC expressed with pASK-IBA2 could be successfully purified from periplasm via a C-terminal strep-tagII [91]. Size exclusion chromatography and a shift in SDS-PAGE towards a lower molecular weight after DTT-treatment demonstrated, that ifnar1-EC was monomeric and carried disulfide bonds. Since yields were low (50 µg/l), *E. coli* were cultivated in a 10 l fermenter. In order to tether ifnar1-EC to chelator surfaces, the strep-tagII was exchanged by a deca-histidine-tag. This exchange led to protein aggregation probably during IMAC. Based on all results with expression in *E. coli*, it was decided to stop expression with this organism. The expression of ifnar1-EC in *P. pastoris* was also proposed to deliver low yields by applying a complicated purification and deglycosylation procedure [63].

Spodoptera frugiperda 9 (*Sf*9) in combination with the baculovirus AcNPV [92] was chosen as an alternative new expression host to address the problems of low yields, folding and stability. Compared to *E. coli* or *P. pastoris,* insect cells are phylogenetically closer to human cells promising a higher probability of successful expression of human proteins compared to bacteria or yeast. The disulfide bond formation and especially the glycosylation during the secretory pathway were expected to increase solubility as well as stability of

heterologously expressed proteins. This was successfully demonstrated for the expression of gp130, IL-6R [9] and several other cytokine receptors in *Sf*9.

Baculoviruses (family *Baculoviridae*) belong to a group of large, double-stranded DNA viruses that infect specifically different insect species as their natural hosts. They were not known to propagate in any non-invertebrate host, which makes handling very simple. During an infection cycle a variety of viral proteins responsible for replication and budding were expressed. By inserting a gene of choice into the baculoviral genome heterologous protein expression was possible.

In baculoviruses several genes were replaced by heterologous genes, which were transcribed during the virus replication cycle. The genes of interest had to be inserted into the virus genome via homologous recombination. Two different procedures for homologous recombination were available using a cloning vector as a gene shuttle. In the Bac-to-Bac system (Invitrogen) the recombination and selection of positive clones takes place in *E. coli*, transfected with the viral genome. The product of the recombination, the "bacmid", was then transfected to *Sf*9 cells starting viral infection. The alternative to this system is the recombination directly in the host cells with the advantage to prevent the time consuming selection in *E. coli*. In this study a linearized genomic viral DNA and the transfer vector were co-transfected into *Sf*9 cells allowing recircularization of the virus DNA by homologous recombination. Since only circularized virus DNA is able to be transcribed and replicated, homologous recombination acts simultaneously as a selection marker for successful gene insertion. In this process also the heterologous gene is inserted into the virus genome. Here, with respect to time and economic reasons, a baculovirus expression vector system (Baculogold®, BD Bioscience) based on the *Autographa californica* nuclear polyhedrosis virus (AcNPV) was used for generating baculoviruses carrying ifnar1-EC via homologous recombination in *Sf*9 cells.

Ifnar1-EC was cloned into the transfer vector pAcGP67-B, which could be used for all cloning procedures in *E. coli.* It carried several features, which were expected to be necessary for successful ifnar1-EC expression. A polyhedrin promoter with a downstream localized multiple cloning site promoted high expression levels in the late phase of viral replication. The multiple cloning site enables a very flexible handling with respect to insertion of additional linkers. Recombination sequences flanking the cloning region facilitated homologous recombination with the linearized viral DNA. The N-terminal secretion sequence of the viral gp67 protein initiated the secretion pathway of ifnar1-EC, ensuring the formation of disulfide bonds, a specific glycosylation and finally the secretion into the medium. This secretion was also the first step in purification.

3.5.2 Ifnar1-EC sub-fragments and mutants

The amino acid sequence of ifnar1-EC was derived from sequence alignments with other cytokine receptors [60]. Four Ig-like domains of ~100 amino acids were predicted to form two cytokine binding modules indicating two potential ligand binding sites. To elucidate the contribution of each cytokine binding module for ligand binding, ifnar-EC was genetically cut at the predicted linker region. With respect to Ig-like domains and position of the his-tag the products of this procedure were termed H10-SD12 and SD34-H10. In contradiction to the hypothesis of two CBMs, SD2 and SD3 were considered to form the ligand binding site for IFNα2 and IFNβ in a non-classical manner [84]. For the identification of the sub-domains involved in ligand binding H10-SD123 and SD234-H10 were cloned, also to probe differences in the binding sites for IFNα2 and IFNβ. The sequences of SD12, SD34, SD123 and SD234 (Figure 14A) were based on the alignment of different cytokine receptors. Since the linker regions between the individual domains were not well determined, short overlaps were generated in designing the proteins to prevent affecting the structure integrity.

For investigating the role of receptor orientation in forming the ternary complex, H10-tags were fused to the C- or N-termini of ifnar1-EC as well as SD123. Also a constructs of ifnar1-EC with N- and C-terminal tag (SD1234-DT) was expressed to mimic a proposed two-fold attachment to the surface. The immobilization mode of the different ifnar1-EC constructs is schematically shown in Figure 14B.

For investigating the role of the membrane proximal SD4 several constructs were designed. SD4 was replaced by Ig-like domains of human IFNλ receptor (LRSD2) and IL-10 receptor (IL10R2D2) (Figure 15). These constructs addressed the question, if SD4 acts as a spacer or if it has a specific role in complex formation. To verify this question IFN binding on cells (performed in the group of Gilles Uzé, CNRS Montpellier) and on surfaces was investigated. In addition the construct V1V2 deriving from IL-10-R2D2 was cloned. Two amino acid cassettes of ifnar1-EC were re-introduced to get a detailed picture of the arrangement of SD4 with special respect to the C-terminus (Figure 15).

In the cloning strategy (Figure 16) initially SD1234-DT was cloned by an N-terminal linker-insertion of a deca-histdine tag (via *Bam*HI) into the transfection vector pAcGP67-B. H10-SD1234, H10-SD12, SD34-H10, H10-SD123 and SD234-H10 were derived from this construct. For the preparation of SD123-H10 first the sequence without a tag was cloned followed by the insertion of an H10-tag via *Eco*RI, which enables further insertions of other tags or fusion proteins. All other constructs were cloned via classical cloning (PCR and ligation). Mutants with exchanged residues were generated by ligase chain reaction (LCR).
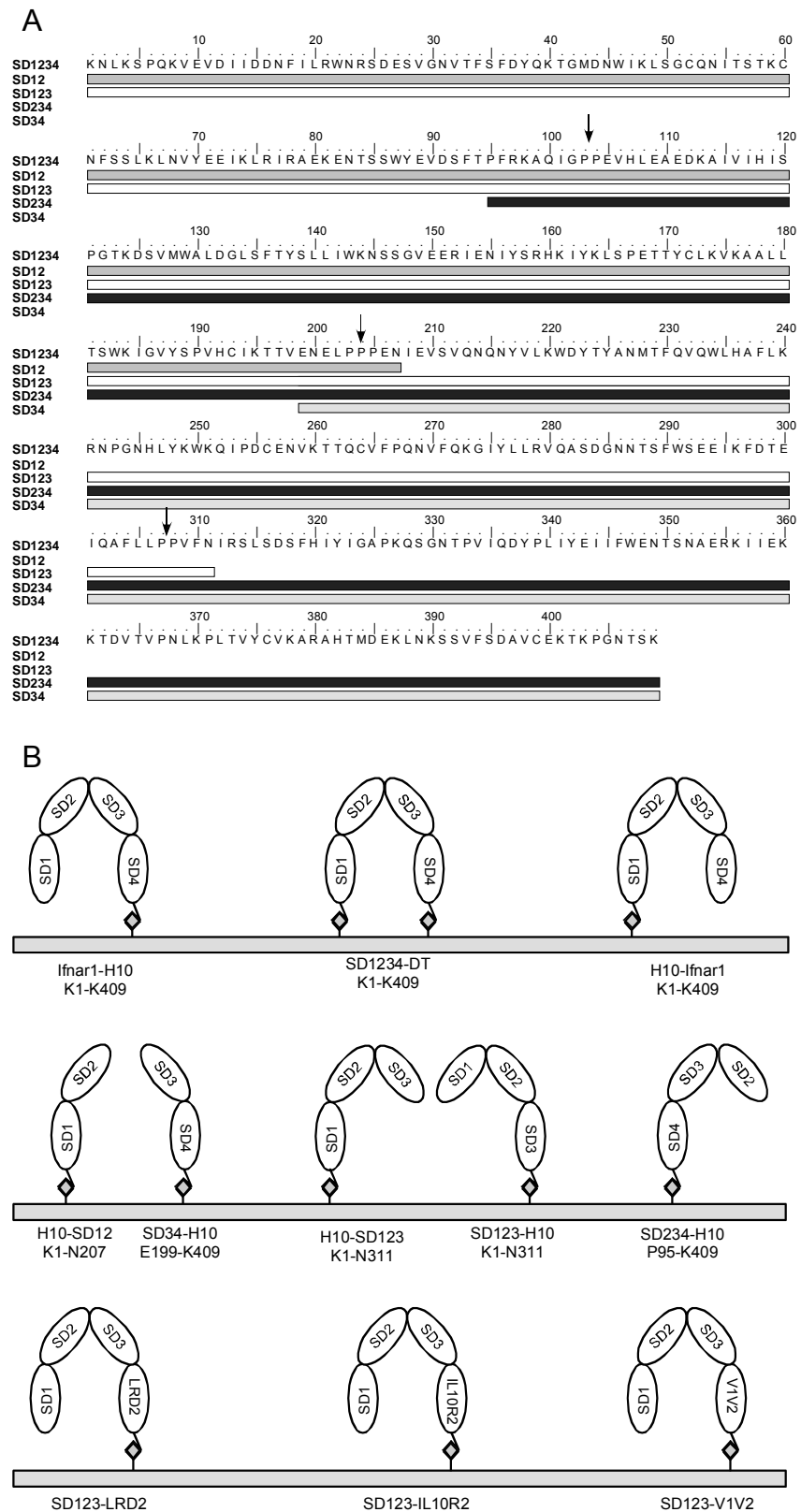
Figure 14   *A: Sequence of ifnar1-EC and the different sub-fragments. The arrows indicate three proline-rich regions of the transition between two Ig-like domains. B: Schematic of ifnar1-EC constructs and their attachment to the surfaces via N- and C-terminal decahistidine-tags.*
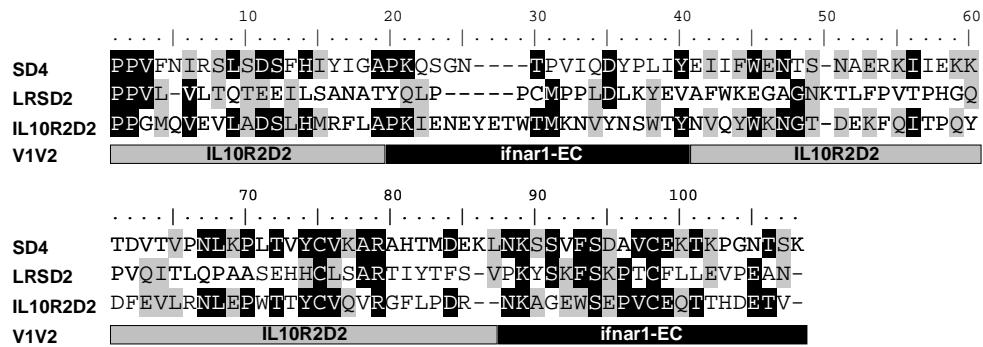
```
              10         20         30         40         50         60
     ....|....|....|....|....|....|....|....|....|....|....|....|....|
SD4  PPVFNIRSLSDSFHIYIGAPKQSGN----TPVIQDYPLIYEIIFWENTS-NAERKTIEKK
LRSD2 PPVL-VLTQTEEILSANATYQLP-----PCMPPLDLKYEVAFWKEGAGNKTLFPVTPHGQ
IL10R2D2 PPGMQVEVTADSLHMRFLAPKIENEYETWTMKNVYNSWTYNVQYWKNGT-DEKFQTTPQY
V1V2  [IL10R2D2]      [ifnar1-EC]        [IL10R2D2]
```

```
              70         80         90        100
     ....|....|....|....|....|....|....|....|....|....|
SD4  TDVTVPNLKPLTVYCVKARAHTMDEKLNKSSVFSDAVCEKTKPGNTSK
LRSD2 PVQITLQPAASEHHCLSARTIYTFS-VPKYSKFSKPTCFLLEVPEAN-
IL10R2D2 DFEVLRNLEPWTTYCVQVRGFLPDR--NKAGEWSEPVCEQTTHDETV-
V1V2  [IL10R2D2]              [ifnar1-EC]
```

Figure 15   Sequence alignment of sub-domain 4 with LRSD2, IL10R2D2 and IL10R2-V1V2. Black: identical residue, grey: homolog residue.
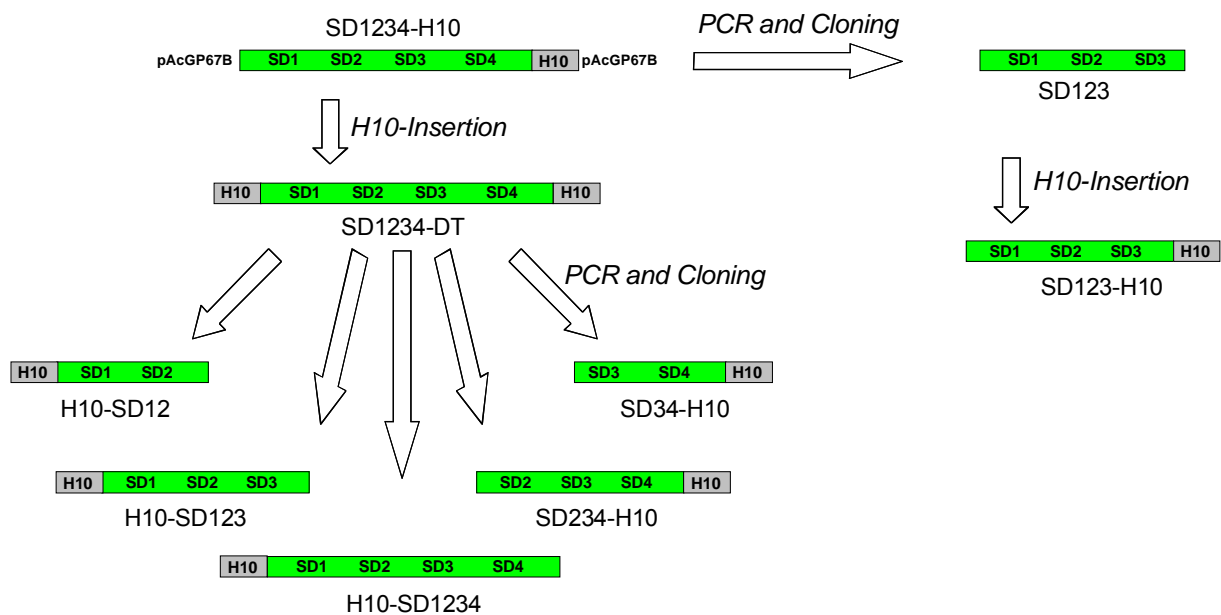

Figure 16   Cloning strategy of different ifnar1-EC sub-fragments. Details in the text.

3.5.3 Detection techniques

Since low affinity for the interaction of ifnar1-EC with IFNα2 and IFNβ was expected, a detection method for monitoring transient interactions was necessary. Therefore label-free solid phase detection by reflectometric interference spectroscopy (RIfS) was applied. This technique is based on the change in optical thickness caused by mass deposition on a glass surface. RIfS detects selectively binding processes at the surface, whereas processes in the bulk are not monitored (Figure 17A). As a read out either the shift of the interference maximum or the interference change at a defined wavelength can be used to monitor protein binding at the surface (Figure 17B). Here, protein immobilization (Figure 17C) or lipid fusion shifted the interference pattern. Since the signal was proportional to immobilized mass, the amount of immobilized protein can be absolutely quantified. Thus the stoichiometry between interaction partners by taking their molecular masses into account can be determined. The affinities of IFN toward ifnar1-EC or ifnar2-EC are calculated from rate constants or

equilibrium signals. A particular advantage for the detection of low affinity interactions are much less critical background signals in RIfS-detection [93] compared to evanescent field detection.
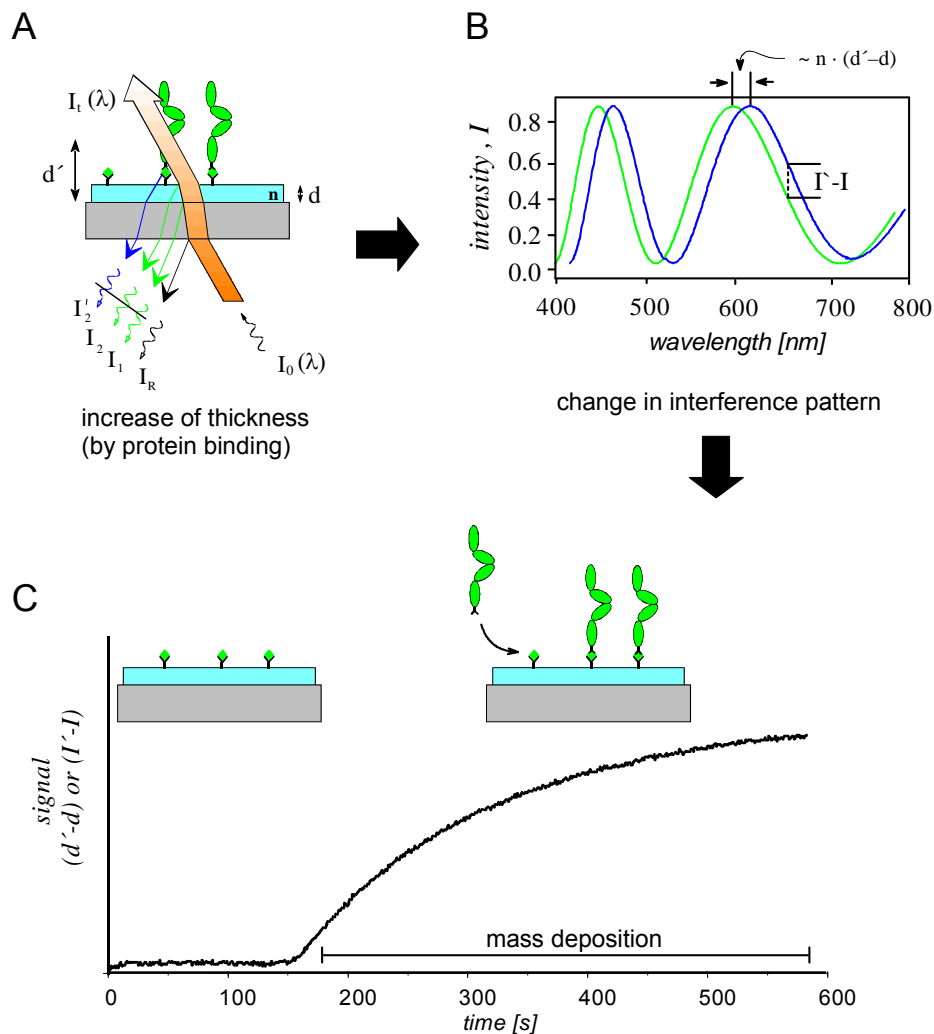

Figure 17   Schematic of RIfS detection method. A: Protein immobilization causes a change in the optical thickness leading to a shift in interference pattern.

Total internal reflection fluorescence spectroscopy (TIRFS) is a surface sensitive method to detect binding processes on surfaces. Here, a total internal reflected light beam generates an evanescent field at the surface, which excitates fluorescence only close to the surface (100-200 nm). Fluorescence detection provided means for more detailed mechanistic analysis. In order to discriminate interactions of different ligands with ifnar1-EC, TIRFS was applied to monitor competition between labeled IFNα2 and unlabeled IFNβ.

For mechanistic understanding of ternary complex dynamics, exchange processes were investigated by chasing labeled with unlabeled IFNα2 at the complex. Another application of TIRFS, also for studying receptor complex dynamics, was probing interactions at very low receptor surface concentrations. Here the receptor surface concentration was

decreased but the ratio between ifnar1-EC and ifnar2-EC was still kept constant. Because of its high sensitivity binding processes at low receptor surface concentrations were monitored.

For all experiments using TIRFS also the RIfS signal was simultaneously monitored as a control. Thus receptor surface concentrations and stoichiometries could be quantified [94] (Figure 18).
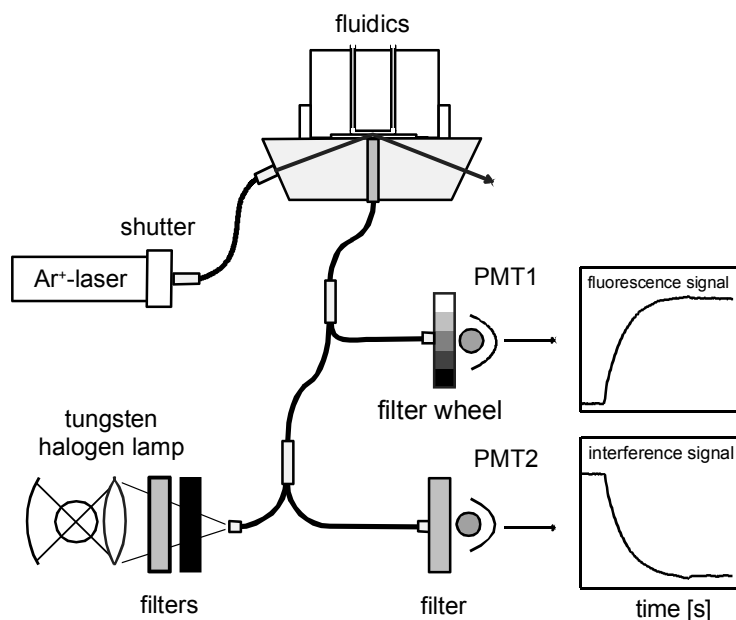

Figure 18   *Schematic of the set-up for simultaneous TIRFS-RIf detection. A laser beam excitates the surface generating the TRIF signal. A filter wheel mediates the specific detection of fluorescence at a photomultiplier (PMT). In parallel light for Rif signal is generated by a halogen lamp, reflected at the surface, filtered and detected at 800 nm by the second photomultiplier.*

3.5.4 Immobilization techniques

For probing receptor-ligand interaction on surfaces, receptor proteins were tethered in a site-specific manner onto the signal-transducer by their C-terminal decahistidine-tag (H10-tag). Since histidine coordinates transition metal ions, his-tagged proteins could be tethered to metal loaded chelator surfaces. In this case a new class of multivalent chelators [95] was used for ifnar1-EC and ifnar2-EC immobilization.

Two modes of chelator surfaces were used in this work. First the chelator was covalently linked to a PEG-polymer brush (Figure 19A). The advantages of this method were the stability of the surface and a simple handling of the chip, which could be used for days. The chelator was fixed very tightly to the polymer brush, so immobilized proteins were predicted to have no lateral mobility (non-fluid support). This immobilization technique was applied for probing individual interactions, because no receptor cross-talk was expected.

To mediate receptor cross-talk between ifnar1-EC and ifnar2-EC, lateral fluidity was required. For this reason a multivalent chelator headgroup (bis-NTA) covalently linked to a lipid, a so called chelator lipid [95] (Figure 19C) was used. It was integrated into a solid supported lipid bilayer (Figure 19B). Thus, immobilized ifnar1-EC and ifnar2-EC were expected to be properly oriented to each other in a ligand induced signaling complex. In all experiments with co-immobilized ifnar1-EC and ifnar2-EC this fluid support was applied.
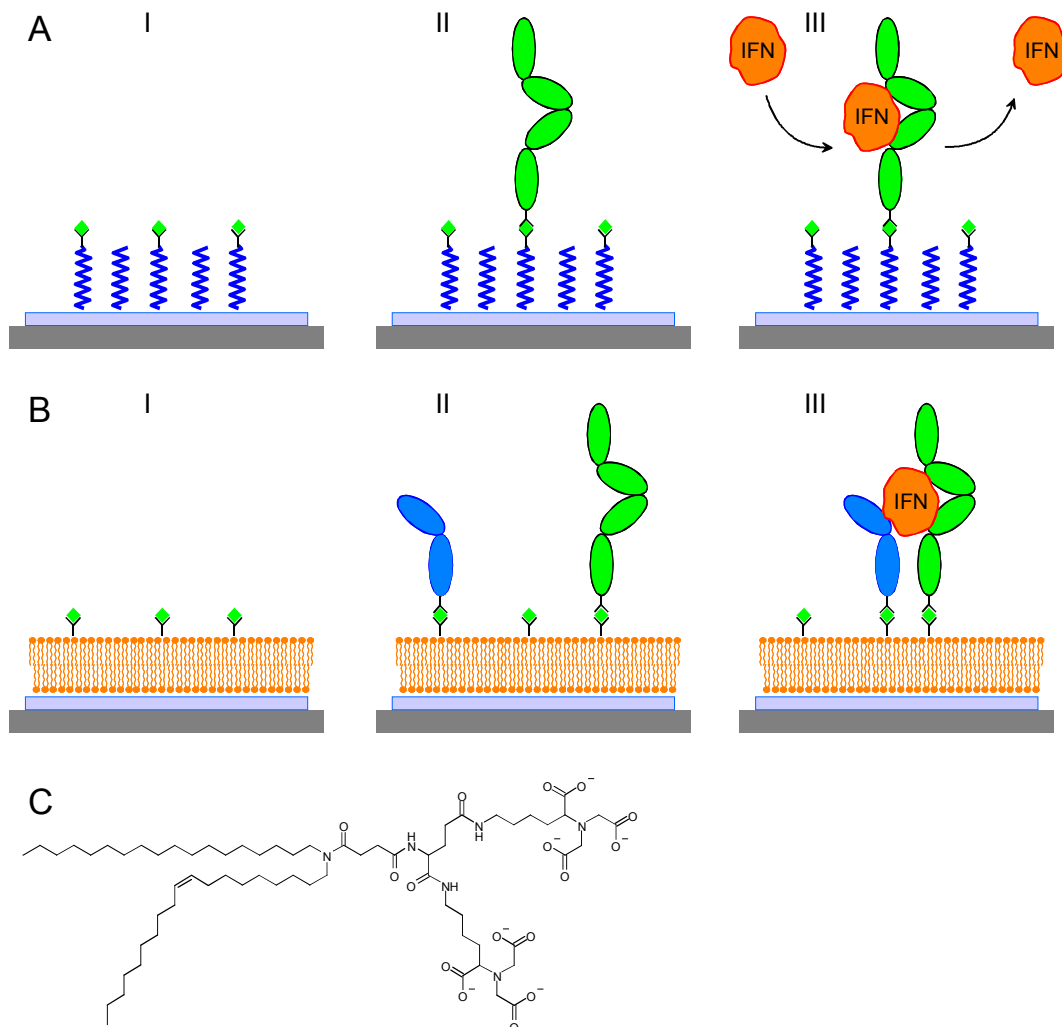
Figure 19   *Probing interactions between IFN and immobilized receptor subunits on different supports. In the first step NTA is loaded with Ni^{2+} (I), then the receptor is immobilized (II). Finally the IFN is injected (III). A: Individual interaction between ifnar1-EC and IFN on a covalently linked Ni^{2+}-NTA. B: Reconstitution of both extracellular domains on supported lipid bilayers mimicking lateral mobility in plane of the membrane. C: Structure of the bis-NTA chelator lipid.*

4 Materials

4.1 Chemicals

Name	Company
4-Chloro-1-naphthol	Sigma-Aldrich
5-Bromo-4-chloro-3-indoylphosphate	Sigma Chemical CO.
Acetic acid 99%	Riedel de Haen GmbH
Acryl amide 30% (w/v)	Carl Roth GmbH
Agar	GibcoBRL
Agarose	Sigma Chemical CO.
ATP	Roche Diagnostics GmbH
Avidin	Fluka Chemie GmbH
Bovine Serum Albumin (BSA)	Sigma Chemical CO.
Bromphenolblue	Merck KGaA
Coomassie Brilliant Blue	Sigma Chemical CO.
D-(+)-Saccharose	Carl Roth GmbH
Dimethylsulfoxide (DMSO)	Fluka Chemie GmbH
EDTA, Disodiumsalt	Carl Roth GmbH
Ethanol, abs.	Riedel de Haen GmbH
Ethidiumbromide	Merck KGaA
Glycerol	Carl Roth GmbH
Glycine	Carl Roth GmbH
HEPES	Sigma Chemical CO.
Imidazole	Sigma Chemical CO.
IPTG	PeqLab
Magnesiumchloride	Riedel de Haen GmbH
Methanol	Riedel de Haen GmbH
N,N-Dimethylformamid (DMF)	Fluka Chemie GmbH
Nitrotetrazoliumblue (NBT)	Sigma Chemical CO.
Polyethylenglycol	Sigma Chemical CO.
Hydrochloric acid, 37 %	Merck KGaA
Sodiumacetate	Sigma-Aldrich
Sodiumchloride	Riedel de Haen GmbH
Sodiumdodecylsulfate (SDS)	Carl Roth GmbH
Sodiumhydroxide	Riedel de Haen GmbH
Tris	Carl Roth GmbH
Triton X-100	Carl Roth GmbH
Tween 20	Sigma Chemical CO.

Urea	Carl Roth GmbH
Hydrogenperoxide 30%	Merck KGaA

4.2 Cells, Media and Transfection material

Name	Company
Ampicillin	Sigma Chemical CO.
Baculogold linearized baculoviral DNA	BD Bioscience Pharmingen
Fetal Calf Serum (FCS)	Biochrom AG
Penicillin/Streptolysin 100x	PAA laboratories GmbH
Peptone/tryptone from casein	Carl Roth GmbH
Pluronic F68, 10%	Invitrogen
SF900-II insect cell medium	Invitrogen
Tranfection Buffer A & B	BD Bioscience Pharmingen
Yeast extract	Carl Roth GmbH

4.3 Enzymes, plasmids and reaction buffers

Name	Company
1 kb DNA-Ladder	New Engand Biolabs
100 bp DNA-Ladder	New Engand Biolabs
Amp-Ligase	Perbio Scinece
Calf Intestine Alkaline Phosphatase (*CIAP*)	New Engand Biolabs
dNTP-Mix	peqlab laboratories
*Dpn*I	New Engand Biolabs
*Eco*RI	MBI Fermentas
*Endo*H	New Engand Biolabs
NEBuffer 1-4	New Engand Biolabs
NP-40	New Engand Biolabs
NTA-AP-Conjugate	Qiagen GmbH
Nucleobond Plasmid Purification Kit (Midi)	Macherey & Nagel
Nucleospin Plasmid Purification Kit (Mini)	Macherey & Nagel
P7-Buffer (for *PNGaseF*)	New Engand Biolabs
pAcGP67-B plasmid DNA	BD Bioscience Pharmingen
*PNGase*F	New Engand Biolabs

Materials

PNK-Buffer A	MBI Fermentas
Polynucleotide-kinase A (*PNK* A)	MBI Fermentas
*Pst*I	New Engand Biolabs
Pwo-Buffer (+/- MgSO4)	peqlab laboratories
Pwo-DNA-Polymerase	peqlab laboratories
Qiaex II Gel Extraction Kit	Qiagen GmbH
Qiaquick PCR Purification Kit	Qiagen GmbH
T4-DNA-Ligase	MBI Fermentas
T4-Polynucleotide-Kinase	MBI Fermentas
Tango Buffer +/- BSA	MBI Fermentas
Taq-buffer	peqlab laboratories
Taq-DNA-polymerase	peqlab laboratories
Water HPLC grade	Sigma Chemical CO.

4.4 Oligonucleotides for cloning

Name	Sequence	Cloning construct
*Bam*H1_R1-SD2_F	GGG CCC GGA TCC CCA TTT CGC AAA GCT CAG ATT GGT	pAcGP67-B-SD234-H10
*Bam*H1-His 10-B	GAT CGG TGA TGG TGG TGA TGA TGG TGA TGG TGA TGG	N-terminal His10 insertion
*Bam*H1-His 10-F	GAT CCC ATC ACC ATC ACC ATC ATC ACC ACC ATC ACC	N-terminal His10 insertion
His10 *Eco*RI F	AAT TCC ATC ATC ACC ATC ACC ATC ATC ATC ACC ATT	C-terminal His10 insertion
His10 *Eco*RI R	AAT TAA TGG TGA TGA TGA TGG TGA TGG TGA TGA TGG	C-terminal His10 insertion
His10_*Pst*I	GG GGG CTG CAG TTA ATG GTG ATG ATG ATG GTG ATG G	pAcGP67-B-ifnar1-EC-H10
IFNLR SD4 *Eco*R1 Z *Pst*I	CGC GCG CTG CAG TTA GAA TTC GTT GGC TTC TGG GAC CTC CAG	pAcGP67-B-SD123-LRD2
IL-10R2_EcoRI_R	GCG CGC GAA TTC TTT GAC CGT TTC GTC ATG GGT TGT	pAcGP67-B-SD123-IL10R2D2
pAcGP67-B_R1EC	CCC CCC GGA TCC AAA AAT CTA AAA CCT CAA AAA GTA GAG	pAcGP67-B-ifnar1-EC-H10
R1 *Eco*R1 Z PstI	CGC GCG CTG CAG TTA GAA TTC TTT AGA GGT ATT TCC TGG TTT	pAcGP67-B-ifnar1-EC-*Eco*RI
R1-I (PPPEN)Z_1	CCC CCC CTG CAG TCA ATT TTC TGG TGG AGG TAG TTC ATT	pAcGP67-B-H10-SD12
R1-II-F	CCC CCC AGG ATC CGA AAT GAA CTA CCT CCA CCA GAA	pAcGP67-B-SD34-H10
R1-SD3_BZ_PstI	CCC GGG CTG CAG TTA GTT AAA GAC TGG AGG AAG TAG GAA	pAcGP67-B-H10-SD123

SD123 *Eco*RI Z PstI	CGC GCG <u>CTG CAG</u> TTA <u>GAA TTC</u> GTT AAA GAC TGG AGG AAG TAG GAA	pAcGP67-B-SD123-H10	

4.5 Oligonucleotides for mutagenesis

Mutation	Primer sequence
Y70A	AAG CTG AAT GTT **GCT** GAA GAA ATT AAA
R76A	GAA ATT AAA TTG **GCT** ATA AGA GCA GAA
E111A	CAT TTA GAA GCT **GCA** GAT AAG GCA ATA
K113A	GAA GCT GAA GAT **GCG** GCA ATA GTG ATA
W129A	GAT AGT GTT ATG **GCG** GCT TTG GAT GGT
F136A	GAT GGT TTA AGC **GCT** ACA TAT AGC TTA
N155T	GAA AGG ATT GAA **ACT** ATT TAT TCC AGA
L247A	CCT GGA AAC CAT **GCG** TAT AAA TGG AAA
W250A	CAT TTG TAT AAA **GCG** AAA CAA ATA CCT
K251A	AAC CAT TTG TAT AAA TGG **GCA** CAA ATA CCT GAC TGT GAA
D298A	GAG ATA AAG TTT **GCT** ACT GAA ATA CAA
N368D	GTT ACA GTT CCT **GAT** TTG AAA CCA CTG

4.6 Chromatography equipment

Name	Company
Aekta Explorer	Amersham Pharmacia
Aekta Prime	Amersham Pharmacia
Amicon Ultra 0.5 and 15 (5kDa cut off)	Fisher Scientific
HisTrap 1ml	Amersham Pharmacia
HiTrap Chelating (1 ml and 5 ml)	Amersham Pharmacia
HiTrap Sepharose Q (1 ml)	Amersham Pharmacia
Sepharose Q	Amersham Pharmacia
SMART Chromtography System	Amersham Pharmacia
Superdex 200 HiLoad 16/60	Amersham Pharmacia
Superdex 200 Hiload 26/60	Amersham Pharmacia
Superdex 200 HR 10/30	Amersham Pharmacia
Superdex 200 PC 3.2/30	Amersham Pharmacia

4.7 Buffers and solutions for purification and binding assays

Buffer	Composition
IMAC dialysis buffer	50 mM Tris-HCl, pH 8
	200 mM NaCl
IMAC running buffer	50 mM Tris-HCl, pH 8
	500 mM NaCl
IMAC elution buffer	50 mM Tris-HCl, pH 8
	500 mM NaCl
	500 mM Imidazole
IMAC stripping buffer	1 M NaCl
	50 mM EDTA pH 8
IMAC metal loading solution	20 mM $ZnSO_4$
Size exclusion chromatography buffer	20 mM Tris-HCl, pH 8
	200 mM NaCl
RIfS running buffer	20 mM Hepes, pH 7.5
	150 mM NaCl
RIfS imidazole buffer	50 mM Tris-HCl, pH 7.5
	500 mM NaCl
	500 mM Imidazole
RIfS metal loading buffer	20 mM Hepes, pH 7.5
	150 mM NaCl
	15 mM $NiSO_4$
RIfS stripping buffer (HBS)	200mM EDTA pH 8

5 Methods

5.1 Molecular Biology

5.1.1 Overview

For expression of ifnar1-EC and several sub-fragments in *Sf*9 insect cells, genes of interest were cloned into the transfer vector pAcGP67-B via the restriction sites *BamH*I and *Pst*I. The gene of mature ifnar1-EC (amino acids from KNL until TSK) with and without a C-terminal decahistidine-tag was amplified via PCR from an ifnar containing vector (provided from Gilles Uzé, CNRS Montpellier), subsequently digested and cloned into the transfer vector. The same was done to get SD34-H10 and SD234-H10. An additional N-terminal extension ADLGS is expected from the cleavage site of the gp67 secretion sequence in the vector.

SD1234-DT was generated by inserting a linker coding for an H10-tag at the N-terminus of SD1234-H10 into the *Bam*HI site (Figure 20), resulting in a total N-terminal extension of ADLGSH$_{10}$RS. This linker was designed so that only the N-terminal *Bam*HI site was retained. The sub-fragments H10-SD12 and H10-SD123 and also H10-SD1234 were subcloned based on this SD1234-DT construct.

5.1.2 Polymerase Chain Reaction

The Polymerase Chain Reaction (PCR) was used for amplifying certain gene sequences for cloning or further analysis. To provide Ifnar1-EC and different sub- fragments the following PCR-mix was prepared:

Forward-primer (100 pM)	1 µl
Reverse-Primer (100 pM)	1 µl
Template	1-5 ng
dNTPs (10 mM)	2 µl
10x PCR-Buffer (-MgSO$_4$)	5 µl
MgSO$_4$ (25 mM)	8 µl
DNA-polymerase (1 U/µl)	3 µl
Adjusted with HPLC-H$_2$O to 50 µl	

To prepare PCR products for cloning a high fidelity polymerase like *Pwo polymerase* was used. In case of analytical PCR *Taq polymerase* was used. Depending on the expected length of PCR products elongation time varies in the following program:

1. Initial Denaturation	95 °C, 2 min
2. Denaturation	95 °C, 1 min
3. Annealing	55 °C, 1 min
4. Elongation	72 °C, 2 min/kb for *Pwo*, 1 min/kb for *Taq*
5. Final Elongation	72 °C, 10 min

Step 2, 3 and 4 were repeated 25-30 times. 5 µl of the PCR were analyzed by agarose gel electrophoresis. If the expected band appeared on the gel the DNA was purified by PCR purification kit (Qiagen AG) and stored at -20 °C until restriction. To verify proper gene insertion into a cloning vector, bacteria colonies could be used as templates for PCR. After bacteria were suspended with a glass tip into the PCR mix (containing *Taq polymerase*) the reaction was started (35 cycles).

5.1.3 DNA preparation

Plasmid DNA for sequencing was isolated by Nucleospin mini kit (Macherey & Nagel GmbH & Co. KG, Germany). *DNAse* contaminations were observed in these preparations, so mini plasmid DNA was not used for restriction analysis or co-transfection with virus DNA. Midi-DNA prepared by Nucleobond midi kit (Macherey & Nagel) was used for restriction analysis and for co-transfection with Baculogold-DNA. DNA concentration and purity were determined by absorbance at 260 nm and 260/280 nm absorbance ratio (ideal ratio: 1.8).

5.1.4 Restriction of DNA

For all cloning procedures DNA, either plasmids or inserts from PCR, were digested with restriction endonucleases. In general the amount of restriction enzyme and incubation time were adapted to gain a 10-20-fold over digestion. Buffers for single or double digestions correspond to the recommendations of the manufacturer (New England Biolabs Inc. and MBI Fermentas). Additionally restricted vector DNA was dephosphorylated for the final 30 min by adding *calf intestine alkaline phopatase* (*CIAP*). After checking restriction by agarose gel electrophoresis, the DNA was purified by using the PCR purification kit (Qiagen AG).

5.1.5 Ligation

Restricted insert and vector DNA were quantified by agarose gel electrophoresis to apply a molar ratio of 3-5:1 (insert : vector). After mixing DNA 2 µl, reaction-buffer and 1 µl T4-*Ligase* were added. Subsequently the reaction mix was adjusted with HPLC-H_2O to 20 µl volume and incubated for 2-4 h at room temperature.

5.1.6 Transformation

150µl of competent *E. coli* TG-1 cells were thawed on ice and mixed with 10µl of ligation reaction mix. After incubation on ice for at least 30 min cells were plated on pre-warmed agar plates supplemented with 100 µg/ml ampicillin.

5.1.7 Site Directed Mutagenesis

For generating mutants ligase chain reaction (LCR) technique was used. In contrast to PCR only one primer carrying the chosen point mutation annealed to the template

(pAcGP67-B-ifnar1-H10). The high fidelity DNA-polymerase *Pwo* synthesized the whole complementary strand which is subsequently ligated by a thermo stable ligase (*Amp-ligase*). Thus one single stranded, circularized DNA strand was produced per cycle, which is not an exponential amplification like in PCR. A problem of this method was the size of the template (11 kb) making long elongation times and sometimes the addition of *Taq polymerase* necessary.

Before LCR the primer was phosphorylated (section 5.1.8). 150-200 ng plasmid DNA was applied as template. In contrast to PCR elongation time of 20 min, elongation and ligation temperature of 65 °C and 25 cycles were used:

150-200ng	Template-DNA
4 µl	Primer (phosphorylated)
5µl	dNTP-Mix (2 mM)
2.5 µl	NAD$^+$ (10 mM)
5 µl	10 x Puffer (incomplete)
8 µl	MgSO$_4$ (25 mM)
3 µl	*Pwo polymerase* (1 U/µl)
2 µl	*Amp-Ligase* (5 U/µl)
ad 50µl	HPLC-H$_2$O

After purification by the PCR purification kit DNA was digested by *Dpn*I, which specifically cuts methylated DNA. While synthesized DNA was not affected by *Dpn*I, maternal template DNA was removed and only single stranded DNA carrying the chosen mutation should survive this procedure. After *Dpn*I treatment as described by the manufacturer *E. coli* TG-1 cells were transfected with the reaction mix. Colonies were chosen for DNA preparation followed by sequencing. 50-75% of the picked clones carried the mutation and were used for co-transfecting *Sf*9.

5.1.8 Oligonucleotide Insertion

To fuse defined sequences to the C- or the N-terminus of a protein, for example a histidine-tag, a double stranded oligonucleotide carrying the sequence was inserted into the cloning vector. The oligos were designed to fit into a restriction enzyme cutting site in frame of the gene (Figure 20B). By insertion the former cutting site was destroyed to enable cloning of the whole construct into other vectors (Figure 20C).

*Figure 20   Schematic of an N-terminal H10-oligoinsertion into a BamHI site. The vector
pAcGP67-B-ifnar1-EC is cut (A), annealed to the insert (B) and ligated (C).*

In this work either the *Bam*HI site for N-terminal His10-tag or *Eco*RI and *Pst*I sites for C-terminal His10-tag insertion were used. As a representative example the procedure of a His10-tag insertion into the *Bam*HI site is described:

Annealing of the oligonucleotides

*Bam*HI-His10-Forward (100 pM)	1 µl
*Bam*HI-His10-Backward (100 pM)	1 µl
PNK–Buffer A	10 µl
HPLC-H$_2$O	88 µl
1 min 95 °C, 10min 60 °C	

Insert phosphorylation

*Bam*HI-His10	20 µl
ATP (50 mM)	1 µl
PNK-buffer A	2 µl
PNK	1 µl
HPLC-H$_2$O	1 µl
2 h 37 °C, 20 min 80 °C	

Vector restriction and dephosphorylation

pAc-R1H10 (500 ng/µl)	10 µl
*Bam*HI-buffer	2 µl
*Bam*HI	2 µl
CIAP (for the last 30 min)	1 µl
4 h 37 °C, 20 min 80 °C, purification by PCR purification kit (Qiagen)	

Ligation

pAc-R1H10 restriction	1 µl
Insert (1:100)	0.5 µl
Ligase-buffer	2 µl
T4-Ligase	1 µl
HPLC-H$_2$O	15.5 µl
2-4 h at room temperature	

The ligation mixture was used for *E. coli* transformation as described in section 5.1.6. Proper insertion and orientation were checked by colony PCR using *Bam*HI-His10-Forward in combination with a standard backward sequencing primer (section 5.1.2). Positive clones were picked and mini DNA was sequenced.

5.1.9 Sequencing

All sequencing services were done by Scientific Research and Development GmbH. As sequencing primers pAc-SeqF, pAc-SeqR and sometimes mutation primers were used. Sequences were checked with BioEdit Sequence Alignment software.

5.2 Insect cell culture

5.2.1 Monolayer culture of Sf9 cells

Monolayer cultures of *Spodoptera frugiperda* (*Sf*9) insect cells were grown at 27 °C in SF900 II medium (10 U/ml penicillin, 0.1 mg/ml streptomycin, 0.2% pluronic acid and 5% fetal calf serum). Healthy cells generally doubled every 18-24 hours and were subcultured when a closed confluent layer occurred (3 times a week). For a passage medium and floating cells were replaced by fresh, pre-warmed medium. Cells with passage numbers >55 were discarded.

5.2.2 Shaking culture of Sf9 cells

For expression cultures up to a volume of 500 ml *Sf*9 cells were cultivated in shaker flasks at 27 °C. The cultures were incubated in less than 50% of the total flask volume and under defined shaking conditions (<200 ml at 110 rpm, >200 ml at 60 rpm). To get cells in the dynamic growth phase cell density was kept between 0.3×10^6 cells/ml and 3×10^6 cells/ml. Cells in the stationary phase (>5 $\times 10^6$ cells/ml) were discarded.

5.2.3 Co-transfection of Sf9 cells

The co-transfection procedure was carried out as described in the Baculogold manual (BD Bioscience Pharmingen). To safe expensive linearized viral DNA, a scale-down protocol was established for 1/5 of the original DNA amount:

> ➢ 0.2×10^6 *Sf*9 cells were seeded into a 12-well-culture plate (~30% confluence). The volume per well was at least >500µl to prevent cells from drying out. The procedure was continued until cell attachment.
> ➢ 1.25 µl (0.5 µl) linearized Baculogold-DNA and 0.5 µg plasmid (1-5 µl from Midi preparation) were mixed and incubated for 5 min.
> ➢ Medium was replaced by 250 µl transfection buffer A (BD Bioscience).

> ➢ 250 µl transfection buffer B (BD Bioscience) was mixed with the DNA.
> ➢ Buffer B was carefully added to cells drop by drop, after 2-3 drops the plate was slightly moved back and forth to facilitate efficient mixing. Under the microscope small crystals were observed after a few minutes.
> ➢ The culture plate was prevented from drying out by covering with parafilm and incubated for 4-5 hours at 27 °C.
> ➢ Cells were washed two times with 1 ml SF900 II medium.
> ➢ The recommended incubation time of 4-5 days was expanded to 8-9 days to increase virus titer. After this time 500µl of the supernatant (P0) containing viruses was added to a fresh 5 ml monolayer culture and incubated additional 7 days (P1). After 2-3 days signs of infection should be observed (proliferation stop, size increase and floating, Figure 21B).
> ➢ Cells were removed by centrifugation and the supernatant was stored in darkness at 4 °C or alternatively shock frozen at -80 °C. For preparation of P2 again 500 µl of P1 were added to a fresh 10 ml monolayer culture.
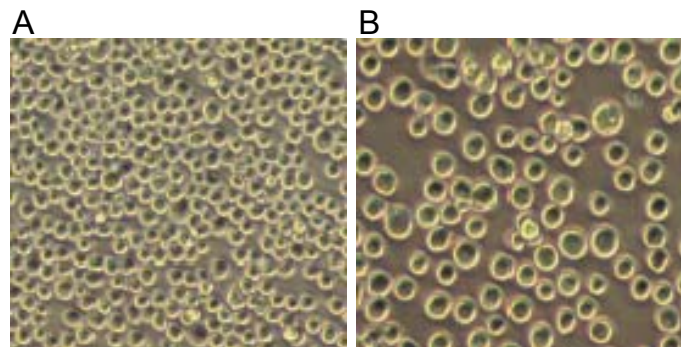

Figure 21   *Comparison of infected and uninfected Sf9-monolayers. A: Uninfected cells. B: Infected cells 3 days after infection with 1% P2.*

5.2.4 Infection cultures for protein production

For protein production cells were grown in SF900 II medium supplied with FCS at 27 °C. To avoid mechanical stress 1 liter Fernbach flasks were used at 60 rpm to cultivate 250-500 ml cells. When a cell density of $2-2.5 \times 10^6$ cells/ml was reached the culture was infected with 1 % virus amplification P2. After an incubation time of 3-4 days cells were harvested by centrifugation (5000 rpm, 5min) and the supernatant was shock-frozen in liquid nitrogen until protein purification.

5.3 Protein purification and characterization

5.3.1 Overview of proteins

In order to investigate interactions between extracellular domains of ifnar and ligands all proteins were purified to homogeneity and well characterized with respect to concentration and stability. IFNα2 and ifnar2-EC were expressed in *E. coli*, refolded from inclusion bodies and purified by anion exchange and size exclusion chromatography [86]. The IFNα2 mutant S136C was site-specifically labeled with Alexa Fluor 488 (AF-488) maleimide (Molecular Probes), and was further purified by desalting and a final step of anion exchange chromatography. Maltose binding protein (MBP) containing an N-terminal His10-tag was expressed in *E. coli* TG-1 transformed with the pMAL-c2x vector (New England Biolabs). Subsequently it was purified from cytoplasm via IMAC and SEC as described below. The purification of ifnar1-EC and all corresponding sub-fragments and mutants are described in more detail in the following chapters.

5.3.2 Immobilized metal chelate affinity chromatography (IMAC)

*Sf*9 supernatant contained several molecules acting as chelators which were able to remove metal ions from the IMAC-columns. After adjusting the supernatant to dialysis conditions (20 mM Tris/HCl, pH 8.0, 200 mM NaCl), it was dialyzed twice for at least 3 h and once over night against 4 L dialysis buffer. After removal of cell fragments and precipitates by centrifugation (15000 rpm, 15 min) the solution was ready for IMAC procedure.

Before every run, an IDA-column (5 ml HiTrap Chelating, Amersham Pharmacia) was conditioned with 25 ml stripping buffer (50 mM EDTA, pH 8.0, 1 M NaCl), 25 ml water, 50 ml ZnSO$_4$ (20 mM) and 25 ml running buffer (50 mM Tris, pH 8.0, 500 mM NaCl). The resin was loaded with a flow rate of 5 ml/min and 20 mM imidazole to prevent unspecific binding. After loading the column was washed again with 40 mM imidazole until the baseline was stable. The protein was then eluted by an imidazole gradient (length: 20 ml, target: 500 mM imidazole, fraction size: 2 ml). Protein-containing samples were identified by SDS-PAGE, pooled and stored at 4 °C until size exclusion chromatography.

5.3.3 Size exclusion chromatography (SEC)

To remove aggregates and imidazole and also to adjust protein samples to defined buffer conditions (20 mM Tris/HCl, pH 8.0, 200 mM NaCl) size exclusion chromatography (SEC) was used. Since deca-histidine-tags were observes to carry metals from IMAC, samples were adjusted to 1mM EDTA and centrifuged (5 min, 13000 rpm, RT) before injection. Depending on sample volume different columns were used (Table 2). In analytical SEC samples were centrifuged after thawing and subsequently injected.

Table 2   Columns for size exclusion chromatography

Column name	Flow rate max.	Pressure max.	Sample volume	Exclusion volume	Bed volume
Superdex 200 PC 3.2/30	100 µl/min	1.5 MPa	50 µl	~ 0.8 ml	~ 2.4 ml
Superdex 200 HR 10/30	500 µl/min	1.5 MPa	500 µl	~ 7.5 ml	~ 21 ml
Superdex 200 HiLoad 16/60	1.5 ml/min	0.5 MPa	4.0 ml	~ 50 ml	~ 122 ml
Superdex 200 Hiload 26/60	4 ml/min	0.5 MPa	10.0 ml	~ 110 ml	~ 320 ml

5.3.4 Protein concentration

After size exclusion chromatography protein fractions were pooled and concentrated by ultrafiltration (equilibrated Amicon ultra 15) at 3000 rpm until volume reduction to <3 ml. Membranes were washed after usage with sterile water and stored at 4 °C for several months.

5.3.5 Protein concentration determination

Protein concentrations were determined by UV/Vis-spectroscopy. Taking the theoretical extinction coefficients (e.g. 84.000 $M^{-1}cm^{-1}$ for ifnar1-EC determined with ProtParam Software from expasy.ch) into account, the concentration was calculated. As a representative example a UV/Vis-spectrum of ifnar1-H10 is shown (Figure 22), also containing the expected "tryptophane shoulder" at 290 nm. Proteins were then aliquoted and shock-frozen at 10-60 µM concentration in liquid nitrogen.
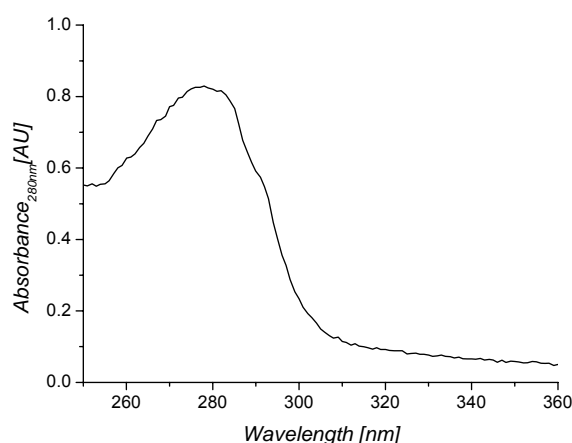

Figure 22   UV/Vis-Spectrum of a 10 µM ifnar1-EC sample in TBS buffer after SEC and spin concentration.

5.3.6 Deglycosylation

Proteins expressed and secreted from *Sf*9 insect cells were expected to be N-glycosylated. Ifnar1-EC carries 9 potential N-glycosylation sites. To analyze protein glycosylation the deglycosylation enzymes *Endo*H and *PNGase*F were used.

Analytical deglycosylation was done under denaturing conditions. Samples with 20 µM concentrations were incubated at 100 °C and 1% SDS / 100 mM DTT for 10 min to unfold and reduce the protein. After cooling and addition of NP40 (for SDS inhibition) enzymes were added to deglycosylate the samples as described in the manufacturer's manual. Deglycosylation efficiency was then investigated by SDS-PAGE.

Preparative deglycosylation using *PNGase*F (New England Biolabs) was carried out directly in protein sample buffer according to the instructions of the manufacturer (8h at room temperature). These samples were used for analytical size exclusion chromatography and binding assays to verify activity of deglycosylated protein.

5.3.7 Western-Blot

To detect His-tagged proteins Western-Blot analysis was performed as described below by using an NTA conjugate of *alkaline phosphatase*.

- ➤ Blotting the SDS-PAGE for 60-90 min at 100 mA to a nitrocellulose membrane
- ➤ Washing 3x5 min with PBS
- ➤ Blocking accessible binding sites for 1 h with 3% BSA in PBST
- ➤ Washing 3x10 min with PBST
- ➤ 1 h incubation with Ni-NTA-AP-conjugate (1:1000 in TBST)
- ➤ Washing 3x10 min with TBST
- ➤ Washing 10min with AP-buffer
- ➤ Developing with 10 µl NBT and 60 µl BCIP in 20 ml AP-buffer until blue color appeared
- ➤ Reaction was stopped by addition of water

5.3.8 CD-Spectroscopy

For CD spectroscopy, proteins at 20-40 µM concentration were extensively dialyzed against 20 mM Pi pH 8.0, 150 mM sodium fluoride. Circular dichroism spectra were recorded on a Jasco J-810 CD spectrometer equipped with a Jasco PTC-423S Peltier temperature control system using quartz cuvettes with 0.2 mm path lengths at 22 °C. Secondary structure composition was calculated using the estimation software Jasco Spectra Manager Version 1.53.00.

5.4 Protein interactions on surfaces

5.4.1 Detection system

Lipid bilayer assembling, receptor immobilization protein interactions and surface conditioning were monitored by Rif(S). This label-free detection technique monitors binding on the surface of a thin silica interference layer [96, 97], and therefore was compatible with fluorescence detection. In this study two different set-ups were applied. In one set-up the shift of the interference maximum was used as read out. In the other set-up light intensity at a certain wave length was correlated with mass deposition.

Binding curves were obtained from the shift of the interference spectrum of the silica layer: a shift of 1 nm corresponds to approximately 1 ng protein per mm² on the surface. Measurements were carried out in a flow chamber with an acquisition rate of 1 Hz under continuous flow-through conditions as described [96, 97]. Binding of fluorescence-labeled proteins was monitored by TIRFS using a home-built setup [94]. A 25 mW argon ion laser was used for fluorescence excitation at 488 nm. Typically a low excitation power of 2-3 mW focused onto an area of 1-2 mm² was used in order to minimize photo bleaching. Fluorescence was collected by an optical fiber and detected by a photomultiplier tube through a band pass filter. The same transducer slides as for RIfS detection were used as substrates, and all processes on the surface were monitored simultaneously by single-wavelength RIfS detection at 800 nm. Continuous flow-through conditions were maintained for all experiments. Data were acquired with a time resolution between 1.5 s and 16 s depending on the kinetics of the process. Photobleaching was minimized by closing the shutter of the excitation source between the measurements.

5.4.2 Vesicle preparation and bilayer fusion

Before vesicle preparation Hamilton syringes were washed extensively with methanol and chloroform. SOPC in chloroform was mixed with 1–5 mol% of a bis-NTA chelator lipid. After removing the solvent by vacuum evaporation (20 min) and resuspension into HBS buffer (15 min), small unilaminar vesicles (SUV) were prepared by sonication (15 min on ice). The transducer surface was incubated for at least 15 min in freshly prepared mixture of one part 30% (v/v) hydrogen peroxide and two parts concentrated sulfuric acid. After extensive washing with water, the transducer was mounted immediately into the flow cell. SUVs at a concentration of 250 µM were injected and bilayer formation was followed by RIfS-detection (Figure 23). Vesicle fusion should appear rapidly with a signal intensity of 5 nm. For every measurement the bilayer was conditioned by sequential 50 sec injections of 500 mM imidazole pH 8.0, 200 mM EDTA pH 8.0, and 15 mM $NiSO_4$ (in HBS), 270 µl each (Figure 23B). Bilayers could be used for one day of measurements or until an air bubble occurred.
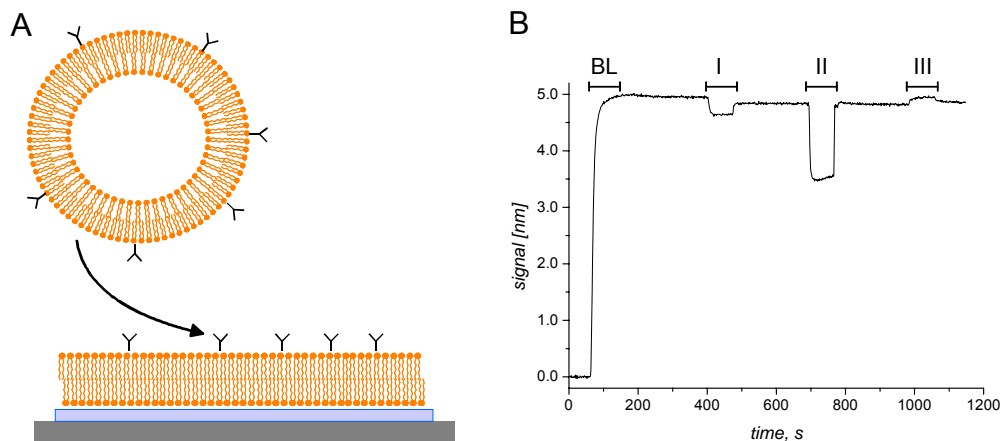
Figure 23   A: Cartoon of vesicle fusion to a glass surface. B: Detection of bilayer assembly (BL) and the injections of imidazole (I), EDTA (II) and Ni^{2+} (III) as detected by RIfS.

5.4.3 Protein interaction experiments

For probing individual interactions proteins were immobilized via their H10-tag to a PEG polymer brush carrying bis- or tris-NTA head groups (non-fluid support). To investigate ternary complex assembly, receptors were co-immobilized on a lipid bilayer to achieve lateral mobility of the individual proteins in plane of the membrane (fluid support). Protein immobilization and ligand binding was always monitored by RIfS, additionally fluorescence labeled samples were also simultaneously detected by TIRFS. Depending on the targeted surface concentration (signal intensities 0.2-2 nm), receptors at concentrations between 50 nM and 300 nM were injected for 470 sec. In order to check proper attachment of the receptors after every injection the surface was washed for 100-200 s with a flow rate of 1 ml/min. Depending on the ligand and the goal of the experiment different injection (50 or 220 s) and washing times were used. For studying IFNβ, which is known to bind metal ions, excess of coordination sites was blocked by injection of 3-5 µM MBP-H10 before binding experiments. After every binding experiment either lipid or covalent surfaces were conditioned as described above (section 5.4.2).

6 Results

6.1 Protein Biochemistry

6.1.1 Purification of ifnar1-EC and sub-fragments

Ifnar1-EC and all sub-fragments and mutants were expressed in *Sf*9 cells with an N-terminal secretion sequence of the baculovirus protein gp67. It was expected that the target protein was secreted via the secretory pathway into the medium. This secretion process was required for disulfide-bond formation and probable glycosylation. Both features were necessary to enable proper folding and protein stability. Proteins were extracted from the medium by using their C- or N-terminal decahistidine-tag for immobilized metal affinity purification (IMAC). As a representative example for all constructs the purification of ifnar1-EC with a C-terminal H10-tag by using a Zn^{2+}-IDA resin is shown in Figure 24. Ifnar1-EC eluted at ~180 mM imidazole (Figure 24A) and SDS-PAGE analysis demonstrated the successful extraction as well as the efficient purification to homogeneity (Figure 24B).
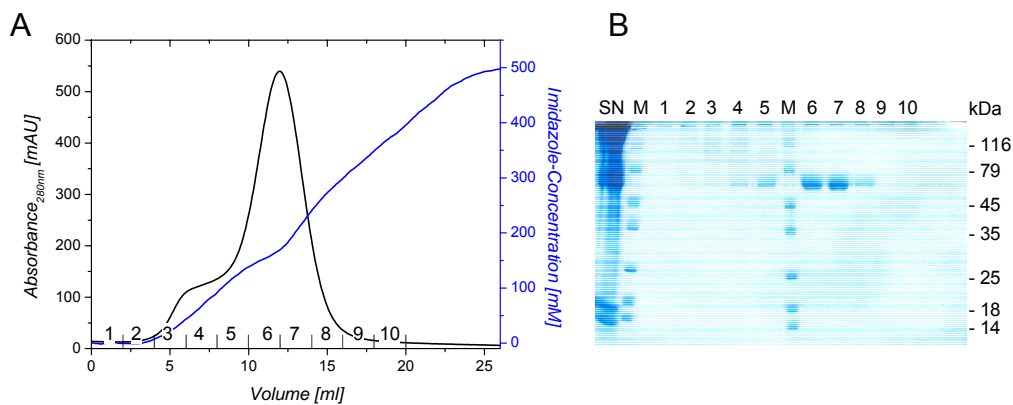
Figure 24　　*IMAC of Sf9 supernatant containing ifnar1-EC. A: Chromatogram of the imidazole gradient. B: SDS-PAGE of collected elution fractions (1-10) and applied supernatant (SN).*

In the next step, aggregates as well as imidazole were removed by size exclusion chromatography. Ifnar1-EC eluted in a symmetric peak at a retention volume expected for the monomer (Figure 25A). In SDS-PAGE, a molecular mass of approximately 57 kDa was observed (Figure 25B), indicating glycosylation of ifnar1-EC in the insect cells. From analytical SEC it was concluded that ifnar1-EC was monomeric by taking the retention volume of ifnar2-EC and IFNα2 into account (Figure 26). In order to identify ifnar1-EC as the purified protein, a Western-Blot detecting the H10-tag was carried out. All fractions of a monomer peak determined from SDS-PAGE led to a corresponding band in Western-Blot (Figure 25C). Also Western-Blot analysis with anti-ifnar1 antibodies confirmed the identity of the purified protein.
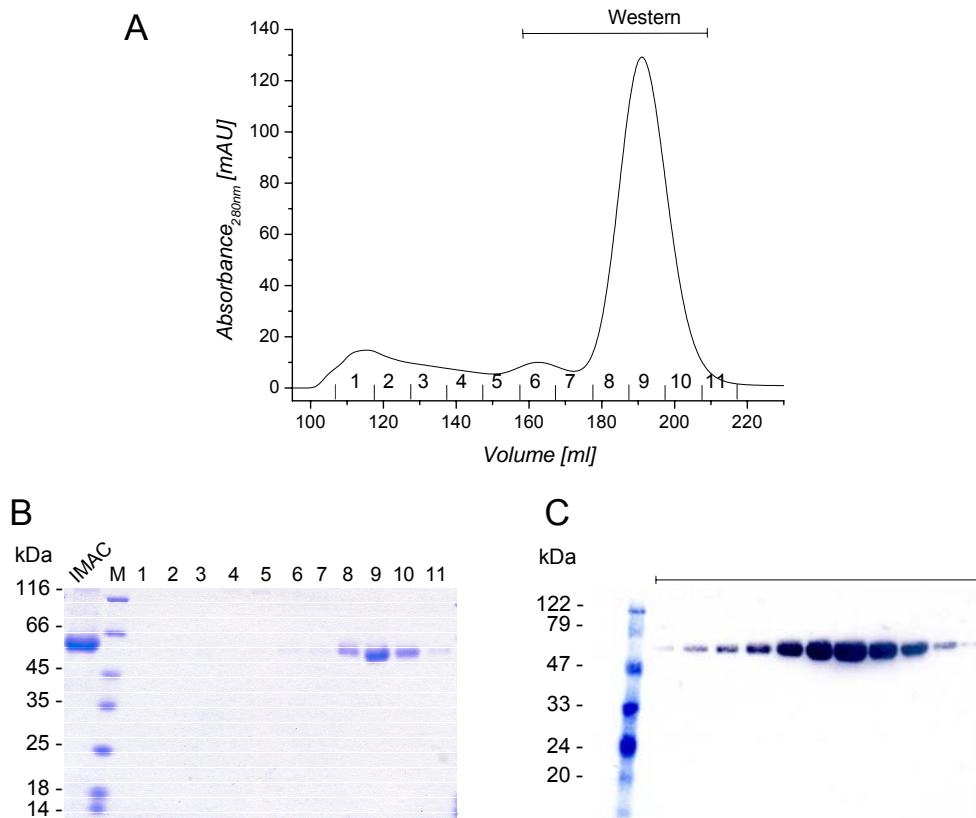
Figure 25   Size exclusion chromatography (Superdex 200 HR 26/60) of ifnar1-EC from IMAC: Chromatogram (A) and corresponding SDS-PAGE (B); 1-11, fractions; M, Marker; IMAC, loaded sample. C: Western-Blot of an ifnar1-EC monomer peak from SEC for His-tag detection with Ni-NTA-AP conjugate.

The purified ifnar1-EC was shock-frozen in liquid nitrogen and stored at -80 °C. After two cycles of freezing and thawing < 5 % aggregation was observed in analytical SEC (Figure 26). Thus a very efficient purification strategy for ifnar1-EC purification, ending up with a purity of > 95% and a yield of stable, monomeric protein of ~ 10 mg/l, was established.
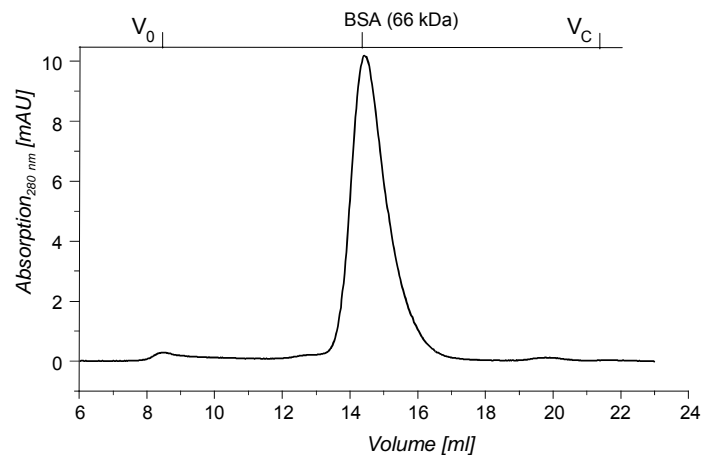
Figure 26   Analytical SEC (Superdex 200, 10/30) with ifnar1-EC after two cycles of freezing and thawing. V_0: Exclusion volume; V_c: Bed volume.

This strategy was successfully applied to the purification of all sub-fragments and mutants (Figure 27). The sub-fragments as well as the double tagged ifnar1-EC (SD1234-DT) were purified equally to the wild-type protein in yields of 5-10 mg/l cell culture. Since all sub-fragments were glycosylated, monomeric in gel filtration and stable, they were used for further biochemical characterization and binding experiments.
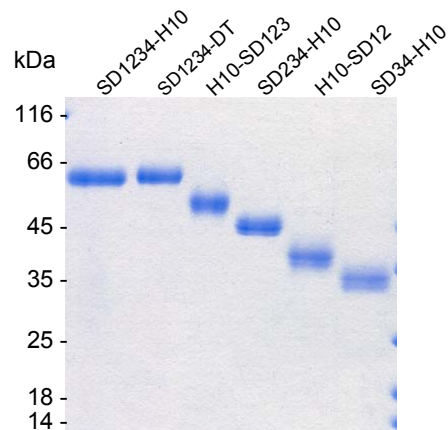

Figure 27   *SDS-PAGE of the purified sub-fragments after IMAC and size exclusion chromatography under reducing conditions. In agreement with the sub-fragment definition ifnar1-EC is named SD1234-H10.*

The replacement of SD4 by homologous receptor domains was more critical (Figure 28). SD123-IL10R2D2 was > 90 % aggregated as demonstrated by SEC (Figure 28B) and not used for any further experiments. Fusing this domain to SD123 seemed to prevent proper folding. Interestingly SD123-IL10V1V2, which differs from SD123-IL10R2D2 by two short ifnar1-EC sequences (3.5.2), was purified in amounts equal to wild-type protein (Figure 28B, C). SD123-LRD2 was purified as a dimer, probably caused by a third cysteine on LRD2 (Figure 28B, C). However, this construct was stable and active and therefore used for binding experiments.
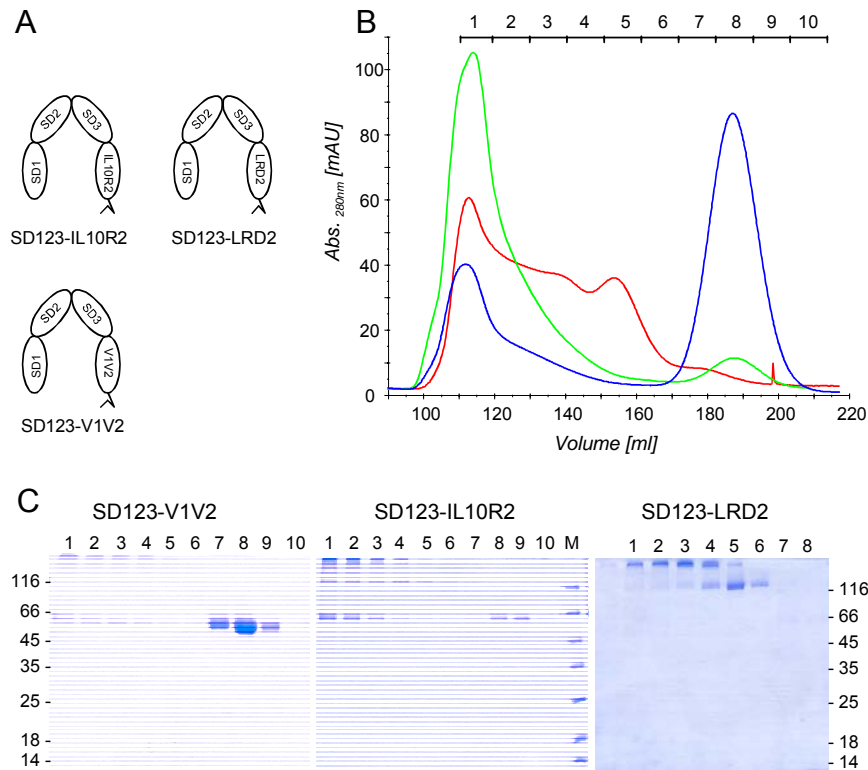
Figure 28   *A: Cartoon of the ifnar1-EC constructs with SD4 substituted with homologous receptor domains of IL10 (IL10R2D2 and V1V2) and IFNλR (LRD2). B: SEC of SD123-IL10V1V2 (blue), SD123-IL10R2D2 (green) and SD123-LRD2 (red). C: Corresponding SDS-PAGEs under oxidizing conditions (Fractions: 1-10, M: Marker).*

6.1.2 Protein deglycosylation

For purified ifnar1-EC a single, yet broadened band corresponding to a molecular mass of approximately 57 kDa was observed in SDS-PAGE in contrast to a calculated mass of 49 kDa. This difference suggested substantial glycosylation of the protein. In order to identify the type of glycosylation, the deglycosylation enzymes E*ndo*H and *PNGase*F were used. While *Endo*H cleaves specifically hybrid and high mannose structures (Figure 29A), *PNGase*F cleaves all glycosylation types including the complex type (Figure 29B). For *Endo*H no degycosylation of ifnar1-EC was observed, but removal of the glycans with *PNGase*F yielded a protein with an apparent molecular mass of 49 kDa corresponding to the expected molecular mass (Figure 29D, E).

In an additional SDS-PAGE analysis the formation of disulfide bonds was investigated. Under non-reducing conditions the band of deglycosylated ifnar1 was shifted to a lower molecular mass compared to the reduced protein, indicating internal disulfide bonds formation (Figure 29E) leading to a faster migration in SDS-PAGE. All these results led to the conclusion, that ifnar1-EC was oxidized, site specifically glycosylated and secreted into the medium via the secretory pathway of *Sf*9.

For the sub-fragments similar shifts as well as band broadening and even multiple bands were observed (Figure 29C). Significant shifts between SD123 and SD234 as well as

SD12 and 34 were observed, suggesting different grades of glycosylation as predicted in Table 3. For all proteins the apparent molecular mass shifted to the expected mass after *PNGase*F treatment (Table 3) confirming a complete expression of the sub-fragments. Interestingly also the small difference of 12 amino acids between the single and the double-tagged ifnar1-EC could be detected by SDS-PAGE.
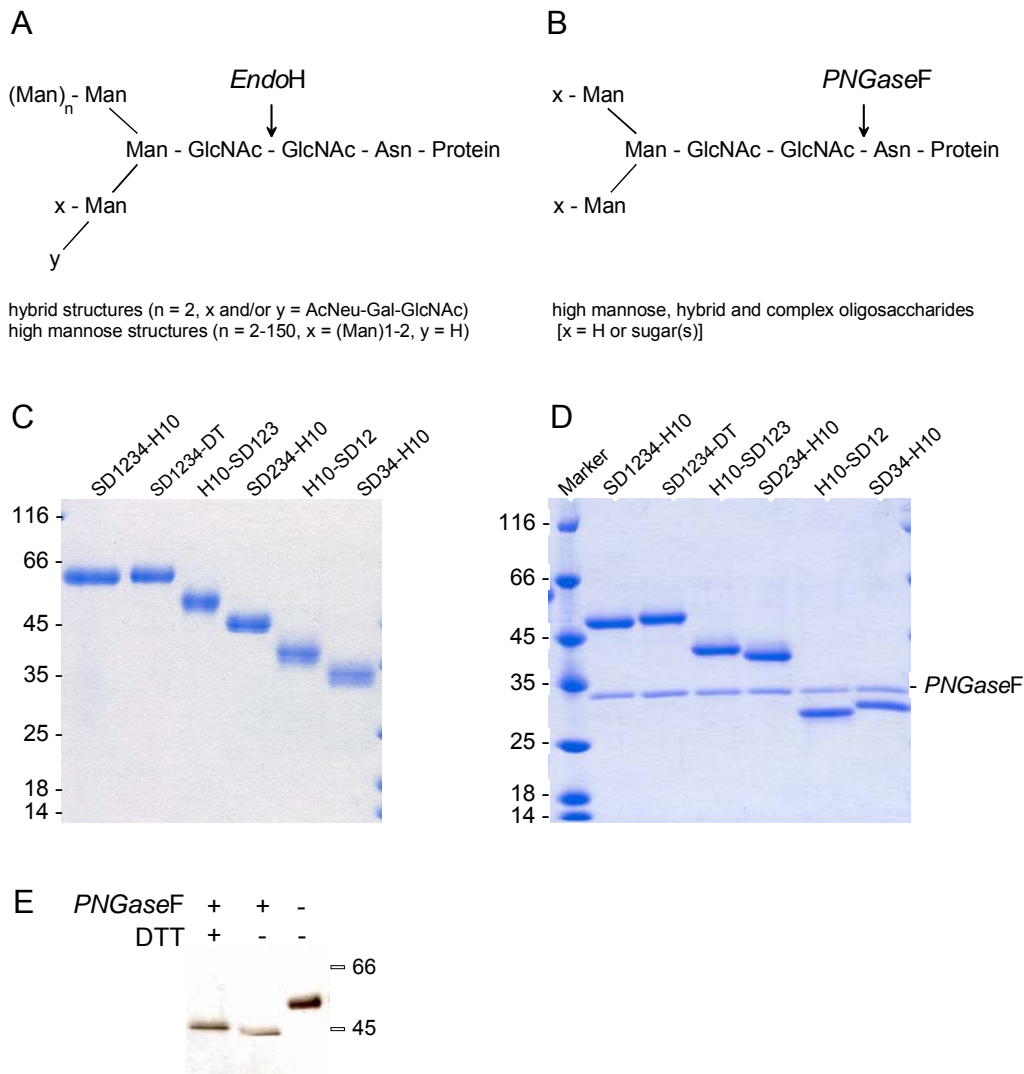

Figure 29   *A, B: Schematic of EndoH (A) and PNGaseF (B) cleavage sites. C, D: SDS-PAGE of the purified sub-fragments after IMAC and size exclusion chromatography without (C) and with PNGaseF treatment (D) under reducing conditions. E: SDS-PAGE of purified ifnar1-EC after deglycosylation with PNGaseF under non-reducing and reducing conditions in comparison to the non-deglycosylated protein.*

6.1.3 Further biochemical characterization

Ifnar1-EC and sub-fragments were investigated by analytical SEC with and without deglycosylation. The rather broad, asymmetric peaks observed for the glycosylated proteins (Figure 30A) became more sharp and symmetric, and slightly shifted towards higher elution volumes after deglycosylation (Figure 30B). While no significant difference between ifnar1-EC (SD1234-H10) and SD1234-DT was detectable, H10-SD123 was eluted with

substantially higher apparent molecular size than SD234-H10, despite the very similar apparent molecular mass observed in SDS-PAGE. This difference suggests a different spatial and possibly non-symmetrical arrangement of the Ig-like domains in these two proteins. Also between H10-SD12 and SD34-H10, a small, but reproducible and significant shift was observed, indicating a different structural organization of these to potential CBMs.
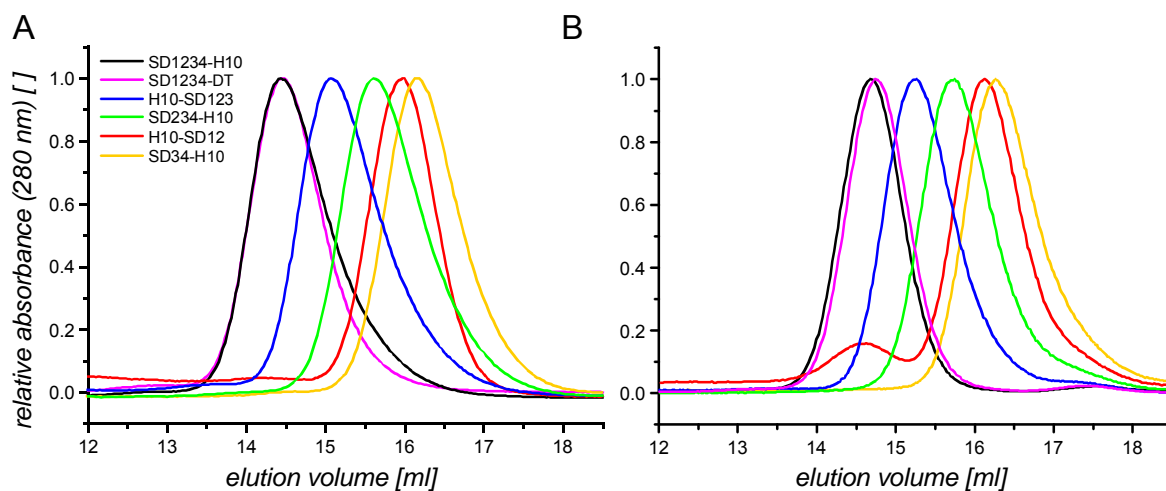

Figure 30   Analytical SEC of the purified sub-fragments before (A) and after deglycosylation with PNGaseF (B). Color coding as shown in the inset.

In order to confirm proper folding the secondary structure was investigated by CD-spectroscopy (Figure 31). The anticipated secondary structure of mainly β-sheet (Table 3) was confirmed for all sub-fragments by CD spectroscopy corroborating appropriate folding of the protein.
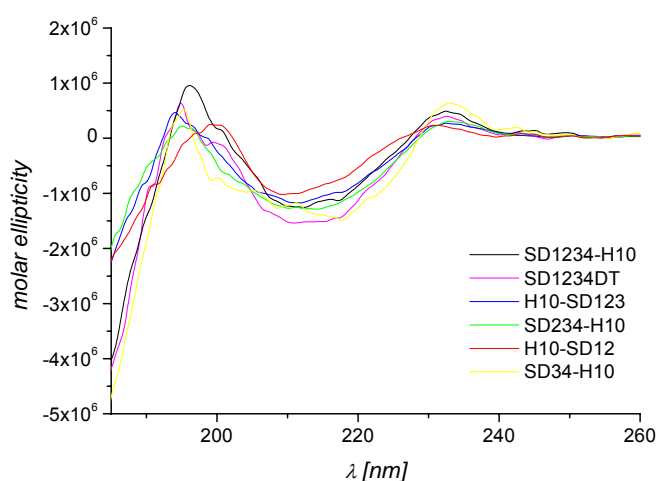

Figure 31   CD-spectrum of ifnar1-EC and sub-fragments for secondary structure analysis (color coding in the inset).

In Table 3 all results of the biochemical analysis for ifnar1-EC and its sub-fragments are summarized. For all the following binding experiments glycosylated proteins were used.

Table 3   *Biochemical properties of ifnar1-EC sub-fragments.*

Name	ifnar1-H10	ifnar1-DT	SD12	SD34	SD123	SD234
Sequence[1]	K1-K409	K1-K409	K1-N207	E199-K409	K1-N311	P95-K409
H10-tag[2]	C	C, N	N	C	C, N	C
Total no. of aa[3]	424	436	224	226	326	325
MM (expected) [98]	49.0	50.6	25.8	26.2	37.9	37.4
MM[4] (found) [kDa]	57.3	-	31.1	29.4	45.3	42.2
MM[5] (deglyc.) [kDa]	49	50	29	30	40	39
pot. glycos. Sites[6]	9	9	5	4	7	5
β-sheet/α-helix/RC[7]	84/2/14	78/2/20	70/4/26	77/01/22	76/3/21	75/2/23

[1]*First and last amino acid accord to the predicted mature sequence.* [2]*Position of the decahistidine tag(s).* [3]*Number of amino acids including additional residues derived from cloning strategy and tag-insertion.* [4,5]*The molecular masses were estimated from MALDI (for glycosylated proteins) and from SDS-PAGE (for deglycosylated proteins).* [6]*The potential glycosylation sites were predicted by NetNGlyc 1.0 Server.* [7]*The secondary structures were determined by CD-spectroscopy.*

6.2 Dissection of interferon receptor assembling

6.2.1 Stoichiometry of the IFN receptor complex in solution

The formation of a stable complex with a 1:1:1 stiochiometry for recombinant ifnar1-EC, ifnar2-EC and IFNβ was shown in analytical SEC [63]. Only in presence of ifnar2-EC this interaction was detectable. Thus a cooperative effect of ifnar2-EC was proposed. In order to investigate stoichiometry, affinity and possible cooperative effects in solution, the interactions between ifnar1-EC, ifnar2-EC and IFNα2/β were also analyzed by SEC. For IFNα2 either in complex with ifnar2-EC or alone no detectable interaction with ifnar1-EC could be detected up to µM concentrations (data not shown). This result indicated low affinity (K_D ~ µM range) for the IFNα2/ifnar1-EC interaction, which prevents stable complex formation. In contrast to IFNα2, IFNβ was expected to have a higher affinity towards ifnar1-EC. IFNβ samples (formulated Rebif®, 5-10 µg/ml) were supplied with additives (> 10 mg/ml HSA) stabilizing IFNβ for clinical applications, which made the detection at a wavelength of 280 nm very difficult. For monitoring specifically the receptor subunits, ifnar1-H10 and ifnar2-H10 were labeled through a tris-NTA-fluorescein conjugate. This conjugate stoichiometrically and stably interacts with a his-tag and enables detection at 490 nm (fluorescein absorbance). In parallel an IFNα2 mutant (IFNα2-HEQ) was used. On IFNα2-HEQ H57, E58 and Q61 were replaced by alanines leading to a 40-fold increased affinity towards ifnar1 comparable with that of IFNβ (personal communication with Gideon Schreiber).

For IFNα2-HEQ as well as for IFNβ a stable binary complex with ifnar1-EC was detected (Figure 32A) and identified by SDS-PAGE (Figure 32B), which also confirmed the activity of the proteins. Interestingly only a minute shift of ifnar1-EC signal in SEC was observed for both IFNs. Thus IFN binding to ifnar1-EC did not seem to enhance the hydrodynamic radius significantly. Probably ligand binding compensated the increase of molecular weight by a structural arrangement of the sub-domain structure. However, a stable binary complex for ifnar1-EC with IFNβ as well as IFNα2-HEQ was clearly demonstrated. This result contradicted to the observation, that ifnar1-EC only interacted with IFNβ in the presence of ifnar2-EC [63]. Probably the minute shift between ifnar1-EC and the binary complex was not detected.

Separately, isolated IFNα2-HEQ (~ 20 kDa) and ifnar2-EC (~ 25 kDa) eluted at the expected retention volume (Figure 32C). Ifnar2-EC together with IFNα2-HEQ shifted to a higher molecular weight, which agreed with a binary complex formation (~ 45 kDa). Interestingly, ifnar1-EC showed a significant shift compared to this binary complex. The different molecular weights (57 kDa for ifnar1-EC, 45 kDa for ifnar2-EC-IFNα2) could not explain these different retention volumes. A probably more stretched structural arrangement

of the four sub-domains of ifnar1-EC in contrast to a more compact arrangement in the ifnar2-EC/IFNα2-HEQ complex was indicated. The retention volume of the ternary complex of IFNα2-HEQ/ifnar1-EC/ifnar2-EC was in agreement with the molecular weight expected for a 1:1:1 complex (~100 kDa, Figure 32). All three proteins in the complex were identified by SDS-PAGE (Figure 32D). In order to prepare quantitative amounts of the ternary complex, it was necessary to concentrate the mixture of ifnar1-EC/ifnar2-EC/IFNα2-HEQ (up to 100 µM). As a consequence aggregation was observed as a "shoulder" (Figure 32C). At this concentration aggregation was also observed separately for ifnar1-EC and ifnar2-EC (data not shown). Thus, this observation did not indicate a stoichiometry higher than 1:1:1.
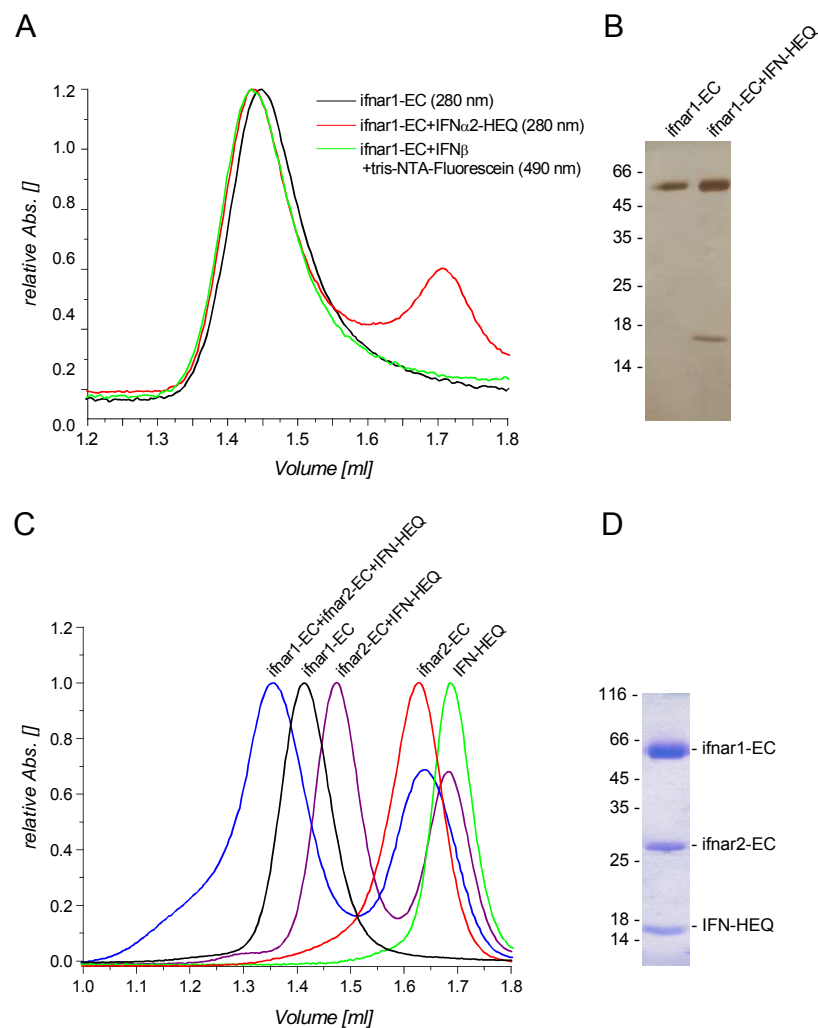

Figure 32   *Analytical SECs of complexes and individual proteins on a Superdex 200 3.2. A: Binary complex of IFNα2-HEQ, IFNβ and ifnar1-EC. The complex with IFNβ was detected at 490 nm via an NTA-fluorescein conjugate binding to the his-tag. B: SDS-PAGE of the binary complex of ifnar1-EC/IFNα2-HEQ C: Ternary complex and individual proteins. D: SDS-PAGE of the ternary complex collected at 1.3 ml retention volume.*

6.2.2 Interaction of ifnar2-EC with IFNα2 and IFNβ on solid support

From analytical SEC different affinities for IFNα2 and IFNβ towards ifnar1-EC were qualitatively proposed. Also the proposed cooperative effect of ifnar2-EC on the ifnar1-EC/IFN interaction [63] has not been confirmed. Thus, in order to quantitatively investigate differences between individual IFNs with respect to stoichiometry, affinity and cooperativity, an *in vitro* binding assay is required.

Binding of IFNα2 to immobilized tag-less ifnar2-EC without a his-tag (ifnar2-tl, i.e. tag-less) has been studied before on different surfaces [93]. Here all receptor proteins were immobilized via their C-terminal deca-histidine-tags in a site-specific and oriented manner to the surface. To exclude any influence of this immobilization mode on the activity, individual interactions of immobilized ifnar2-EC with IFNα2 and IFNβ were probed on a PEG polymer brush carrying a multivalent chelator head group (Figure 33A). IFNα2 interacted specifically with ifnar2-EC (Figure 33B) and the stoichiometry as determined from the relative binding amplitudes was 1:1. Thus, stable and oriented tethering through a decahistidine-tag retained the protein fully functional on the surface. From concentration dependent binding curves, a k_d value of 0.010 ± 0.002 s^{-1}, a k_a value of $(3 \pm 1) \cdot 10^6$ M^{-1}s^{-1} and a K_D value of 3 ± 1 nM were determined. These values are in excellent agreement with the values obtained for ifnar2-tl immobilized via monoclonal antibodies [93]. The association phase was significantly biased by mass transport limitation as indicated by the systematic deviation from the model (Figure 33D). Also the dissociation phase deviated significantly from a single exponential decay indicating rebinding (Figure 33D), in agreement to what has been reported before [93]. The interaction of IFNβ with immobilized ifnar2-EC had been investigated only at increased ionic strength in order to overcome its otherwise strong non-specific binding to the surface [76]. At the PEG polymer brush surface used in this study, no significant non-specific binding of IFNβ was detectable at physiological ionic strength after fully blocking the chelator head groups with MBP-H10 (Figure 33B). Under these conditions, IFNβ bound substantially tighter to ifnar2-EC compared to IFNα2 (Figure 33B), while from the relative signals, a 1:1 stoichiometry between ifnar2-EC and IFNβ was confirmed. The dissociation was very slow with an estimated k_d value of 0.0005 s^{-1}. From the I47A mutant of ifnar2-EC, IFNβ dissociated with a rate constant of 0.005 ± 0.002 s^{-1} (Figure 33C). From this value, the k_d value of approximately 0.0005 s^{-1} was confirmed for the wild-type complex, assuming the same 10-fold difference as observed at high ionic strength [76]. Thus, the half-life of the complex with ifnar2-EC is probably about 20-fold higher for IFNβ compared to IFNα2. The observed association was strongly mass transport limited (Figure 33E) indicating that the association rate constant k_a is well above $5 \cdot 10^6$ M^{-1}s^{-1}. The high k_a can be explained by electrostatic rate

enhancement, as IFNβ is positively charged and ifnar2-EC is strongly negatively charged at physiological pH.

The strong dependence of the complex stability on the ionic strength suggests that electrostatic forces also stabilize the interaction of IFNβ with ifnar2-EC. This effect, however, could also be due to rebinding on the surface, which is dependent on the k_a, and thus also on the ionic strength. Therefore the contribution of rebinding by injecting ifnar2-tl at high concentration (10 µM) during the dissociation phase was investigated (Figure 33F, G). In both cases, a significantly faster dissociation was observed resulting in corrected dissociation rate constants of $0.012 \pm 0.003 \text{ s}^{-1}$ for IFNα2 and $\sim 0.001 \text{ s}^{-1}$ for IFNβ. No significant differences in binding parameters of ifnar2-EC attached via a C-terminal H10-tag compared to immobilization via antibodies were detected. Also rebinding effects were not demonstrated to influence binding parameters dramatically. Thus this immobilization mode could be applied for all following binding experiments.
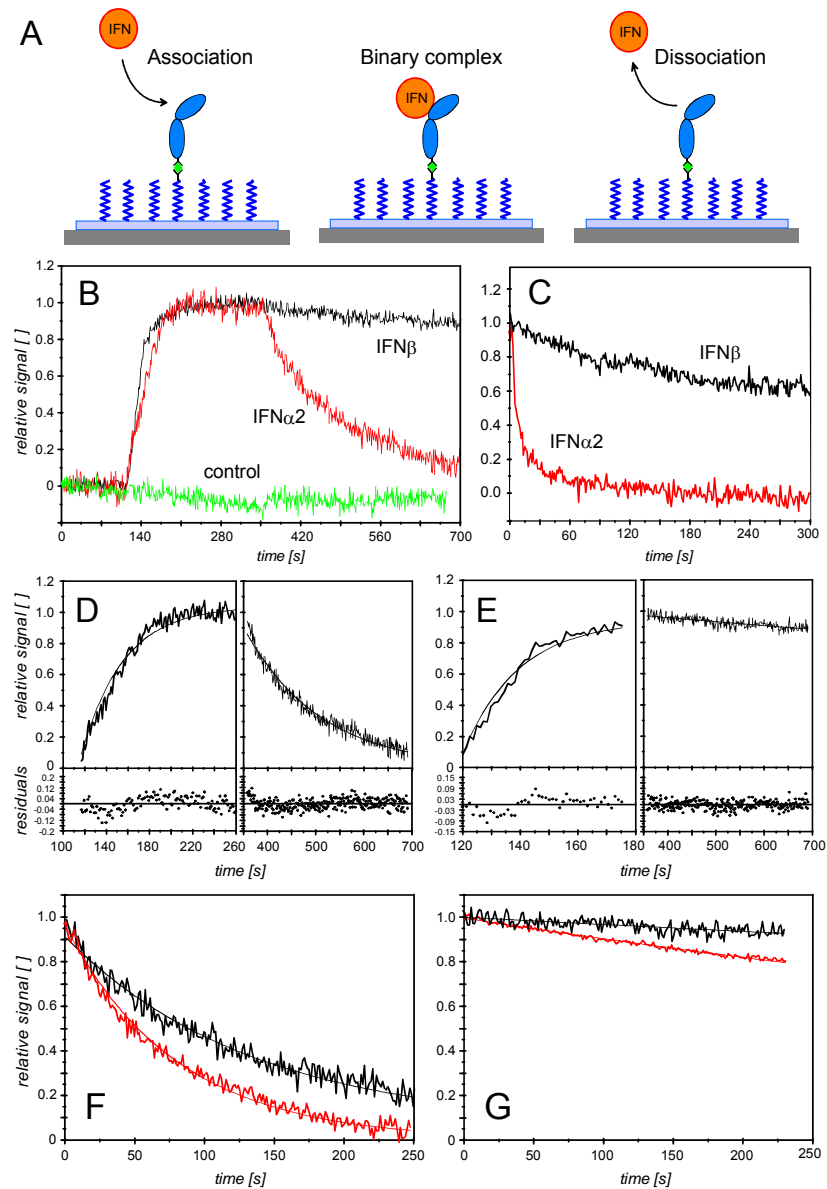
Figure 33 *Interaction of IFNα2 and IFNβ with ifnar2-EC tethered onto a PEG polymer brush. A: Cartoon of the binding experiment. B: Binding curve for 50 nM IFNα2 (red) and 50 nM IFNβ (black) to ifnar2-EC in comparison to 50 nM IFNβ exposed to immobilized MBP (green). C: Dissociation of IFNα2 and IFNβ from immobilized ifnar2-EC I47A. D: Fit and residuals for association and dissociation of IFNα2 shown in B. E: Fit and residuals for association and dissociation of IFNβ shown in B. F, G: Dissociation of IFNα2 (F) and IFNβ (G) from immobilized ifnar2-EC in absence (black) and in presence (red) of 10 µM ifnar2-tl.*

6.2.3 Interaction of IFNs with ifnar1-EC

In order to characterize the interaction with IFNα2 and IFNβ, ifnar1-EC was immobilized on a PEG polymer brush through its C-terminal his-tag (Figure 34A) and IFN in varying concentrations was injected. Binding of IFNα2 to immobilized ifnar1-EC was only detectable at concentrations above 300 nM and rapid dissociation was observed (Figure 34B). This interaction was entirely specific as confirmed by control experiments without ifnar1-EC on the surface (data not shown). From the equilibrium responses R_{eq} observed for IFNα2 at concentrations between 100 nM and 100 µM, titration curves were obtained. A K_D value of 5 ± 2 µM was determined by fitting a Langmuir isotherm (Figure 34C). Hence, the affinity of IFNα2 towards ifnar1-EC is about three orders of magnitude lower than for ifnar2-EC. The maximum binding signal R_{max} obtained from such titration corresponded to a 1:1 interaction between ifnar1-EC and IFNα2 assuming full activity of the immobilized ifnar1-EC. In addition IFNα2 S136C was characterized with respect to experiments with fluorescence labeled ligand. Here no differences to binding parameters determined for IFNα2 wild-type were observed (Table 4). The fast dissociation of IFNα2 ($k_d \sim 1$ s^{-1}) was resolved by TIRFS detection in a recent publication [94].

Before measuring the binding of IFNβ to ifnar1-EC excessive binding sites on the surface were blocked by MBP-H10 (not shown). The interaction of IFNβ with immobilized ifnar1-EC was much more stable compared to the binding of IFNα2 (Figure 34D). Association and dissociation phases were well fitted by mono-exponential models (Figure 34E). From the fitting, a k_a value of $(3 \pm 2) \cdot 10^5$ M^{-1}s^{-1} and a k_d value of 0.017 ± 0.004 s^{-1} were obtained. The binding signals corresponded to a 1:1 stoichiometry between IFNβ and ifnar1-EC.

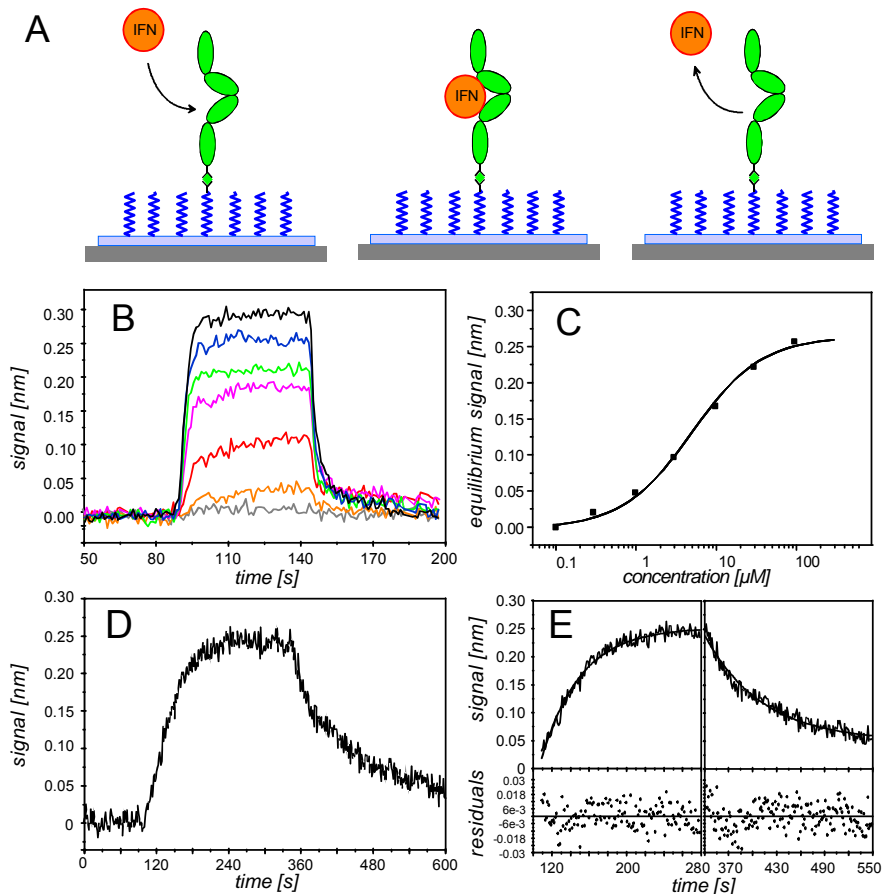*Figure 34*   *Binding of IFNs to immobilized ifnar1-EC on a PEG polymer brush. A: Cartoon of the single interaction binding experiment. B: Binding of IFNα2 in various concentrations (100 nM, 300 nM, 1 μM, 3μM, 10 μM, 30μM and 100 μM) to immobilized ifnar1-EC. C: Equilibrium response of IFNα2 binding to ifnar1-EC vs. concentration and the fitted Langmuir isotherm. D: Binding of 50 nM IFNβ to immobilized ifnar1-EC. E: Monoexponential fit to the association and dissociation shown in D.*

In order to identify a possible cooperative effect of ifnar2-EC, binding experiments with a stoichiometric complex of IFNα2 with ifnar2-tl were carried out (Figure 35A). This complex with a life-time of ~100 s can be assumed static during the time-scale of the interaction with ifnar1-EC. Binding curves for 0.1 and 10 μM IFNα2-ifnar2-tl-complex are shown in Figure 35B. The relative binding signals obtained from a full titration (data not shown) confirmed a 1:1 stoichiometric ratio between the IFNα2-ifnar2-tl complex and immobilized ifnar1-EC. A K_D value of 4 ± 2 μM was obtained, which was not significantly different from the K_D determined for IFNα2 alone. This result suggests the interaction between IFN and ifnar1-EC is not stabilized by cooperative interactions.

Similar to IFNα2, no significant differences in the binding rates were observed for ifnar2-tl-bound IFNβ compared to free IFNβ (Figure 35B, C). Also a 1:1 stoichiometric ratio was confirmed. For free as well as ifnar2-tl-bound IFNβ a K_D value of 50 ± 30 nM was obtained. The interaction of the IFNβ-ifnar2-tl complex with ifnar1-EC was also investigated

in solution by a binding inhibition assay (Figure 36). The K_D obtained from this experiment was 30 ± 10 nM, i.e. in good agreement with the K_D determined for the interaction at the surface.

In order to check if immobilized ifnar1-EC interacts with ifnar2-EC alone, several binding experiments were performed. Up to ifnar2-tl concentrations of 50 µM no binding signal could be observed, indicating a K_D > 100 µM. Since binding activity of both proteins was checked before, a direct interaction between the two extracellular domains of ifnar in the detectable concentration range could be excluded. These results underline the observation, that no cooperative effect for the IFN binding to ifnar1-EC could be detected after the pre-formation of an IFN-ifnar2-tl complex.
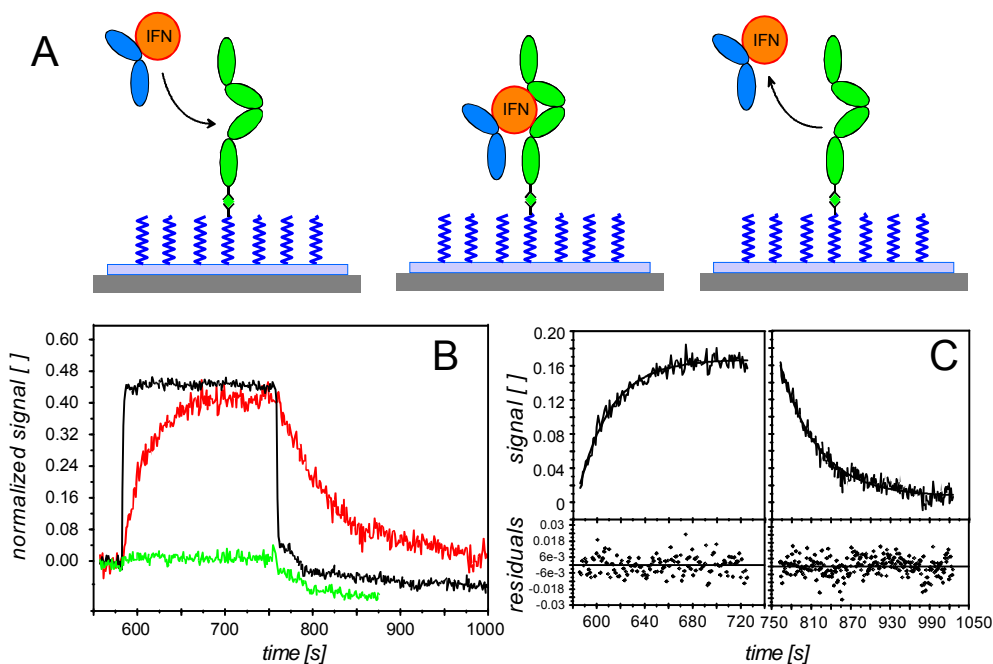

Figure 35   Interaction of immobilized ifnar1-EC with IFN-ifnar2-tl binary complex. A: Cartoon of the binding experiment. B: Binding of 100 nM IFNβ-ifnar2-tl (red), 100 nM IFNα2-ifnar2-tl (green) and 10 µM IFNα2-ifnar2-tl (black) to immobilized ifnar1-EC in comparison (normalized to the amount of ifnar1-EC on the surface). C: Fit of single exponential models to the association and dissociation phase for the interaction of 100 nM IFNβ-ifnar2-tl with ifnar1-EC as shown in E, and the residuals of the fit.

Thus, the affinity of ifnar1-EC to IFNβ is two orders of magnitude higher than for IFNα2. Intriguingly, the association rate constant of IFNβ binding to ifnar1-EC is at least an order of magnitude lower compared to the binding to ifnar2-EC. The individual affinities were not influenced by the interaction with soluble ifnar2-tl indicating non-cooperative binding.
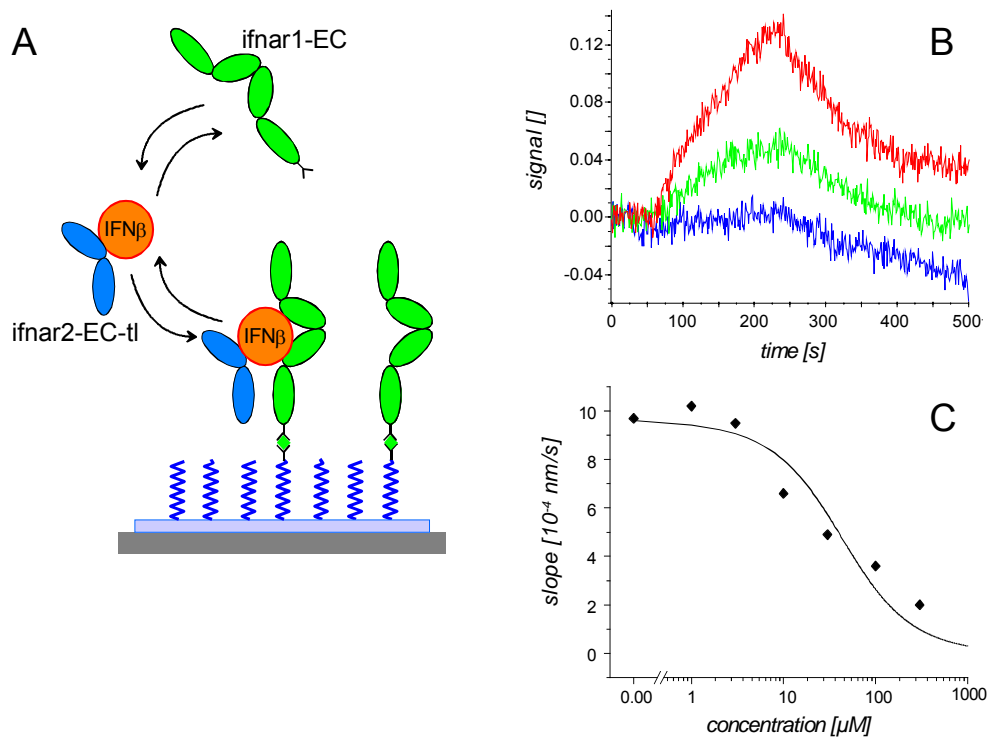
Figure 36   Binding inhibition assay with ifnar1-EC in solution. A: Binding of IFNβ-ifnar2-tl (20 nM) on immobilized ifnar1-EC with various ifnar1-EC concentrations in solution (300nM (red), 30nM (green), 0 nM (blue)). B: Initial slopes of the binding inhibition assay.

Table 4   Rate and equilibrium constants of the interaction with ifnar1-EC IFNs and different mutants. Mean values and standard deviations were determined from at least three independent experiments. IFNα2 S136C was labeled with OG-488 or AF-488 at the additional cysteine. k_a values were calculated from K_D and k_d.

	Ifnar1-EC		
IFN	k_a [$M^{-1}s^{-1}$]	k_d [s^{-1}]	K_D [nM]
IFNα2 wt	~ 2 ·10^5	~ 1	5000 ± 2000
IFNα2 S136C	~ 2 ·10^5	~ 1	~5000
IFNα2 / ifnar2-tl	~ 2.5 ·10^5	~ 1	4000 ± 2000
IFNα2 R149A	~ 2 ·10^5	~ 1	5000 ± 2000
IFNβ	(3 ± 2)·10^5	0.017 ± 0.004	50 ± 30
IFNβ / ifnar2-tl	(4 ± 2)·10^5	0.019 ± 0.004	50 ± 30

6.2.4 Interaction of ifnar1-EC sub-fragments with IFNα2 and IFNβ

In order to identify the ligand binding epitopes for IFNα2 and IFNβ several ifnar1-EC sub-fragments were prepared. These fragments were termed H10-SD12, SD34-H10, H10-SD123 and SD234-H10 (SD1234-H10 for ifnar1-EC). The influence of the N-terminal attachment (relevant for H10-SD12 and H10-SD123) on ligand binding was investigated with an N- and C-terminal attached construct termed SD1234-DT(Figure 37A). The reduced surface binding capacity observed for SD1234-DT compared to SD1234-H10, as well as imidazole-induced dissociation experiments (Figure 37B) confirmed that both histidine-tags were involved in tethering the protein to the surface. Interaction of IFNα2 and IFNβ with immobilized SD1234-DT is shown in Figure 37C, D. The K_D of the interaction with IFNα2 was determined from the equilibrium response, while the rate constants of the interaction with IFNβ were determined by fitting exponential functions to association and dissociation phase of the binding curves (Figure 38C, D). Furthermore, the k_d of the dissociation of IFNα2 (Figure 38B) from immobilized SD1234-DT was determined by TIRFS (k_d ~1 s^{-1}). IFNα2 S136C site-specifically labeled with the fluorescence dye Alexa Fluor 488 ($^{AF-488}$IFNα2) was used, which was shown to interact with ifnar2-EC and ifnar1-EC as wild-type IFNα2 (section 6.2.1 and [99]). All dissociation and rate constants obtained for IFNα2 and IFNβ were in agreement to the values observed for ifnar1-EC (SD1234-H10). Thus the additional N-terminal attachment of ifnar1-EC has no effect on ligand binding.

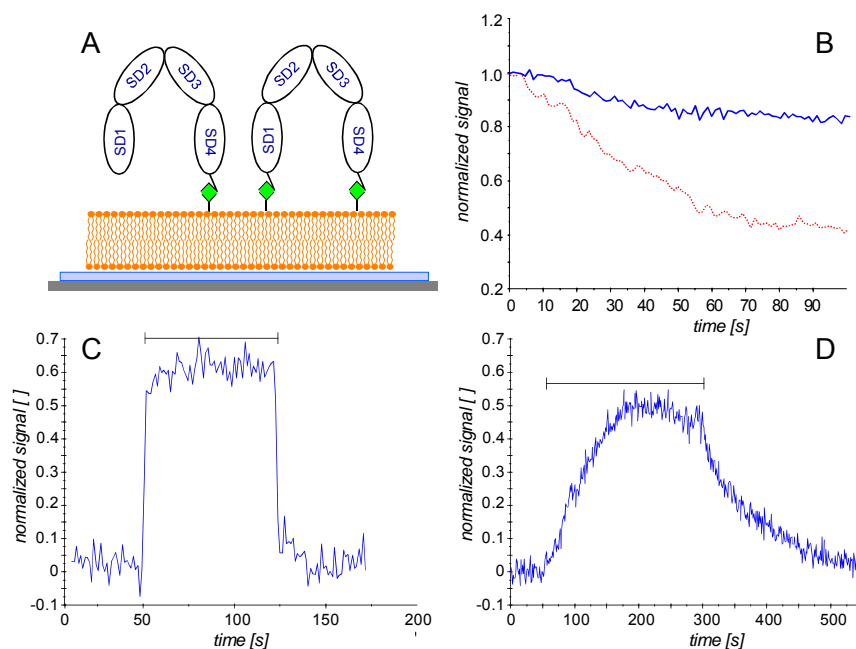*Figure 37*   *Ifnar1-EC immobilization with one C-terminal histidine-tag in comparison to the double-tagged construct SD1234-DT. A: Schematic of immobilization.   B: Dissociation of immobilized SD1234-H10 (red) and SD1234-DT (blue) by 20 mM imidazole. C, D: Binding of IFNα2 (C) and IFNβ (D) to SD1234-DT immobilized on a polymer brush surface as detected by RIfS (the bar marks the injection period).*
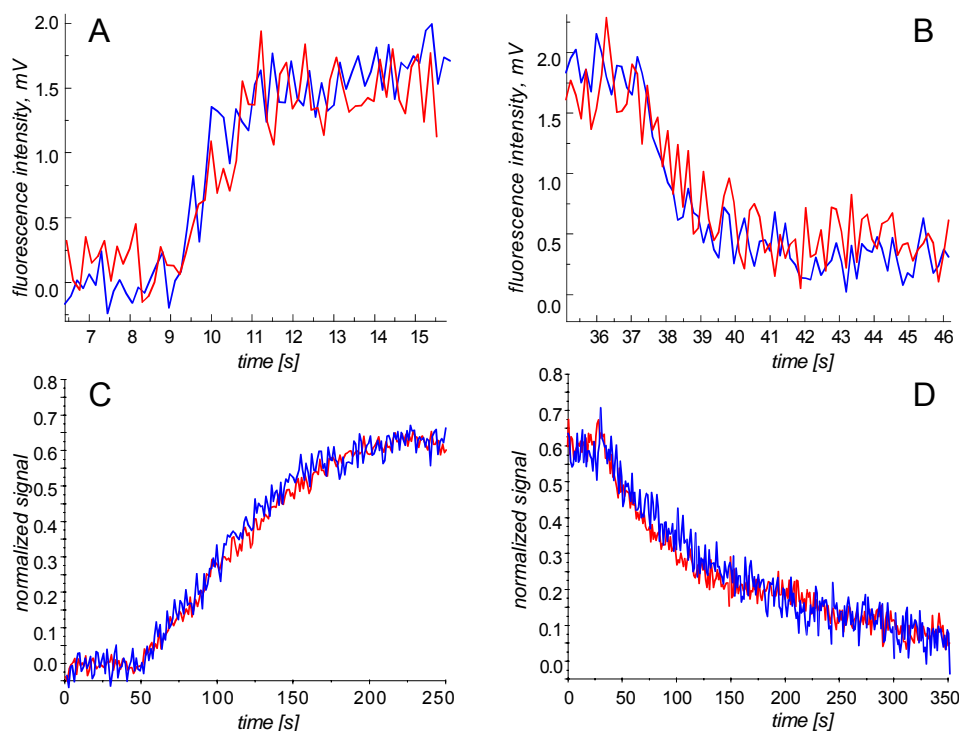
Figure 38   *Analysis of association and dissociation as shown in Figure 37 . A: Association of $^{AF-488}$IFNα2 (200 nM) to SD1234-DT (blue) as detected by TIRFS in comparison to the same experiment carried out with SD1234-H10 (red). B: Dissociation of $^{AF-488}$IFNα2 from SD1234-DT (blue) and SD1234-H10 (red). C: Association of IFNβ2 (100 nM) to SD1234-DT (blue) as detected by RIfS in comparison to the same experiment carried out with SD1234-H10 (red). D: Dissociation of IFNβ from SD1234-DT (blue) in comparison to SD1234-H10 (red).*

In the same manner, binding of IFNα2 and IFNβ was assessed for the sub-fragments. Up to concentrations of 10 µM IFNα2 and 200 nM IFNβ no specific binding was detectable for H10-SD12 and SD34-H10 as well as for SD234-H10 (Figure 39A-C). Thus, the K_D´s of these sub-fragments were >100 µM for IFNα2 and >2 µM for IFNβ. In contrast uncompromised binding of both IFNs was observed for H10-SD123 (Figure 39A-C). The interaction constants determined from these curves were very similar to the values observed for SD1234-H10 (Table 5).
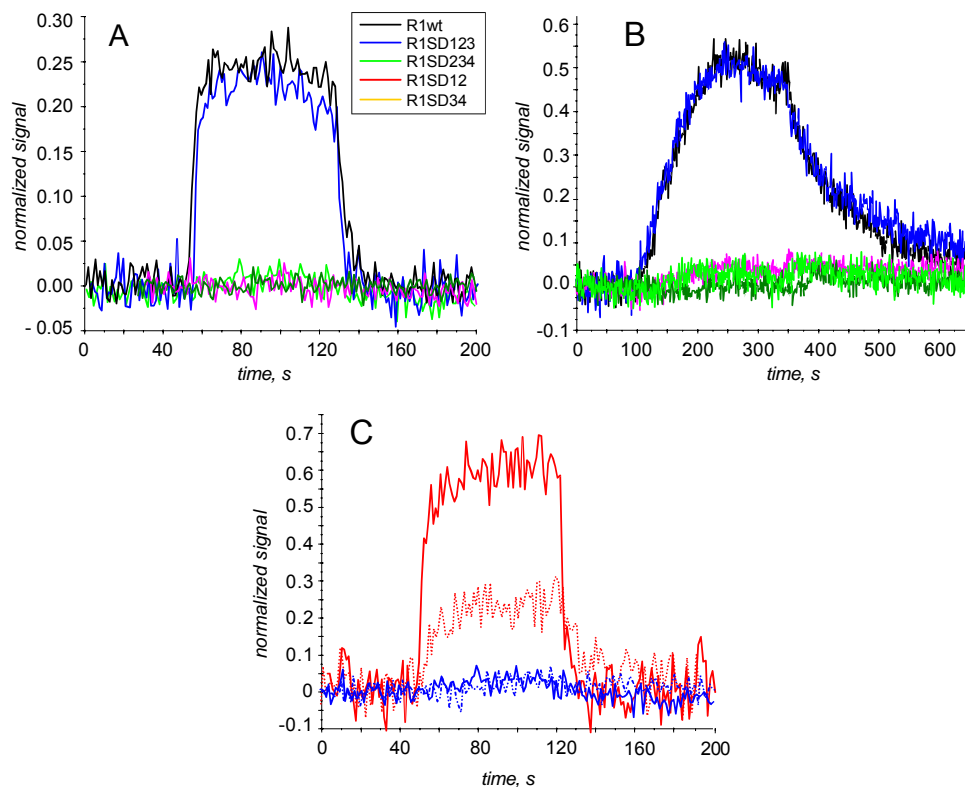
Figure 39   *Binding of IFNα2 and IFNβ to the different sub-fragments immobilized on the transducer surface. A: Response during injection of 1 µM IFNα2 to SD1234-H10, H10-SD123, H10-SD234 H10-SD12, SD34-H10 in comparison (color coding as shown in the inset). Signals were normalized to the molar surface concentration of the immobilized protein. B: Response during injection of 50 nM IFNβ onto SD1234-H10, H10-SD123, SD234-H10, H10-SD12, SD34-H10 in comparison (same color coding as in A). C: Response during injection of 1 µM (·······) and 10 µM (——) IFNα2 onto H10-SD123 (red) and SD234-H10 (blue) in comparison.*

In order to restore ligand binding activity, H10-SD12 and SD34-H10 were co-immobilized in stoichiometric amounts (Figure 40B) onto solid-supported, fluid lipid bilayers in order to allow simultaneous interaction with the ligand (Figure 40A). Still, neither for IFNα2 (Figure 40C) nor for IFNβ (Figure 40D) significant binding was detectable, indicating that the linkage between H10-SD12 and SD34-H10 is required for the formation of an intact binding site.
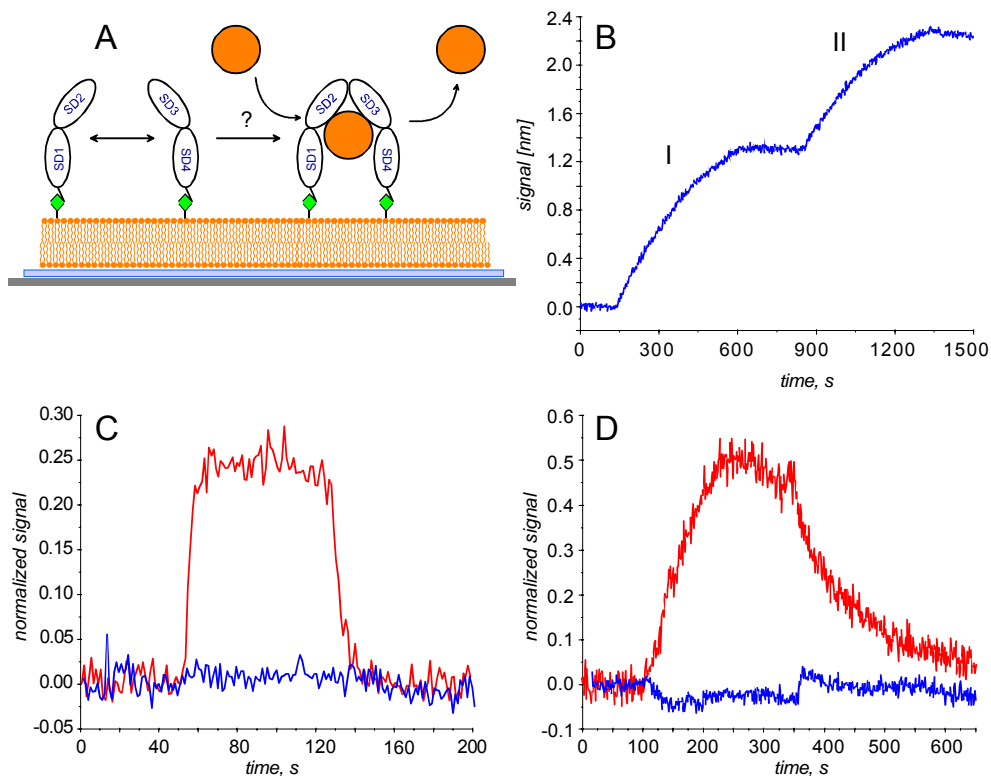
*Figure 40   Co-immobilization of H10-SD12 and SD34-H10 (II) on solid-supported lipid bilayers.
A: Cartoon of the experiment. B: Sequential tethering of H10-SD12 (I) and SD34-H10
(II) to the surface. C,D: Response during injection of 1 µM IFNα2 (C) and 50 nM
IFNβ (D) onto H10-SD12 and SD34-H10 co-immobilized on solid-supported lipid
bilayers in comparison to SD1234-H10.*

To confirm that loss of binding activity for H10-SD12, SD34-H10 and SD234-H10 was
not due to denaturation of the protein during immobilization on the surface, another assay to
assess binding was devised (Figure 41A). Ifnar2-EC was immobilized on the surface
followed by binding of IFNβ which binds quasi-irreversibly to ifnar2-EC (Figure 41B).
Subsequently, binding of SD1234-H10 and the sub-fragments to ifnar2-EC-bound IFNβ was
studied (Figure 41B). In Figure 41C binding of the sub-fragments is compared with that of
SD1234-H10. Again, specific binding was only detectable for the sub-fragment H10-SD123.
All these experiments confirmed that the N-terminal Ig-like domains 1, 2 and 3 on a single
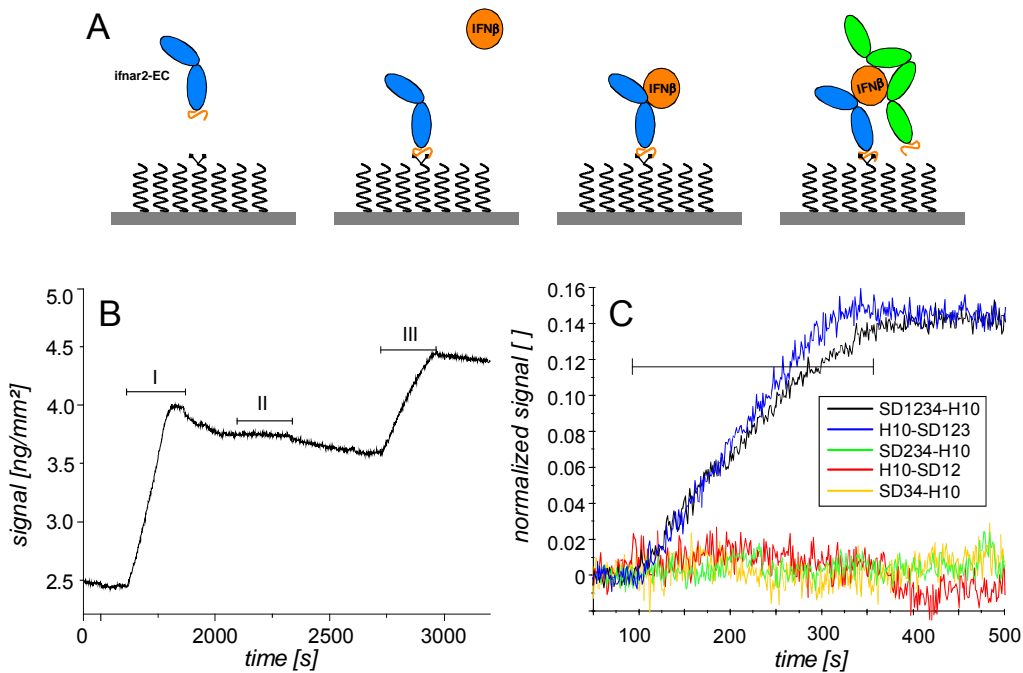polypeptide chain were required for the formation of an intact binding site for IFNα2 and
IFNβ.

Figure 41   *Binding of ifnar1-EC species to the complex of immobilized ifnar2-EC and IFNβ. A: Schematic of the sandwich assay: after immobilization of ifnar2-EC excess chelators are blocked with MBP-H10 (not shown); then, IFNβ binds irreversibly to ifnar2-EC, followed by exposure to the respective ifnar1-EC variant. B: Typical binding of IFNβ (I) to immobilized ifnar2-EC, followed by an injection of 50 nM H10-SD12 (II) and of 50 nM SD1234-H10 (III). C: Binding curves for SD1234-H10 and the sub-fragments in comparison (50 nM each, the color coding is shown in the inset).*

Table 5   *Affinities and rate constants of the interaction with IFNα2 and IFNβ determined for ifnar1-EC (SD1234-H10), SD1234-DT and H10-SD123.*

Ifnar1	IFNα2		IFNβ		
Fragment	k_d	K_D [µM]	k_a [M⁻¹s⁻¹]	k_d [s⁻¹]	K_D [nM]
SD1234-H10	1.0 ± 0.3	~5	$(5 \pm 2) \cdot 10^5$	0.017 ± 0.005	50 ± 20
SD1234-DT	1.0 ± 0.2	~6	$(5 \pm 2) \cdot 10^5$	0.017 ± 0.005	50 ± 20
H10-SD123	1.3 ± 0.2	~8	$(5 \pm 2) \cdot 10^5$	0.019 ± 0.006	70 ± 20

6.2.5 IFNα2 and IFNβ compete for the same binding site on ifnar1-EC

Since the analysis of different sub-fragments did not indicate different binding domains in ifnar1-EC for both IFNα2 and IFNβ, it was investigated whether these two IFNs actually bind competitively to an overlapping epitope. In order to discriminate these two IFNs $^{AF-488}$IFNα2 was used. Binding was monitored in real-time by simultaneous TIRFS-RIf detection [100]. Both the fluorescence and the mass-sensitive signal monitored in real-time during a typical experiment are shown in Figure 42. After immobilization of ifnar1-EC, first 1 µM $^{AF-488}$IFNα2 was injected (Figure 42A (I)), followed by an injection of 1 µM $^{AF-488}$IFNα2

mixed with 100 nM unlabeled IFNβ (Figure 42A (II)), then only 100 nM IFNβ was injected(Figure 42A (III)). The fluorescence signals during the first two injections were compared (Figure 42B). Fast, transient binding of IFNα2 was detectable in the fluorescence channel with a similar characteristic as observed for unlabeled IFNα2 (Figure 34B). The sensitivity of RIf-detection is too low to detect binding at this IFNα2 concentration, because a rather low surface concentration of SD1234-H10 was used for these measurements. When IFNα2 mixed with IFNβ was injected, a decay of the fluorescence signal after the initial, fast rise was observed (Figure 42C). This decay can be ascribed to labeled IFNα2 being exchanged for unlabeled IFNβ, which binds more stably to ifnar1-EC. Binding of IFNα2 is much faster, because of its higher concentration, while the association rate constants are very similar. Binding of IFNβ with its typical association and dissociation characteristics was simultaneously detected on the RIf-channel (Figure 42B (III)). For the IFNβ injection without IFNα2 a very similar binding curve was detected for IFNβ on the RIf-channel while no signal was detectable on the fluorescence channel. More detailed analysis of the binding curves at different concentrations confirmed that the rate constants of the interaction did not change, corroborating competitive binding of IFNα2 and IFNβ to ifnar1-EC.

The same experiment was carried out with H10-SD123 immobilized on the surface. A comparison of the curves for 1 μM IFNα2 in the presence and absence of 100 nM IFNβ is shown in Figure 42D. Very similar shapes of the curves as for ifnar1-EC were obtained, confirming that IFNα2 and IFNβ bind to an overlapping epitope formed by the three N-terminal Ig-like domains of ifnar1-EC.
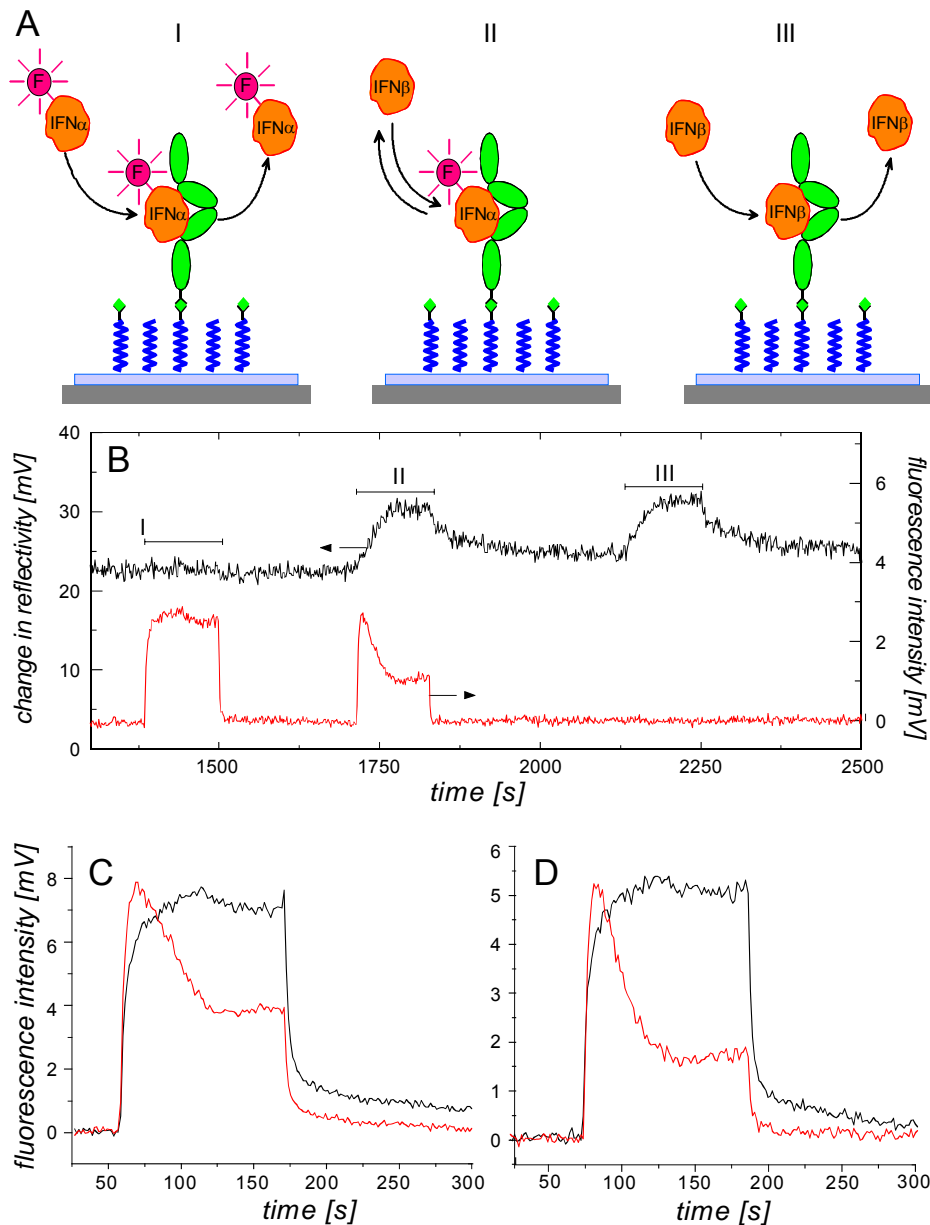
Figure 42   *Competition of IFNα2 and IFNβ for the ifnar1-EC binding site. A: Cartoon of the competition experiment. B: Interference signal (black) and fluorescence signal (red) during injection of $^{AF-488}$IFNα2 (1µM) alone (I), mixed with IFNβ (II) and injection of IFNβ alone (III) on immobilized ifnar1-EC. C: Overlay of the fluorescence signals of injections I (black) and II (red). D: Overlay of the fluorescence signals of injections I (black) and II (red) for the same experiment carried out with immobilized H10-SD123.*

6.2.6 Identification of residues critical for interferon binding

In order to identify individual residues involved in interferon binding, several amino acids on every sub-domain were mutated. Most mutants were expressed in equal amounts like the wild-type protein. The major part of the mutants was also properly folded except W250A as checked by analytical SEC after one freeze and thaw cycle (data not shown). Since interaction studies with wild-type IFNα2 require high amounts of protein (Figure 43A), the high affinity IFNα2 mutant IFNα2-HEQ as well as IFNβ were used for the identification of relevant mutations. For IFNα2-HEQ a K_D value of 70 nM ± 20 nM and dissociation rate

71

constant of ~ 0.025 s^{-1} was determined (Figure 43C), which is comparable to IFNβ. The binding parameters for ifnar1-EC mutants were quantified by RIfS (Figure 43C; D). The results of all titration experiments performed to estimate the K_D are summarized in Table 6.
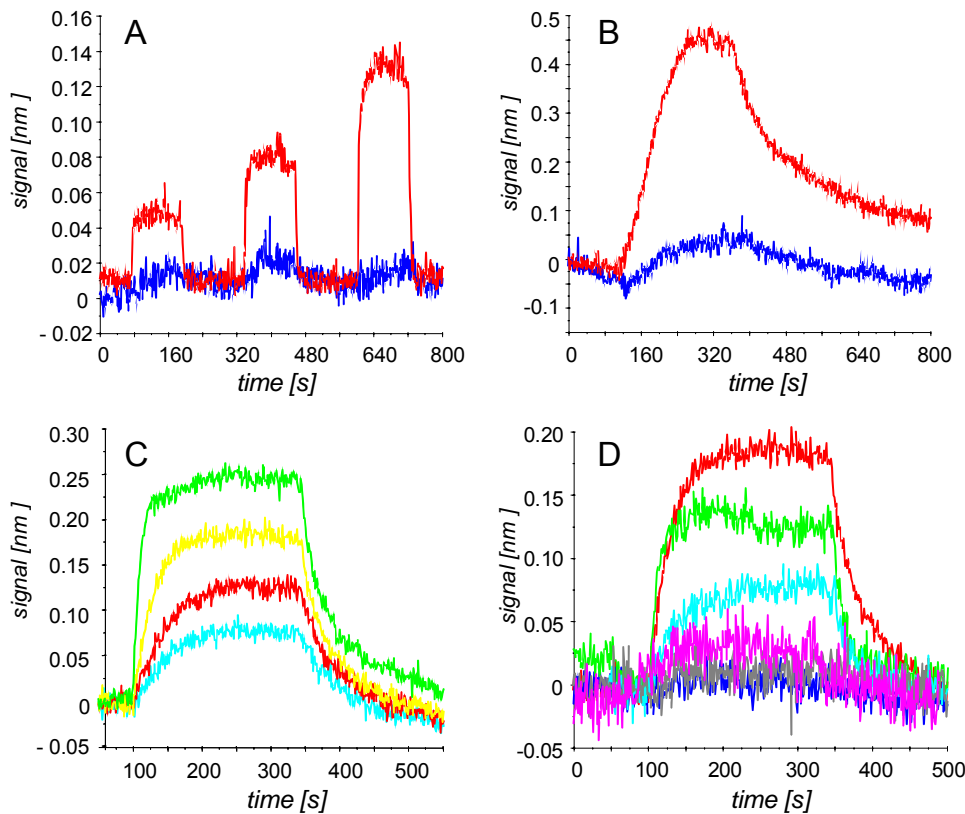

Figure 43   *Interactions of IFNα2, IFNβ and IFNα2-HEQ with different ifnar1-EC mutants immobilized on an NTA-surface. A: Binding curve of IFNα2 (1, 3 and 10μM) on ifnar-EC wild-type (red) and W129A (blue). B: The same experiment with 50 nM IFNβ. C: Binding of IFNα2-HEQ to ifnar1-EC in different concentrations (light blue: 30 nM, red: 50 nM, yellow: 100 nM, green: 300 nM). D: Binding of IFNβ (100 nM) to different immobilized ifnar1-EC mutants (red: wild-type, green: K251A, light blue: N155T, magenta: E111A, grey: F136A, blue: Y70A).*

Residues on SD1 (Y70A) and mainly SD2 (E111A, K113, W129A and F136A) were identified to decrease affinity at least by a factor of 10 for IFNβ as well as for IFNα2-HEQ (Figure 44). Interestingly N155T increased affinity for IFNβ while it reduced affinity for IFNα2-HEQ. However, these results were in good agreement with results obtained from mutagenesis studies on bovine ifnar1-EC [84]. Also on SD3 one residue (K251A) was identified to be involved in binding, but the effect was only minute and only detectable for IFNα2-HEQ. Since SD4 was not expected to be involved in ligand binding, only two mutants were generated on this sub-domain (D298A, N368D). These mutants did not reduce affinity compared to wild-type ifnar1-EC.

Site directed mutagenesis study confirmed that IFNα2 and IFNβ use mainly the same residues on ifnar1 for binding. It is possible, that individual residues accentuate either IFNα2

or IFNβ. But it was concluded, that the same hot spots of binding are involved in the recognition of both IFNs. Thus in case of IFNα2 and IFNβ differential signaling seemed not to be encoded by structural differences in the ligand recognition process.

Table 6   *Dissociation constants determined for different ifnar1-EC mutants determined by titrating IFNα2-HEQ and IFNβ to immobilized receptor.*

Mutant	K_D (IFNα2-HEQ)	K_D (IFNβ)	Remark
Y70A	> 3µM	> 500nM	
R76A	like wild-type	like wild-type	
E111A	340+/-150 nM	> 2µM	
K113A	> 3µM	> 2µM	difficult immobilization
W129A	> 3µM	> 2µM	
F136A	> 3µM	> 2µM	
N155T	200+/-40 M	1+/-0.3 nM	increased affinity for IFNβ k_d=0.0006
L247A	like wild-type	like wild-type	
W250A	-	-	protein aggregation
K251A	130+/-20 nM	like wild-type	
D298A	like wild-type	like wild-type	
N368D	like wild-type	like wild-type	
wild-type	70+/-20 nM	50+/-20 nM	

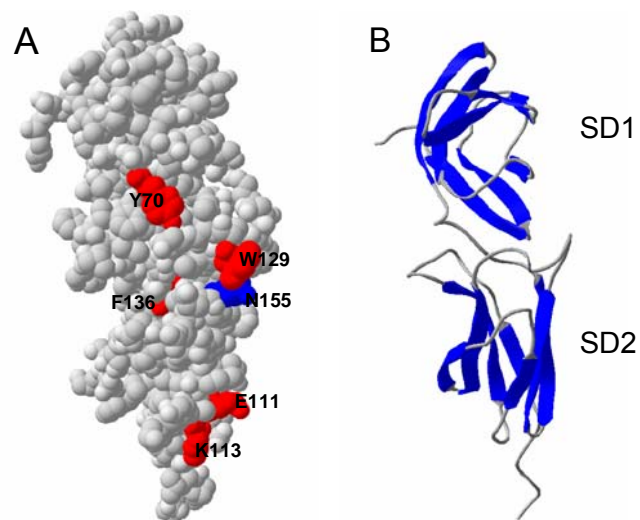*Figure 44*   *A, B: Model of ifnar1-EC SD1 and SD2. The structure is based on the NMR-structure of ifnar2-EC. Residues which decrease affinity toward IFNα2 and IFNβ are depicted in red, N155 is depicted in blue.*

6.3 Complex formation on lipid bilayers

6.3.1 Introduction

In order to investigate stoichiometry and dynamics of ternary complex formation an experimental set-up to simulate the binding processes at the extracellular domains of ifnar was required (Figure 43). The lateral mobility of the plasma membrane was mimicked by a lipid bilayer fused to a glass substrate, which was termed fluid support (Figure 43A). The proper formation and thickness of the bilayer was monitored by RIfS before conditioning (imidazole, EDTA, Ni^{2+}). In the next step proteins were sequentially immobilized via their histidine-tags on a chelatorlipid mimicking the anchoring by the trans-membrane domain (Figure 43B, C). In combination with RIf it was possible to control the absolute and relative surface concentrations of ifnar1-EC and ifnar2-EC. After co-immobilization the complex assembly was induced by IFN-injection (Figure 43D, E). Lateral mobility of the receptor was expected to mediate proper spatial arrangement of the receptor components, but a solid support is expected to reduce porotein mobility (Figure 43F). All experiments probing complex formation and stoichiometry were organized in this sequence.
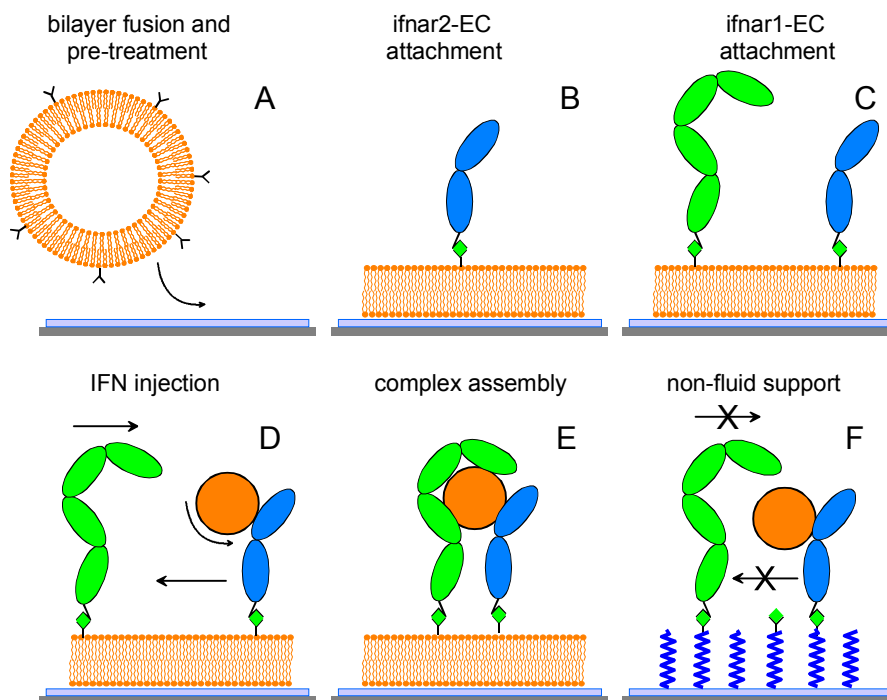
Figure 45   *Schematic of a co-immobilization experiment for probing complex assembly. A unilaminar vesicle fuses to the surface and form a fluid lipid bilayer (I). After per-treatment ifnar2-EC and ifnar1-EC are sequentially immobilized (II+III). Then IFN is injected (IV) initializing complex formation (V). On a non-fluid support by using a PEG polymer brush proper complex formation is not expected (VI).*

6.3.2 Interaction of ifnar1-EC and ifnar2-EC on fluid support

Before co-immobilization of ifnar1-EC and ifnar2-EC any effect of the bilayer on IFN binding had to be excluded by individual interaction experiments on fluid support. When

ifnar1-EC or ifnar2-EC were individually immobilized on solid-supported lipid bilayers (Figure 46A), the binding curves obtained for IFNα2 and IFNβ binding to ifnar2-EC (Figure 46B, C) and ifnar1-EC (Figure 46D, E), respectively, were very similar to the corresponding measurements on the non-fluid polymer brush support. The rate and equilibrium constants obtained from these curves matched the rate constants determined from the measurements on non-fluid support. Neither for IFNα2 nor for IFNβ significant non-specific binding was detectable on the solid-supported lipid bilayers (Figure 46B, D, E).
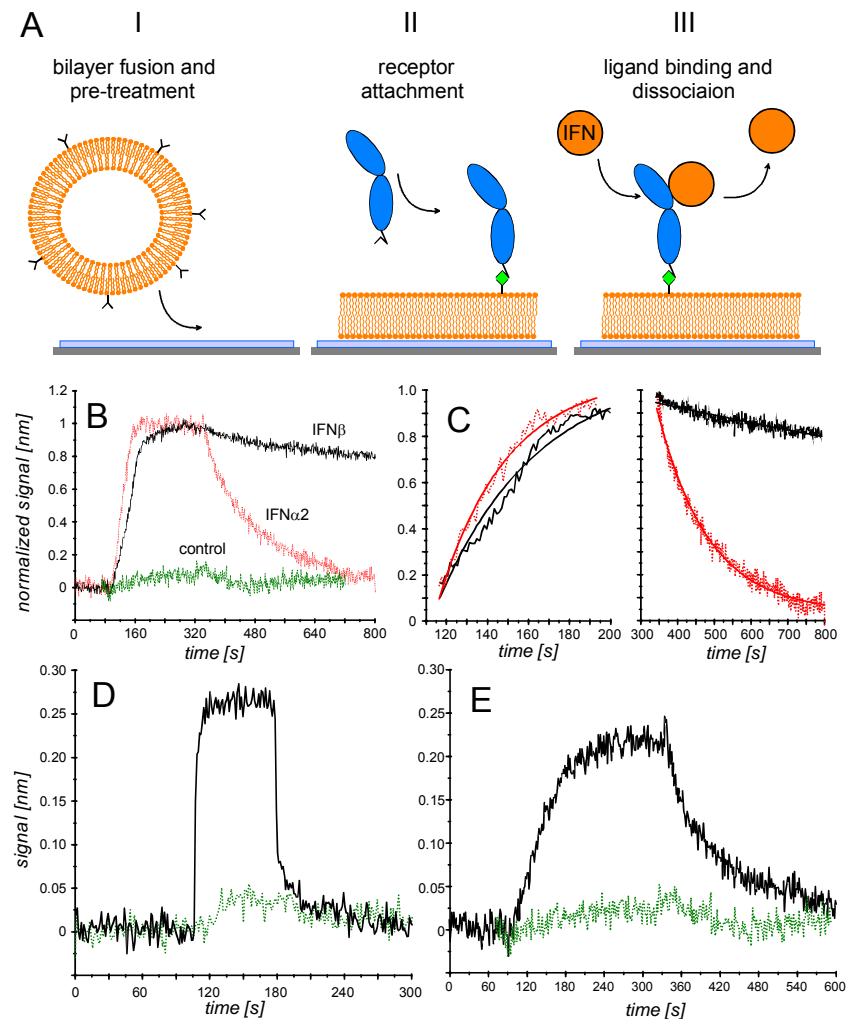

Figure 46   *Ligand binding to ifnar1-EC and ifnar2-EC tethered on solid-supported lipid bilayers as detected by RIfS. A: Cartoon of an experiment probing individual interactions. The unilaminar vesicle fuses to the glass support (I) and subsequently the receptor attached to the surface (II) followed by IFN-injection. B: Interaction of 50 nM IFNα2 (red) and 50 nM IFNβ (black) with ifnar2-EC in comparison to 50 nM IFNβ exposed to a surface loaded with MBP-H10 (green). C: Fit of the association and dissociation curves shown in B. D: Interaction of 10 μM IFNα2 (black) with immobilized ifnar1-EC in comparison to 10 μM IFNα2 exposed to a surface loaded with MBP-H10 (green). E: Interaction of 100 nM IFNβ (black) with ifnar1-EC in comparison to 100 nM IFNβ exposed to a surface loaded with MBP-H10 (green).*

For the investigation of complex assembly ifnar1-EC and ifnar2-EC were sequentially tethered to the surface. Upon co-immobilization binding kinetics of IFNα2 drastically changed

(Figure 47A, B). No significant dissociation was observed within 15 min, and a second injection of IFNα2 did not give any significant signal (data not shown). No dissociation of IFNα2 was discernible only if 1:1 molar ratio for ifnar1-EC and ifnar2-EC was strictly maintained. With a molar excess of ifnar1-EC, partial fast dissociation of IFNα2 was observed, and the amount of stably bound ligand corresponded to the amount of tethered ifnar2-EC (Figure 47C). With a molar excess of ifnar2-EC, a partial dissociation with a rate constant corresponding to the ifnar2-IFNα2 interaction was observed, and the amount of stably bound ligand corresponded to the amount of ifnar1-EC on the bilayer (Figure 47D).
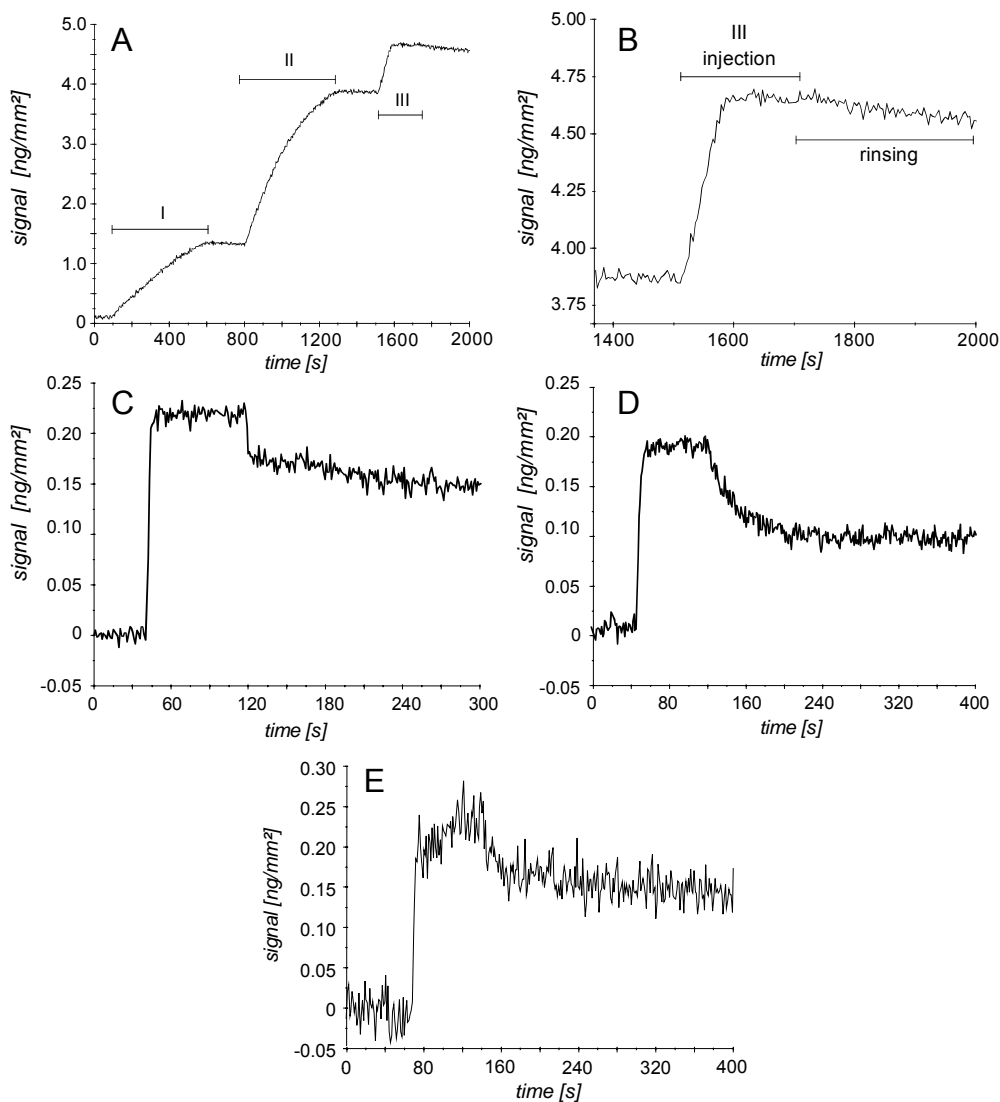
Figure 47   *Ligand binding to ifnar1-EC and ifnar2-EC co-immobilized on solid-supported, fluid lipid bilayers. A: Immobilization of ifnar2-EC (I) and ifnar1-EC (II) in stoichiometric ratio, and interaction with 100 nM IFNα2 (III). B: Enlargement of IFNα2 binding and dissociation as shown in A. C, D: Interaction with 100 nM IFNα2 with an excess of ifnar1-EC (C) and ifnar2-EC (D). Interaction of IFNα2 (1 μM) with deglycosylated ifnar1-EC co-immobilized with ifnar2-EC on lipid bilayer.*

The same results were also obtained for deglycosylated ifnar1-EC (Figure 47E) which demonstrates, that glycosylation has no effect on complex formation. All results confirmed that with IFNα2 a complex with a stoichiometry of 1:1:1 was formed, termed the ternary complex.

Formation of a stable stoichiometric ternary complex was only observed on fluid supports (Figure 48), confirming that orientation and lateral reorganization of the receptor domains were required to obtain maximum binding affinity. This observation was underlined by FRAP experiments. For $^{OG-488}$ifnar2-EC tethered to the chelator lipid, a diffusion constant of 1 ± 0.5 µm²/s was determined, which is very similar to the diffusion constant of GPI-anchored proteins in living cells [101]. No significant change in recovery time was observed upon co-immobilization with ifnar1-EC, while binding of IFNα2 clearly reduced the recovery rate by a factor of 2 (Figure 49). These results also confirmed that no substantial interaction between ifnar1-EC and ifnar2-EC takes place in the absence of the ligand.
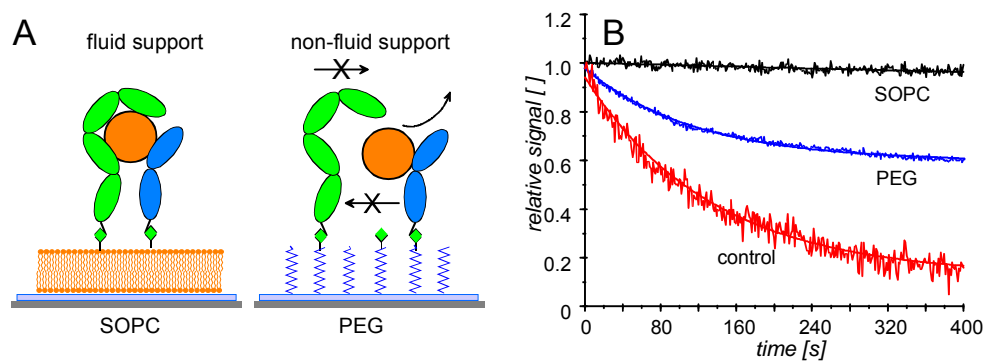
Figure 48   *Fluid and non-fluid support in ternary complex assembling. A: Cartoon of the experiment. B: Dissociation of IFNα2 from the ternary complex with ifnar1-EC and ifnar2-EC on lipid bilayers (black) and on polymer brush support (blue), compared to the dissociation from ifnar2-EC alone (red).*
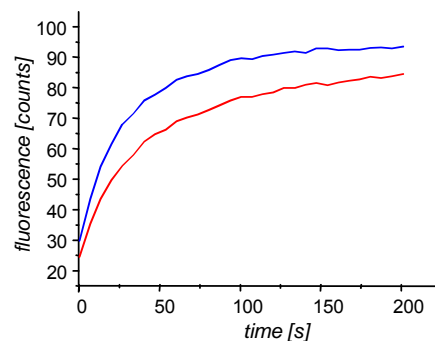
Figure 49   *FRAP experiment carried out with ifnar2-EC S35C labeled with OG488 tethered to chelator lipids in a solid-supported lipid bilayer. Recovery curves of ifnar2-EC OG-488 in presence of ifnar1-EC before (blue) and after (red) addition of 100 nM IFNα2.*

Since for the wild-type proteins no dissociation from the ternary complex was observed, several mutants of ifnar2-EC and IFNα2 forming relatively less stable binary complexes with each other compared to their wild-type counterparts were investigated (Figure 50A, B). IFNα2 dissociated from ifnar2-EC I47A with a rate constant of 0.2 s^{-1} (20-fold higher than wild-type ifnar2-EC). Upon co-immobilization of ifnar-1EC, a k_d of 0.001 ± 0.0002 s^{-1} was observed (Figure 50C). For IFNα2 R149A (K_D: 500 nM, $k_d \sim$ 2 s^{-1}), a dissociation rate constant of 0.01 ±0.003 s^{-1} in presence of tethered ifnar1-EC was observed (Figure 50D).

From these experiments it was estimated, that in presence of ifnar1-EC the apparent affinity is approximately 200-fold higher compared to the affinity towards ifnar2-EC alone. This was mediated by the formation of a ternary complex at high receptor surface concentration.
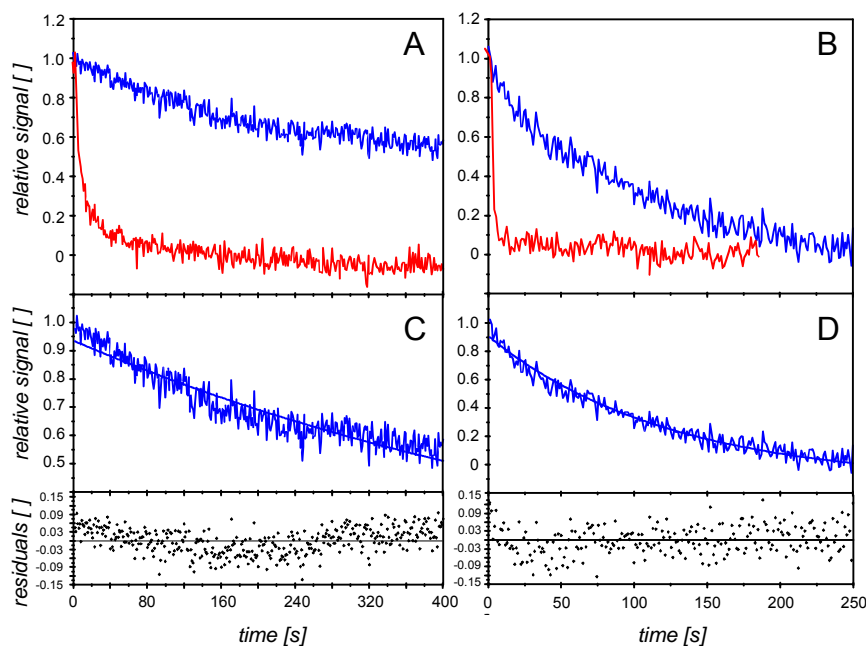

Figure 50   *A, B: Dissociation of IFNα2 from both ifnar1-EC and ifnar2-EC on lipid bilayers (blue) compared to ifnar2-EC alone (red) observed for ifnar2-EC I47A with wild-type IFNα2 (A) and for wild-type ifnar2-EC with IFNα2 R149A (B). C, D: Fit of a mono-exponential decay to the dissociation from the ternary complex shown in A (C) and B (D), and the residuals.*

Table 7   *Rate and equilibrium constants of the interaction with ifnar1-EC and ifnar2-EC determined for different IFNs and different mutants (n.b., no binding detectable). Mean values and standard deviations were determined from at least three independent experiments.*

IFN	Ifnar2-EC			Ifnar2-EC/Ifnar1-EC (co-immobilized on lipid BL at high surface concentrations)		
	k_a [M^{-1}s^{-1}]	k_d [s^{-1}]	K_D [nM]	k_a [M^{-1}s^{-1}]	k_d [s^{-1}]	K_D [nM]
IFNα2 wt	$(3 \pm 1) \cdot 10^6$	0.012 ± 0.002	3 ± 1	$(3 \pm 1) \cdot 10^6$	~0.0001	~0.03
IFNα2 S136C	$(3 \pm 1) \cdot 10^6$	0.013 ± 0.002	3 ± 1	$(3 \pm 1) \cdot 10^6$	~0.0001	~0.03
IFNα2 wt on ifnar2-EC I47A	$(3 \pm 1) \cdot 10^6$	0.20 ± 0.04	60 ± 20	-	0.0012±0.0002	-
IFNα2 R149A	-	~ 2	500 ± 100	-	0.010±0.003	-
IFNβ	> 5·10^6	~ 0.001	< 0.1	-	< 0.0005	-
IFNβ on ifnar2-EC I47A	> 5·10^6	0.003 ± 0.001	< 0.6	-	-	-
IFNβ with 500mM NaCl	> 5·10^6	0.005 ± 0.002	< 1	-	< 0.0005	-

6.3.3 Complex stability depends on receptor surface concentration

All measurements demonstrating a stable ternary complex, however, were carried out at very high receptor surface concentrations (approximately 20-40 fmol/mm², i.e. 20-40% of a monolayer). Thus, simultaneous RIfS/TIRFS detection was carried out to monitor association and dissociation processes under controlled surface conditions at low receptor surface concentrations. Binding of labeled IFNα2 to the receptor on lipid bilayers was measured at different absolute surface concentrations of the receptor in a stoichiometric ratio of ifnar1-EC and ifnar2-EC (Figure 51). At high surface concentration of ifnar1-EC and ifnar2-EC, fluorescence detection principally showed similar dissociation phases like RIfS (Figure 51A). However, a decay of the signal while rinsing was observed. This was not due to ligand dissociation, as stable binding was confirmed by simultaneous RIfS detection (data not shown), but can be ascribed to photobleaching. With decreasing surface concentrations of ifnar1-EC and ifnar2-EC a decreasing stability of the ternary complex was observed (Figure 51B). The dissociation curves were fitted by a single exponential decay (Figure 51B, C), and increasing k_d values were obtained with decreasing surface concentrations. In Figure 51D, the dissociation rate constants were plotted as a function of receptor surface concentration, the corresponding values are listed in Table 8. At the lowest receptor surface concentration of approximately 0.3 fmole/mm² (~200 molecules/µm²), the stability of the ternary complex was only 3-times higher than for ifnar2-EC alone. For surface concentrations of 2-

4 fmole/mm² k_d values corresponding to the affinities which have been observed in binding assays with living cells were determined [102].

Table 8   *Rate and equilibrium constants of IFNα2 binding at different stoichiometric surface concentrations of ifnar1-EC and ifnar2-EC on supported lipid bilayers. K_D was calculated using the average k_a of $(3 \pm 1) \cdot 10^6 \ M^{-1}s^{-1}$*

Ifnar1-EC [fmol/mm²]	k_a [10^6M^{-1}s^{-1}]	k_d [10^{-3}s^{-1}]	K_D [nM]
12 ± 3	1 ± 0.3	0.5 ± 0.1	0.17 ± 0.06
8 ± 2	1 ± 0.3	0.5 ± 0.1	0.17 ± 0.06
5.5 ± 1	3 ± 1	0.6 ± 0.1	0.21 ± 0.07
4 ± 1	4 ± 1	0.8 ± 0.2	0.28 ± 0.1
2 ± 0.4	5 ± 2	1.4 ± 0.2	0.46 ± 0.16
1 ± 0.2	3.5 ± 1	2.1 ± 0.2	0.70 ± 0.24
0.5 ± 0.1	3 ± 1	3.3 ± 0.3	1.11 ± 0.4
0.3 ± 0.1	4 ± 1	4.4 ± 0.4	1.48 ± 0.5
0	4 ± 1	12 ± 1	4 ± 1.5

The association phases of the binding curves normalized to the saturation signal are shown in Figure 51E. At receptor surface concentrations below 8 fmol/mm², the association curves overlayed. These curves were fitted well by a pseudo first-order model (Figure 51F) and gave association rate constants very similar to the interaction of IFNα2 with ifnar2-EC alone (Table 8). At higher surface concentration, significantly lower association rate constants were obtained and systematic deviations from the model, as well as from the other binding curves were observed (Figure 51F). This was probably due to mass transport limitations at these high receptor surface concentrations, which have already been observed for the interaction of IFNα2 with ifnar2-EC alone.
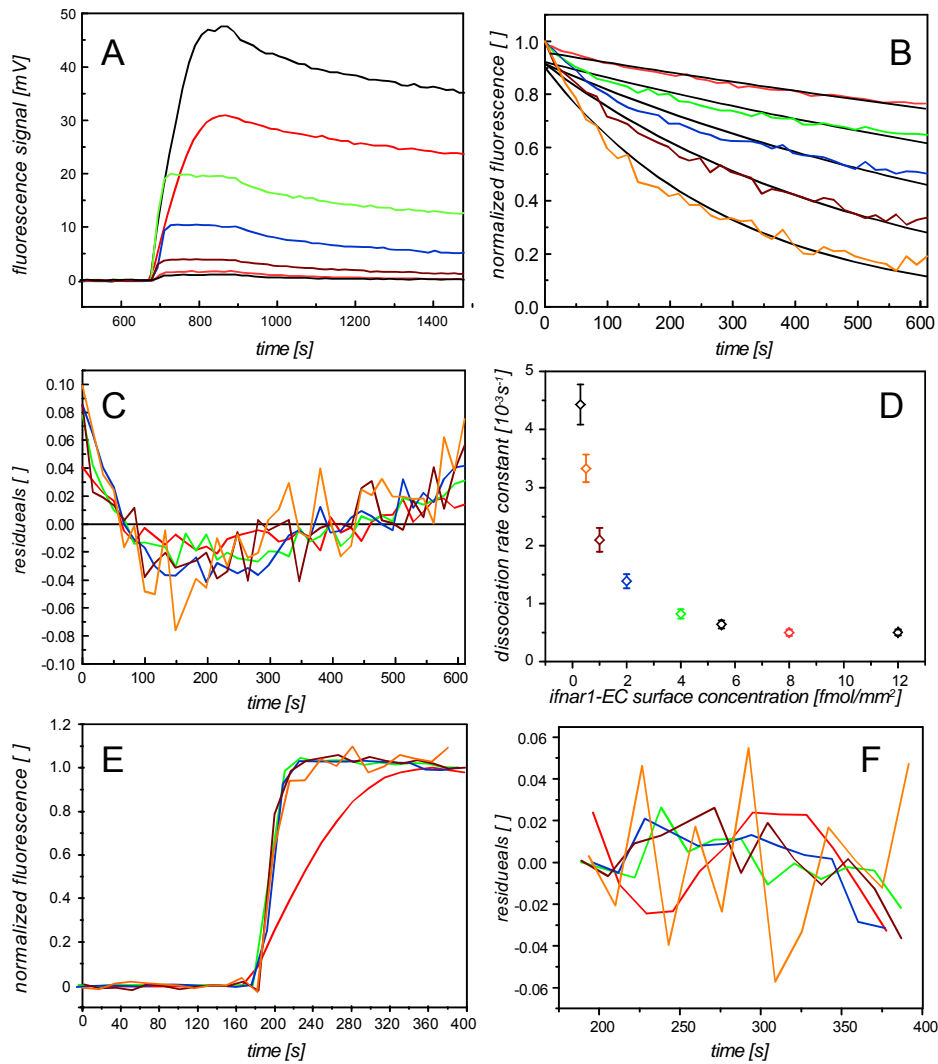
Figure 51   *IFNα2 interaction with ifnar1-EC and ifnar2-EC tethered onto supported lipid bilayers as detected by TIRFS. A: binding of 100 nM AF-488-labeled IFNα2 at different surface concentrations of ifnar2-EC and ifnar1-EC in a stoichiometric ratio (black: 12 fmol/mm²; red 8 fmol/mm²; green: 4 fmol/mm²; blue: 2 fmol/mm²; brown: 1 fmol/mm², orange: 0.5 fmol/mm²). B: dissociation phases of the binding curves shown in A normalized to the signal at the beginning of dissociation (same color coding as A) including the fit curve of a mono-exponential decay (black lines). C: residuals for fitting curves shown in B (same color coding as A). D: dissociation rate constant as a function of the surface concentration of the receptor. E: association phases of binding curves shown in A normalized to the saturation signal (same color coding as A). F: residuals of a first-order association model fitted to the curves shown in E.*

6.3.4 Dynamic exchange processes on the ternary complex

The dependence of the complex stability on the receptor surface concentration suggested that the ternary complex is not static, but stabilized by fast re-association, i.e. the kinetics which depends on the receptor surface concentration. This was further corroborated by the observation that stable ternary complexes were formed at low surface concentrations of ifnar2-EC but high surface concentrations of ifnar1-EC (data not shown). In order to analyze this kinetic stabilization, the apparently stable ternary complex formed with

fluorescence labeled IFNα2 was challenged by injecting unlabeled IFNα2 or ifnar2-tl (Figure 52A). Already at a concentration of 1 µM unlabeled IFNα2 an exchange rate of 0.002 s^{-1} was observed. At the same time the total amount of bound IFN did not change as simultaneously detected by RIfS (data not shown). In contrast no significant change in dissociation kinetics was observed when ifnar2-tl was injected, even at a concentration as high as 10 µM (Figure 52A).
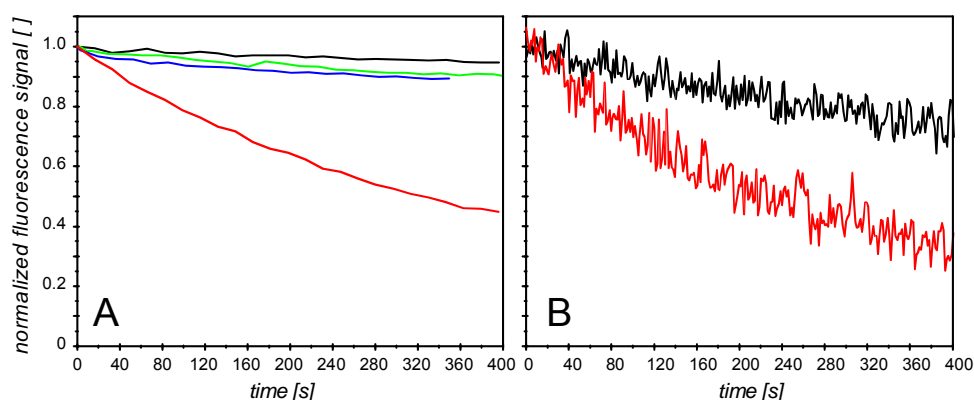

Figure 52   *Chase experiments with fluorescent labeled IFNα2 bound to ifnar2-EC and ifnar1-EC co-immobilized on supported lipid bilayers A: Dissociation of OG-488-labeled IFNα2 (black) at high surface concentrations of both ifnar2-EC and ifnar1-EC, in the presence of 1 µM (green) and 10 µM (blue) ifnar2-tl, and in the presence of 1 µM unlabeled IFN (red). B: Dissociation of OG-488-labeled IFNα2 from the ternary complex at low surface concentration of ifnar2-EC in absence (black) and in presence (red) of 1 µM unlabeled IFNα2.*

Furthermore, even at much lower surface concentrations of ifnar2-EC (~0.5 fmol/mm²), fast exchange was observed in presence of 1 µM unlabeled IFNα2 (Figure 52B). These experiments confirmed that the ligand does not dissociate from the surface and re-associates (rebinding-effect), because then ifnar2-tl should interfere as efficient as IFNα2 does, and the effect should be much less pronounced at low surface concentrations. The fact that the ligand is much faster exchanged than the apparent dissociation rate furthermore corroborates the kinetic stabilization of the ternary complex.

Binding assays with ifnar1 and ifnar2 co-immobilized on lipid bilayers were also carried out with IFNβ. However, very stable binding was observed already for the interaction with ifnar2-EC alone, and thus no substantial difference in stability could be observed in presence of ifnar1-EC. Upon challenging the ternary complex formed with IFNβ by injecting fluorescently labeled IFNα2, no exchange could be observed (data not shown), confirming the anticipated high stability of the ternary complex. Since the already formulated IFNβ could not be labeled appropriately, binding assays at low surface concentration were also not feasible.

6.3.5 Complex formation of ifnar1-EC sub-fragments on lipid bilayers

The direct interaction assays revealed that the binding affinity towards IFNα2 and IFNβ decreased by more than a factor of >20 in case H10-SD12, SD34-H10 and SD234-H10, while nearly full binding affinity was maintained for H10-SD123. Owing to the already low affinity of IFNs towards ifnar1-EC, the residual binding affinity could not be established by these assays. Furthermore the effects of sub-domain deletion on ternary complex formation remained unclear. Therefore ligand binding to ifnar2-EC co-immobilized with ifnar1-EC or its sub-fragments onto a solid-supported fluid lipid bilayer was investigated. It was shown before that with stoichiometric amounts of ifnar2-EC and ifnar1-EC (SD1234-H10) at high surface concentrations (~25-50 fmol/mm²) IFNα2 binds at least 100-times stronger than to ifnar2-EC alone. Thus this binding assay was even more sensitive to low affinities, since the ligand is captured by the high-affinity interaction with ifnar2-EC, and subtle lateral interaction on the surface would be reflected by a decrease in the dissociation rate constant.

For the sub-domains H10-SD12, SD34-H10 (data not shown) and SD234-H10 (Figure 53E) no significant difference in the dissociation kinetics was observed compared to the dissociation from ifnar2-EC alone. Also upon co-immobilization of H10-SD12 and SD34-H10 with ifnar2-EC, no change in the dissociation kinetics was observed (Figure 53A-C). From these assays, a loss of affinity by more than 2 orders of magnitude can be concluded for the sub-fragments H10-SD12, SD34-H10 and SD234-H10. In contrast a strong decrease in the apparent k_d was observed for SD123 co-immobilized with ifnar2-EC (Figure 53D), almost as strong as for ifnar1-EC or SD1234-DT (Figure 53E). A k_d of 0.0002 s^{-1} was estimated by an exponential fit, i.e. two orders of magnitude slower than the dissociation from ifnar2-EC alone. The stability of the ternary complex formed upon co-immobilization with ifnar2-EC was compared in more detail for the variants ifnar1-H10, SD1234-DT and H10-SD123 applying the IFNα2 mutant L30A, which binds ~500-times weaker to ifnar2-EC (k_d ~5 s^{-1}). The curve observed for SD1234-DT (data not shown) was indistinguishable from the curve obtained for SD1234-H10) with a k_d of 0.015 s^{-1}. In case of H10-SD123, slightly faster dissociation was observed (k_d: 0.025 s^{-1}) (Figure 53F). Thus, only small differences in ternary complex stability were observed for H10-SD123 compared to SD1234-H10 and SD1234-DT at these high receptor surface concentrations, confirming that ternary complex formation was possible without SD4.
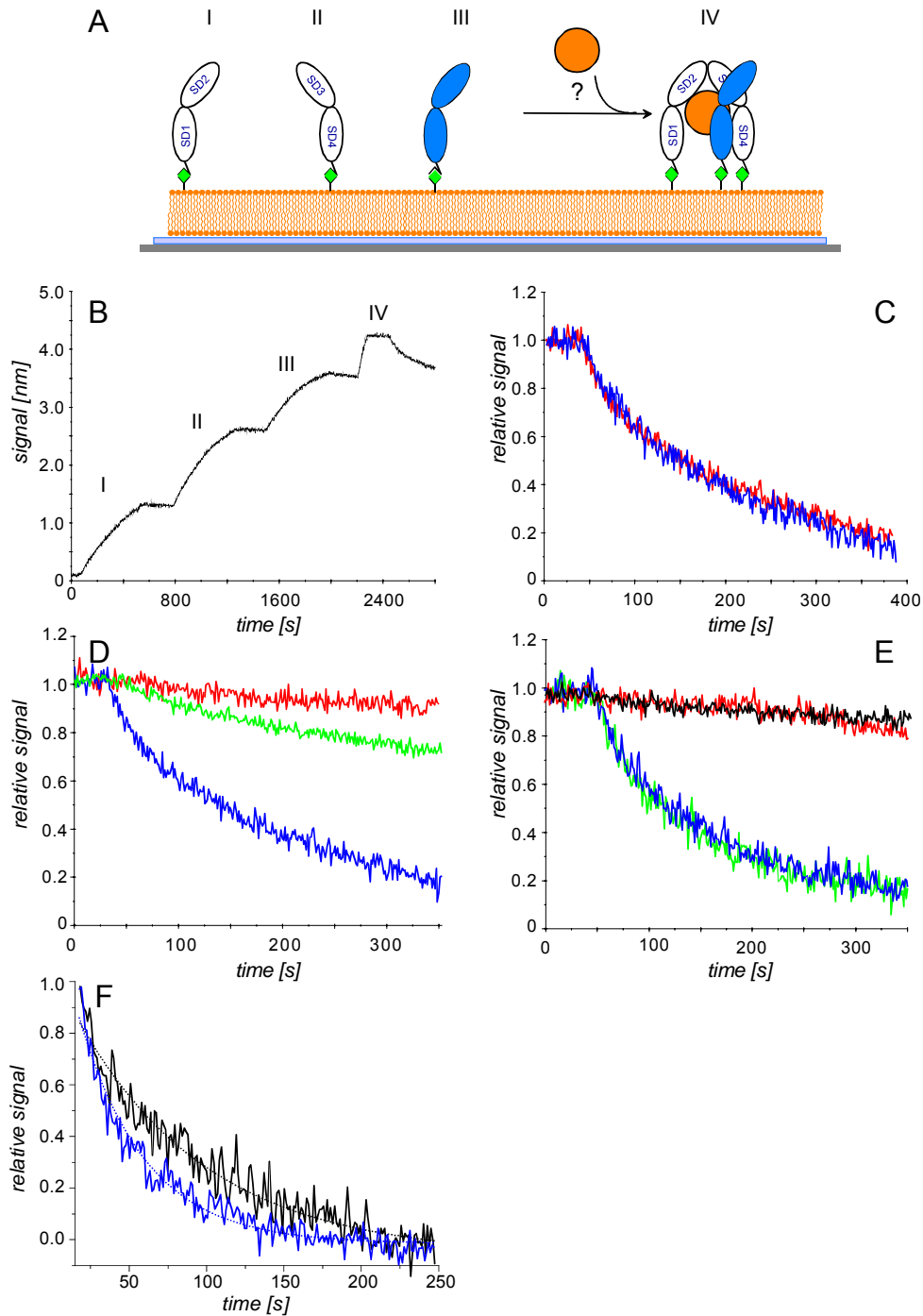
Figure 53   *IFNα2 binding to ifnar2 co-immobilized with different ifnar1-EC sub-fragments onto solid-supported lipid bilayers. A, B: Cartoon (A) and binding (B) of 100 nM IFNα2 (IV) to co-immobilized ifnar2 (I), H10-SD12 (II) and SD34-H10 (III) (blue) compared to ifnar2 alone. C: Enlargement of IFNα2 binding and dissociation as shown in B. D: Dissociation from SD1234-H10 (red), H10-SD123 (green) co-immobilized with ifnar2-EC and ifnar2 alone (blue). E: The same as shown in D with SD234-H10 (green) and SD1234-DT (black). F: Dissociation of IFNα2-L30A from SD1234-H10 (black) and H10-SD123 (blue) co-immobilized with ifnar2-EC. The dotted lines are the mono-exponential fits of these curves.*

Table 9   *Dissociation rate constants of the interaction with IFNα2 and IFNα2 L30A determined for different ifnar1-EC constructs on fluid lipid bilayers at high surface concentrations (20-40 fmol/mm²).*

Ifnar1 Fragment	IFNα2/ifnar2-EC k_d[s^{-1}]	IFNα2 L30A/ifnar2-EC k_d[s^{-1}]
SD1234-H10	~0.0001	0.015 ± 0.003
SD1234-DT	~0.0001	0.017 ± 0.003
H10-SD123	~0.0002	0.025 ± 0.003

6.3.6 Understanding of the role of SD4 in ternary complex assembling

In order to study the effect of sub-domain deletion on ternary complex formation *in vivo*, ligand binding was analyzed in HEK293T cells overexpressing ifnar2 with different constructs of ifnar1-EC fused to the ifnar1 transmembrane and cytoplasmic domains. This work was done in collaboration with Gilles Uzé and José Van der Heyden (CNRS, Montpellier). Binding of IFNα2 and ifnar1 surface expression were quantified by FACS and the results are summarized in Figure 54. As expected for SD234 no increase in ligand binding was detectable. Interestingly for SD123 as well as for constructs with substituted SD4 (SD123-LRD2 and SD123-IL10R2D2) no high affinity ligand binding was observed (Figure 54B). Interestingly SD123-IL10V1V2, carrying two sets of amino acid sequences identical to ifnar1-SD4, was comparable to wild-type ifnar1. These results indicated that SD4 has an important function for the assembling of the ternary complex *in vivo*.
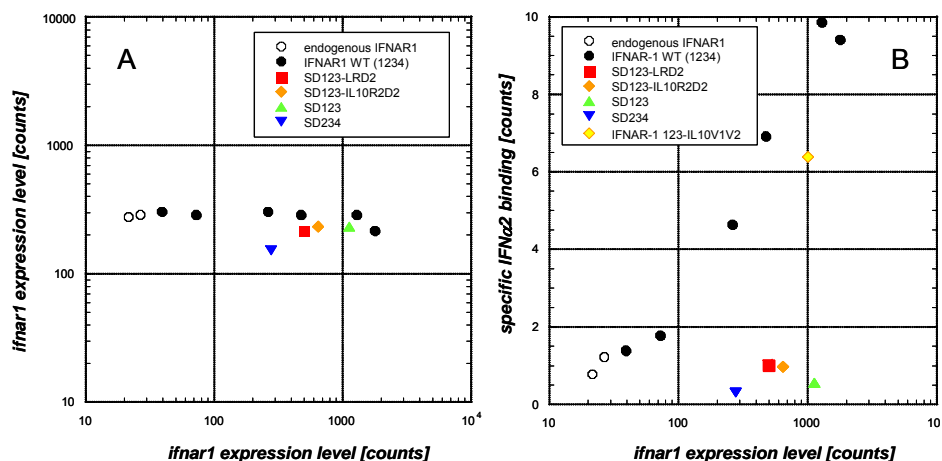
Figure 54   *A, B: Cell surface binding of IFNα2 on HEK293T cells over-expressing ifnar2 and different amounts of ifnar1. HEK293T cells were co-transfected with plasmids encoding EGFP, ifnar2 and ifnar1. The EGFP positive population was analyzed in FACS for the cell surface expression level of ifnar1 and ifnar2 (A) and for specific binding of $^{AF-488}$IFNα2 (B). The binding of $^{AF-488}$IFNα2 is expressed relative to the binding level measured on cells transfected with EGFP and ifnar2 alone (open circles).*

For a better understanding of the role of SD4, ternary complex assembling was studied with several ifnar1-EC fragments and variants in more detail *in vitro*. SD123-LRD2 with a C-terminal H10-tag (SD123-LRD2-H10), as well as SD1234 with an N-terminal H10-tag (H10-SD1234) and SD123 with a C-terminal H10-tag (SD123-H10) were expressed in *Sf*9 insect cells and purified to homogeneity (section 6.1.1). As expected from the previous analysis, direct binding of IFNα2 and IFNβ was unaltered compared to SD1234-H10 for all these proteins (data not shown). Ternary complex assembling was studied by TIRFS-RIf detection with $^{AF-488}$IFNα2 at ~3 fmol/mm² receptor surface concentration. This surface concentration is a good representation of the cell surface receptor density and more than one order of magnitude lower than the receptor surface concentrations used in the ternary complex formation assays described above.

A comparison of ligand dissociation curves for different fragments is shown in Figure 55B. For SD1234-H10, significantly faster ligand dissociation was observed compared to high receptor surface concentration, as expected for less efficient kinetic stabilization at these lower receptor surface concentrations. Under the same conditions, substantially faster dissociation was observed for SD123-LRD2-H10 than for SD1234-H10, in agreement with the low affinity observed for this variant on the cell surface. The dissociation kinetics, however, was still 4-5-times slower than from ifnar2-EC alone, indicating that the ternary complex still assembled, yet with a much lower efficiency.

In order to test the role of orientation on surface affinity, ligand dissociation from ternary complexes formed with H10-SD1234, SD123-H10 and H10-SD123 under the same conditions (i.e. receptor surface concentrations) was investigated. Strikingly, also for H10-SD1234, substantially faster ligand dissociation from the ternary complex was observed than for SD1234-H10. For both H10-SD123 and SD123-H10 ligand dissociation from the ternary complex was similarly fast as observed for SD123-LRD2-H10. However, by increasing the receptor surface concentration, the decrease in ligand binding affinity could be compensated (Figure 55C), suggesting less efficient recruitment of these ifnar1 constructs on the lipid bilayer. Tethering ifnar1-EC through both N- and C-terminus onto the membrane (SD1234-DT) only had a minor effect on ligand dissociation (Figure 55D). Interestingly, it was observed, that the construct SD123-IL10V1V2 was comparable to wild-type ifnar1-EC in terms of complex stability (Figure 56). Probably the back-mutated regions in this domain were responsible for mediating the contribution of ifnar1-EC SD4 in complex assembly.

Taken together, these results indicate that SD4 and its anchoring to the lipid bilayer plays a key role for the efficiency of ifnar1 recruitment into the ternary complex without being responsible for ligand recognition.
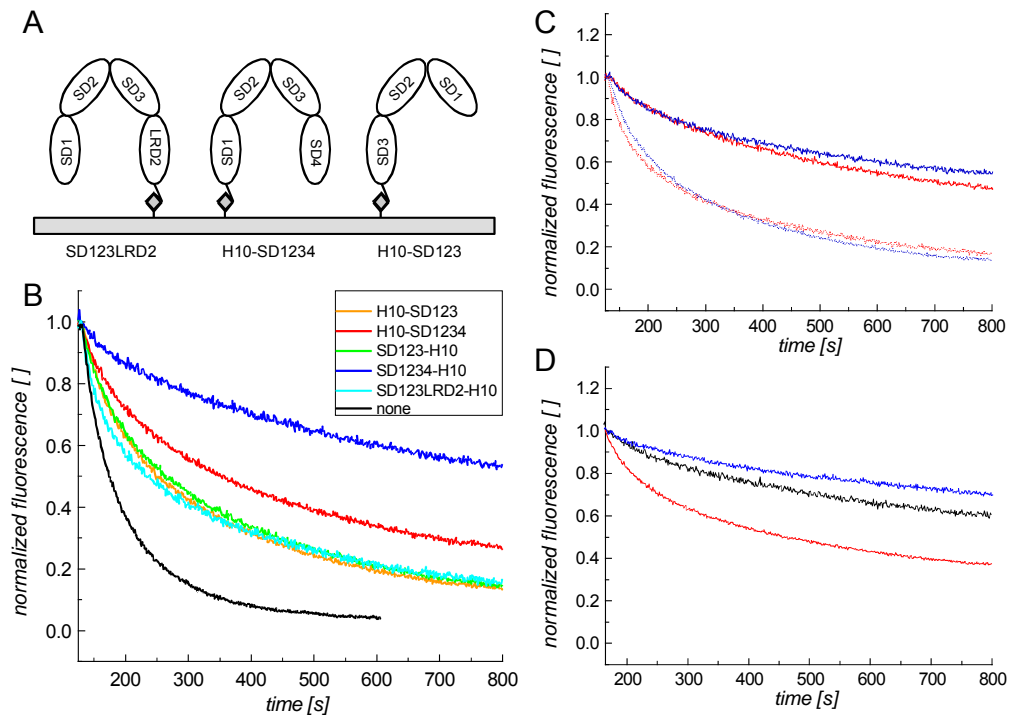
Figure 55   *Comparison of different constructs to investigate the role of SD4 in complex assembly. A: Schematic of the constructs SD123-LRD2-H10, H10-SD1234 and H10-SD123 and their attachment to the lipid bilayer. B: Dissociation of IFNα2 from ifnar2-EC co-immobilized with different constructs of ifnar1-EC on lipid bilayers (receptor surface concentration ~3 fmol/mm²). C: Dissociation of IFNα2 from ifnar2-EC co-immobilized with H10-SD123 (red) and SD123-LRD2-H10 (blue) at different surface concentrations (solid line: ~7 fmol/mm²; dotted line: ~3 fmol/mm²). D: Dissociation of IFNα2 from ifnar2-EC co-immobilized with SD1234-H10 (blue), H10-SD1234 (red), and SD1234-DT (black) on supported lipid bilayers (receptor surface concentration ~4 fmol/mm²).*
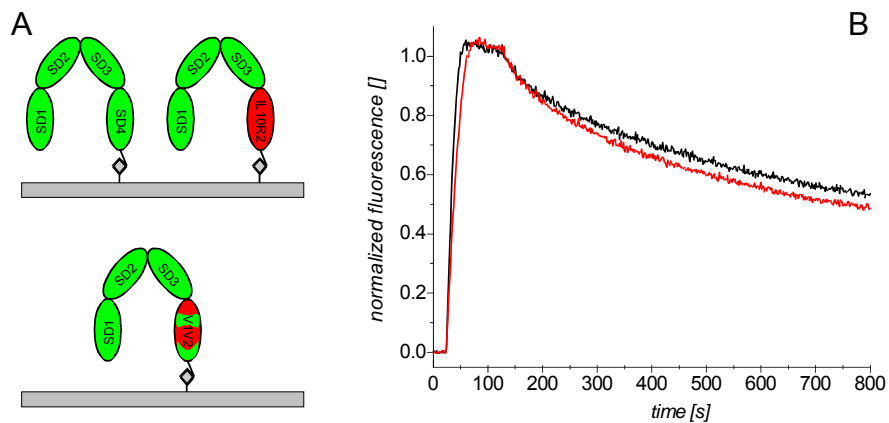
Figure 56   *A: Cartoon of SD123-V1V2 and SD123-IL-10-R2D2. B: Interaction of 100 nM [AF-488]IFNa2-S136C with ifnar1-EC (black) or SD123-IL10V1V2 (red) co-immobilized with ifnar2-EC.*

87

6.3.7 Single particle analysis

In order to get an intial view on the structure of the ternary complex, single particle analysis was applied. This work was done in collaboration with Gideon Schreiber, Weizmann Institute of Science. In the structural model (Figure 57) all results of the previous chapters were underlined. IFNα2 mediates the cross-linking of ifnar1-EC and ifnar2-EC via direct ligand-receptor interactions. As expected, no contact between the two receptor subunits was observed and SD4 was confirmed not to be involved in ligand binding.

Figure 57   Structure of the ternary complex calculated from single particle analysis.

7 Discussion

This work investigated the ligand induced assembly of the type I interferon receptor in order to understand the molecular basis of differential signaling by different interferons. An efficient expression and purification system to produce active and functional ifnar1-EC was established for *in vitro* binding assays. With quantitative amounts of all involved proteins individual interaction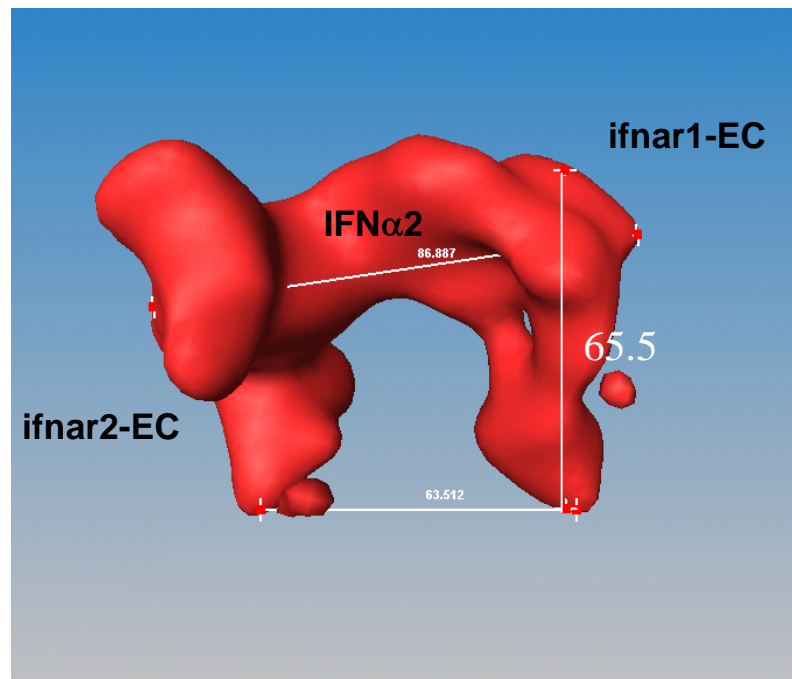s between receptor subunits were probed by solid phase detection in terms of stoichiometry, dynamics and binding site identification. By co-immobilizing ifnar1-EC and ifnar2-EC on lipid bilayers ternary complex formation with respect to stabilization and architecture was investigated. Finally a binding mechanism with ifnar1 as a key element explaining differential signaling was proposed.

7.1 Expression, purification and biochemical characterization

The expression and purification strategy applied for ifnar2-EC and IFNα2, i.e. denaturation, reduction and refolding, did not work for ifnar1-EC. Also fusion to MBP and expression in different *E. coli* strains with an oxidizing cytoplasm did not lead to properly folded protein. Secretion of ifnar1-EC into *E. coli* periplasm ended up with monomeric ifnar1-EC, but low yield and stability supported the decision to choose an alternative strategy. Since expression in *P. pastoris* did also not significantly increase yield or stability (personal communication with from Robert Arduini), *Sf*9 insect cells were chosen as expression host. In this work a novel expression strategy for ifnar1-EC in insect cells was successfully established. By combining the advantages of genetic engineering in baculovirus with the processing machinery of *Sf*9 secretion pathway, an efficient expression system for ifnar1-EC was developed. The yield of ~10 mg/l cell culture was an increase by factor 200 compared to *E. coli* periplasm. The glycosylation was demonstrated to be essential for protein stability, whereas ifnar1-EC from *E. coli* periplasm precipitated either during expression or purification. In contrast to *P. pastoris* [63] glycosylation in *Sf*9 was defined, which enabled a comfortable handling of ifnar1-EC, because deglycosylation was not necessary. Also successful formation of disulfide bonds as expected for cytokine receptor domains was confirmed.

In order to localize binding sites and to investigate complex architecture, several ifnar1-EC sub-fragments, mutants and chimeras were expressed. All sub-fragments were confirmed to be properly folded like the wild-type, confirming independent folding of the Ig-like domains. Probably the chosen cutting sites between the predicted Ig-like domains led to folded proteins with no hydrophobic areas causing aggregation. Also the position of the his-tag did not seem to influence expression and folding, indicating the localization of the protein termini at the surface. Like ifnar1-EC all sub-fragments and constructs had disulfide bonds

and were glycosylated. By comparing the molecular masses of different sub-fragments the predicted 9 glycosylation sites were probable.

In SEC analysis H10-SD123 and SD234-H10 differed in size before deglycosylation, but the shift in the apparent molecular weight was also reproducible for the deglycosylated proteins. These results indicated a different structural arrangement of 3 Ig-like domains of each terminus. It seems that SD1, 2 and 3 were organized in a more stretched manner than SD2, 3 and 4, a first sign for a non-symmetrical structural arrangement of the sub-domains. This was underlined by comparable observations with SD12 and SD34, indicating the non-symmetrical arrangement of these to potential CBMs.

Ifnar1-EC mutants were also expressed and purified in yields comparable to the wild-type protein. An exception was W250A. This residue may play an important role in structure integrity. Interestingly mutants with an exchanged SD4 showed very different properties. SD123-IL10R2D2 was > 90 % aggregated, but by exchanging two special sets of residues yield and stability were completely restored (V1V2). This observation indicated that these two sets of amino acids were important for a proper folding of SD4. The dimerization of SD123-LRD2 was probably mediated by a free cysteine in LRD2. However, despite dimerization SD123-LRD2 was immobilized and still active. Thus, expression of ifnar1-EC in *Sf*9 was proved to be a powerful tool for the preparation of ifnar1-EC variants and possibly other cytokine receptors.

7.2 Dissection of interferon receptor assembling

One major challenge was to dissect the individual contributions of the different interactions between ifnar1, ifnar2 and IFNs involved in formation of a signaling complex. For the first time, kinetics and thermodynamics of ifnar1-EC ligand binding was quantitatively investigated *in vitro*. Ifnar1 was clearly identified as the low affinity receptor component in ifnar. The association constant K_A ($1/K_D$) towards IFNα2 as well as IFNβ was three orders of magnitude lower compared to ifnar2. This confirmed a two-step binding process. In the first step ifnar2 binds to IFN, in the second step ifnar1 binding mediates complex formation.

A striking observation was the drastically higher affinity of IFNβ towards both ifnar1 and ifnar2 compared to IFNα2, monitored by RIfS as well as SEC. These results are in agreement with the fact, that the complex of ifnar1 and ifnar2 with IFNβ is stable in immuno-precipitation, while it is not with IFNα2 [71, 73]. These differences in affinity towards ifnar1 and ifnar2 also mean that IFNβ engages ifnar more efficient than IFNα2 does. For IFNα2 mutants a clear correlation between affinity towards ifnar2-EC and anti-viral activity has been shown [80]. The antiviral activity of IFNβ is only by a factor of 2-4 higher than for IFNα2, and

not by orders of magnitude. However, saturation of activity has been also observed for GH with substantially enhanced binding affinities [18]. While the reason for this saturation is not fully clear, it is very well possible, that this effect is different for different types of responses. Differential efficiencies in the engagement of ifnar1 (and ifnar2) by IFNβ compared to IFNα2 could then explain that in contrast to IFNα, IFNβ shows additional gene activation at lower (i.e. physiological) concentrations, while at higher concentration similar activities were observed [75]. Although cross-linking of the receptor components by specific interactions with different sites on the ligand is still the basic paradigm for how signal activation is induced, the mode of how this is achieved is currently under controversial debate. Probably even different modes apply for different systems. Increasingly, pre-association of the receptor chains has been postulated [28], [35], and their activation by conformational changes induced by the ligand. In the case of class I cytokine receptors, stem-stem contacts between the membrane-proximal, extracellular receptor domains have been shown to be important for the formation of stable ternary complexes, namely growth hormone receptor (GHR) [15],[103], interleukin-4 receptor [104] and interleukin-6 receptor [105]. Though the affinities of such receptor-receptor interactions have not been quantified yet, cooperative stabilization by inter-receptor and ligand-receptor contacts was clearly shown. Gel filtration assays carried out with recombinant ifnar1-EC, ifnar2-EC and IFNβ [63] indicated a similar scenario for the type I interferon receptor. For both IFNα2 and IFNβ, such cooperative interaction could be clearly excluded, as a significant difference in the affinity of the interaction of ifnar1-EC with IFNα2 alone and in complex with ifnar2 was not detected. Furthermore, no direct interaction between ifnar1 and ifnar2 could be detected, neither by solid phase detection, nor by FRAP. These results suggest a different mode of interaction for this member of the class II cytokine receptor superfamily compared to the members class I family mentioned above. This is in good agreement with the observation that the binding site for IFNα is not located on the membrane-proximal tandem Ig-like domains, but at the hinge between the two extracellular tandem Ig-like domains [82, 84].

Characterization of the binding site of human ifnar1 *in vivo* has been hampered by the extremely low affinity towards its ligands: the high-affinity interaction with ifnar2 dominates binding to the cellular receptor, while binding to ifnar1 alone is too transient to be appropriately detectable. Therefore, most information about ligand recognition by ifnar1 stem from experiments with bovine ifnar1-EC, which binds human IFNα's with much higher affinity [83, 84]. Here, for the first time ligand binding to different sub-fragments of human ifnar1-EC was analyzed *in vitro* in order to better define ligand recognition. The architecture of ifnar1-EC with its four Ig-like domains suggests potentially two cytokine binding modules. The sub-fragments addressed the question of Ig-like domains' spatial arrangement

By direct ligand binding assays, it was clearly shown that these potential CBMs, SD12 and SD34, separately do neither interact with IFNα2 nor with IFNβ. Even when co-immobilized on a fluid support, which allowed lateral rearrangements, the binding site was not restored. It was concluded that the linkage between SD2 and SD3 is absolutely critical for ligand binding. Out of the two sub-fragments containing three Ig-like domains – i.e. with an intact linkage between SD2 and SD3 – only SD123 retained its ligand binding activity. These results have an interesting relationship to the observations in SEC. The differences in the apparent molecular size indicated an asymmetric architecture of the 4 Ig-like domains of ifnar1 and not simply two, linked symmetric CBMs.

No differences in terms of sub-domains required for ligand recognition were found for IFNα2 and IFNβ, which have been suggested to bind to different epitopes on ifnar1 [82]. Direct competition experiments could show that the binding sites of IFNα2 and IFNβ are at least overlapping, if not congruent. This was also supported by site directed mutagenesis, since all involved residues affected the interaction with IFNα2-HEQ as well as IFNβ. All these studies suggest that ifnar1 is recognized in a very similar manner by these IFNs.

7.3 Complex formation on lipid bilayers

For characterizing the role of individual interactions for ligand-induced receptor assembly, the ternary complex formation with the extracellular receptors tethered in an oriented fashion on supported membranes was investigated. Based on combined fluorescence and label-free detection receptor assembling was studied on a mechanistic level, which may help to explain how differences in receptor engagement by IFNα2 and IFNβ results in differential signaling.

A very stable ternary complex was observed at high surface concentrations of ifnar1 and ifnar2. Compared to the binding to ifnar2 alone IFNα2 binding was extremely stable, decreasing the apparent k_d by factor 200. With respect to the very low affinity of ifnar1-EC toward IFNα2 and the transient interaction of these proteins, the mode of stabilization was investigated in detail. Ternary complex stability was demonstrated to be dependent on receptor surface concentration. This surface concentration dependency as well as the possibility to exchange the bound ligand with much faster rates than the apparent dissociation rate constant confirmed kinetic rather than static stabilization of the complex. In combination with the fact that interactions between ifnar2-EC and ifnar1-EC were not observed, a two-step assembling mechanism was suggested (Figure 58): After binding of IFN to ifnar2 (k_1), ifnar1 transiently associates to the complex. Owing to the low life-time of the IFNα2-ifnar1 interaction, the complex dissociates (k_{-2}) and re-associates (k_2) in a fast

manner (on a second scale). At lower receptor surface concentrations the re-association kinetics is slowed down and kinetic stabilization is diminished, leading to faster dissociation of IFN (k_{-1}).
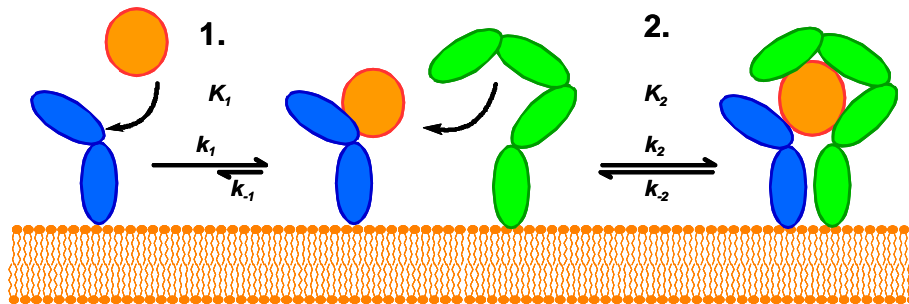

Figure 58   Model of two-step formation and kinetic stabilization of the ternary complex upon IFN binding

Depending on the receptor surface concentrations only part of the ligand bound is involved in the ternary complex. The fraction is defined by the equilibrium dissociation constant for the interaction of ifnar2-EC-IFN complex with ifnar1-EC on the surface ($K_2 = k_{-2}/k_2$). From cellular interaction assays, a 10-20-times decrease in K_D due to ifnar1 has been observed for IFNα2. Taking this into account and furthermore assuming that the biophysical environment is in principle mimicked appropriately, these results have several important implications for the mechanism of receptor assembling: (i) The formation of a stable pre-formed receptor-complex by interactions mediated via the extracellular domains as suggested for other receptors [26], [28], [106] is very unlikely; (ii) the receptor components are in some way co-localized on the surface of the plasma membrane, as random distribution of several hundred receptors on the plasma membrane would not be sufficient for gaining 10-20-times increased stability. This is in line with the observation that ifnar1 and ifnar2 are located in caveolae [107]; (iii) different receptor concentrations not only lead to different apparent binding affinities, but also different fractions of IFN involved in the ternary complex.

As a consequence of this model ifnar1 can explained as the limiting factor for complex formation, which controls the efficiency of complex formation by the variation of k_2 (K_2). This hypothesis is also supported by the experiments elucidating the role of SD4. This sub-domain does not seem to play a significant role for ligand recognition and is also not required for ternary complex formation with ifnar2-EC. In cells, however, no high affinity ligand binding site was observed in the absence of SD4 or when it was exchanged by a corresponding domain of homologous cytokine receptors. In addition the analysis of these constructs *in vitro* indicated that ternary complex formation is still possible, although recruitment efficiency is substantially impaired if SD4 is absent or exchanged. The decrease of ligand binding stability observed for N-terminally attached or impaired ifnar1 constructs reflect an increase in K_2 (decrease in k_2). This drop in surface binding affinity can be ascribed to a decrease in the surface association rate constant, which was shown to be enhanced on

the membrane in terms of successful collisions [100]. Non-optimal orientation of the ligand binding site of ifnar1 on the membrane probably reduces the collision efficiency, and thus reduces the surface association rate constant and the surface affinity constant.

One of the key questions is how differential signaling of IFNα2 and IFNβ is encoded in the mechanism of receptor assembly. IFNα2 and IFNβ neither differ in the stoichiometry of their individual interactions with the receptor subunits nor in the stoichiometry of the components in the ternary complex. It was also shown that both IFNs are recognized via the same binding domains and residues. The only major difference between these two IFNs was the affinity towards ifnar1, which was ~ 100-fold higher for IFNβ than for IFNα2. Results indicated that ifnar1 recruitment is likely to be the limiting factor in IFN signal activation. This leads to the hypothesis, that differential signaling is encoded in the affinity of ifnar1 towards different IFNs. As one possibility, different signaling pathways could require different amounts of ternary complexes. It is also probable, that for several pathways a certain complex stability is required. In case of IFNα2 and IFNβ, the antiviral and the antproliferative activity are examples for differential signaling. For antiviral activity lower concentrations of ternary complex are required than for antiproliferative activity. Since IFNβ has a higher affinity towards ifnar1, a higher absolute number of complexes per cell are expected compared to IFNα2, which explains a higher antiproliferative effect of IFNβ. IFNβ was also demonstrated to induce signaling in cancer cells with a reduced ifnar1 level, but IFNα2 had no effect [108]. Affinity of individual IFNs toward ifnar1 seems to be an important element of differential signal activation. Ifnar1 surface concentration was also demonstrated to be correlated with complex formation efficiency. Differences between individual cell types in IFN response could be explained by the variation of ifnar1 surface concentration. Cells could control their sensitivity to different IFNs by their ifnar1 surface expression level. As a conclusion of this work ifnar1 was proposed to be the key element in IFN mediated differential signaling.

7.4 Outlook

One aspect which has not been taken into account so far is the role of the trans-membrane domains. It is possible that they have an effect on complex formation. Therefore ifnar1 and ifnar2 carrying the trans-membrane domains have to be expressed and reconstituted. By comparison with the established assays on chelator surfaces the contributions of these domains could be elucidated.

To achieve a more detailed picture of the complex architecture, a more detailed view to the structure of ifnar1-EC as well as the ternary complex is necessary. By applying the knowledge of protein immobilization on lipid bilayers 2D crystallization would be the first step in structure biology. With this technique the arrangement of the four ifnar1-EC sub-domains with respect to the sub-domains of ifnar2-EC can be estimated. The 3D-analsis by X-ray crystallography is then the next challenging project, but in case of success the structure of the ternary complex would be a milestone in cytokine receptor research. Also FRET studies in solution and on surfaces would generate additional information about conformational changes during complex assembly.

For the identification of additional residues involved in ligand binding, the site directed mutagenesis of ifnar1-EC has to be continued. By double mutant cycle analysis interaction pairs can be identified and their binding enthalpy can be determined. Also the role of individual residues in the formation of the ternary complex has still to be investigated.

8 Abbreviations

2-5A-sythase	2-5-oligoadenylat-systhase
AcNPV	*Autographa californica* nuclear polyhedrosis virus
ATP	adenosintriphosphate
bp	base pair(s)
BL	bilayer
BSA	bovine serum albumin
CD	circular dichroism
CIAP	calf intestine alkaline phosphatase
CP	cytoplasmic domain
CSF	colony-stimulating factor
dNTP	desoxy-nucleotidetriphosphate
DT	double tagged
DTT	dithiothreitol
E. coli	*Escherichia coli*
EC	extracellular domain
EGF	epidermal growth factor
EPO	erythropoietin
FCS	fetal calf serum
FRAP	fluorescence recovery after photobleaching
G-CSF	granulocyte colony-stimulating factor
GH	growth hormone
GM-CSF	granulocyte and macrophage colony-stimulating factor
H10	deca-histidine-tag
HBS	Hepes buffer saline
HSA	human serum albumin
IDA	Iodo-diacetic acid
IFN	interferon
ifnar	interferon alpha receptor
ifnar1	type I interferon receptor subunit 1
ifnar2	type I interferon receptor subunit 2
Ig	immunoglobulin
IL	interleukin
IL-10R2D2	interleukin-10 receptor domain 2
IMAC	immobilized metal affinity chromatography
ISGF	interferon-stimulated gene activating factor
ISRE	interferon-stimulated regulatory elements

JAK	Janus-activated kinase
k_a	association rate constant
kDa	kilo Dalton
K_D	dissociation constant
k_d	dissociation rate constant
LCR	ligase chain reaction
LRD2	lambda receptor domain 2
MBP	maltose binding protein
MHC	major histocompatibility complex
NAD	nicotinamidadeninetriphosphate
NMR	nuclear magnetic resonance
NTA	nitroso-tetra-acetic acid
P. pastoris	*Picchia pastoris*
PAGE	polyacrylamide gelelectrophoresis
PBS(T)	phosphate buffer saline (Tween)
PCR	polymerase chain reaction
PI-3-K	phospatidyl-inositol-3-kinase
PKR	protein kinase R
Pwo	*Pyrococcus woesei*
Rif(S)	reflectance interference spectroscopy
RNA	ribonucleic acis
rpm	rounds per minute
SD	sub-domain
SDS	sodiumdodecylsulfate
SEC	size exclusion chromatography
*Sf*9	*Spodoptera frugiperda* 9
SOPC	stearoyl-oleoyl-phosphatidycholine
STAT	signal transducer and activator of transcription
TAP	transporter associated with antigen processing
Taq	*Thermophilus aquaticus*
TBS(T)	Tris buffer saline (Tween)
TIRFS	total internal reflection fluorescence spectroscopy
tl	tag-less
TMD	transmembrane domain
TNF	tumor necrosis factor

9 References

1.   Wells, J.A., *Binding in the growth hormone receptor complex.* Proc Natl Acad Sci U S A, 1996. **93**(1): p. 1-6.

2.   Syed, R.S., S.W. Reid, C. Li, J.C. Cheetham, K.H. Aoki, B. Liu, H. Zhan, T.D. Osslund, A.J. Chirino, J. Zhang, J. Finer-Moore, S. Elliott, K. Sitney, B.A. Katz, D.J. Matthews, J.J. Wendoloski, J. Egrie, and R.M. Stroud, *Efficiency of signalling through cytokine receptors depends critically on receptor orientation.* Nature, 1998. **395**(6701): p. 511-6.

3.   de Vos, A.M., M. Ultsch, and A.A. Kossiakoff, *Human growth hormone and extracellular domain of its receptor: crystal structure of the complex.* Science, 1992. **255**(5042): p. 306-12.

4.   Wilson, I.A. and L.K. Jolliffe, *The structure, organization, activation and plasticity of the erythropoietin receptor.* Curr Opin Struct Biol, 1999. **9**(6): p. 696-704.

5.   Hage, T., W. Sebald, and P. Reinemer, *Crystal structure of the interleukin-4/receptor alpha chain complex reveals a mosaic binding interface.* Cell, 1999. **97**(2): p. 271-81.

6.   Zhang, J.L., I. Simeonowa, Y. Wang, and W. Sebald, *The high-affinity interaction of human IL-4 and the receptor alpha chain is constituted by two independent binding clusters.* J Mol Biol, 2002. **315**(3): p. 399-407.

7.   Hiraoka, O., H. Anaguchi, A. Asakura, and Y. Ota, *Requirement for the immunoglobulin-like domain of granulocyte colony-stimulating factor receptor in formation of a 2:1 receptor-ligand complex.* J Biol Chem, 1995. **270**(43): p. 25928-34.

8.   Chow, D., X. He, A.L. Snow, S. Rose-John, and K.C. Garcia, *Structure of an extracellular gp130 cytokine receptor signaling complex.* Science, 2001. **291**(5511): p. 2150-5.

9.   Skiniotis, G., M.J. Boulanger, K.C. Garcia, and T. Walz, *Signaling conformations of the tall cytokine receptor gp130 when in complex with IL-6 and IL-6 receptor.* Nat Struct Mol Biol, 2005. **12**(6): p. 545-51.

10.   Walter, M.R., W.T. Windsor, T.L. Nagabhushan, D.J. Lundell, C.A. Lunn, P.J. Zauodny, and S.K. Narula, *Crystal structure of a complex between interferon-gamma and its soluble high-affinity receptor.* Nature, 1995. **376**(6537): p. 230-5.

11.   Bach, E.A., M. Aguet, and R.D. Schreiber, *The IFN gamma receptor: a paradigm for cytokine receptor signaling.* Annu Rev Immunol, 1997. **15**: p. 563-91.

References

12. Walter, M.R. and T.L. Nagabhushan, *Crystal structure of interleukin 10 reveals an interferon gamma-like fold.* Biochemistry, 1995. **34**(38): p. 12118-25.

13. Walter, M.R., *Strucure of interleukin-10/interleukin-10R1 complex: a paradigm for class 2 cytokine activation.* Immunol Res, 2002. **26**(1-3): p. 303-8.

14. Argetsinger, L.S., G.S. Campbell, X. Yang, B.A. Witthuhn, O. Silvennoinen, J.N. Ihle, and C. Carter-Su, *Identification of JAK2 as a growth hormone receptor-associated tyrosine kinase.* Cell, 1993. **74**(2): p. 237-44.

15. Cunningham, B.C., M. Ultsch, A.M. De Vos, M.G. Mulkerrin, K.R. Clauser, and J.A. Wells, *Dimerization of the extracellular domain of the human growth hormone receptor by a single hormone molecule.* Science, 1991. **254**(5033): p. 821-5.

16. Wells, J.A. and A.M. de Vos, *Structure and function of human growth hormone: implications for the hematopoietins.* Annu Rev Biophys Biomol Struct, 1993. **22**: p. 329-51.

17. Pearce, K.H., Jr., M.H. Ultsch, R.F. Kelley, A.M. de Vos, and J.A. Wells, *Structural and mutational analysis of affinity-inert contact residues at the growth hormone-receptor interface.* Biochemistry, 1996. **35**(32): p. 10300-7.

18. Pearce, K.H., Jr., B.C. Cunningham, G. Fuh, T. Teeri, and J.A. Wells, *Growth hormone binding affinity for its receptor surpasses the requirements for cellular activity.* Biochemistry, 1999. **38**(1): p. 81-9.

19. Atwell, S., M. Ultsch, A.M. De Vos, and J.A. Wells, *Structural plasticity in a remodeled protein-protein interface.* Science, 1997. **278**(5340): p. 1125-8.

20. Cunningham, B.C. and J.A. Wells, *High-resolution epitope mapping of hGH-receptor interactions by alanine- scanning mutagenesis.* Science, 1989. **244**(4908): p. 1081-5.

21. Philo, J.S., K.H. Aoki, T. Arakawa, L.O. Narhi, and J. Wen, *Dimerization of the extracellular domain of the erythropoietin (EPO) receptor by EPO: one high-affinity and one low-affinity interaction.* Biochemistry, 1996. **35**(5): p. 1681-91.

22. Watowich, S.S., A. Yoshimura, G.D. Longmore, D.J. Hilton, Y. Yoshimura, and H.F. Lodish, *Homodimerization and constitutive activation of the erythropoietin receptor.* Proc Natl Acad Sci U S A, 1992. **89**(6): p. 2140-4.

23. Wrighton, N.C., F.X. Farrell, R. Chang, A.K. Kashyap, F.P. Barbone, L.S. Mulcahy, D.L. Johnson, R.W. Barrett, L.K. Jolliffe, and W.J. Dower, *Small peptides as potent mimetics of the protein hormone erythropoietin.* Science, 1996. **273**(5274): p. 458-64.

24. Livnah, O., D.L. Johnson, E.A. Stura, F.X. Farrell, F.P. Barbone, Y. You, K.D. Liu, M.A. Goldsmith, W. He, C.D. Krause, S. Pestka, L.K. Jolliffe, and I.A. Wilson, *An*

antagonist peptide-EPO receptor complex suggests that receptor dimerization is not sufficient for activation. Nat Struct Biol, 1998. **5**(11): p. 993-1004.

25. Johnson, D.L., F.X. Farrell, F.P. Barbone, F.J. McMahon, J. Tullai, D. Kroon, J. Freedy, R.A. Zivin, L.S. Mulcahy, and L.K. Jolliffe, *Amino-terminal dimerization of an erythropoietin mimetic peptide results in increased erythropoietic activity.* Chem Biol, 1997. **4**(12): p. 939-50.

26. Livnah, O., E.A. Stura, S.A. Middleton, D.L. Johnson, L.K. Jolliffe, and I.A. Wilson, *Crystallographic evidence for preformed dimers of erythropoietin receptor before ligand activation.* Science, 1999. **283**(5404): p. 987-90.

27. Cohen, J., H. Altaratz, Y. Zick, U. Klingmuller, and D. Neumann, *Phosphorylation of erythropoietin receptors in the endoplasmic reticulum by pervanadate-mediated inhibition of tyrosine phosphatases.* Biochem J, 1997. **327 (Pt 2)**: p. 391-7.

28. Remy, I., I.A. Wilson, and S.W. Michnick, *Erythropoietin receptor activation by a ligand-induced conformation change.* Science, 1999. **283**(5404): p. 990-3.

29. Constantinescu, S.N., T. Keren, M. Socolovsky, H. Nam, Y.I. Henis, and H.F. Lodish, *Ligand-independent oligomerization of cell-surface erythropoietin receptor is mediated by the transmembrane domain.* Proc Natl Acad Sci U S A, 2001. **98**(8): p. 4379-84.

30. Guo, C., K.E. Georgiadis, S.K. Dower, D. Holowka, and B.A. Baird, *Interleukin 1 (IL-1) causes changes in lateral and rotational mobilities of IL-1 type I receptors.* Biochemistry, 1999. **38**(5): p. 1618-25.

31. Damjanovich, S., L. Bene, J. Matko, A. Alileche, C.K. Goldman, S. Sharrow, and T.A. Waldmann, *Preassembly of interleukin 2 (IL-2) receptor subunits on resting Kit 225 K6 T cells and their modulation by IL-2, IL-7, and IL-15: a fluorescence resonance energy transfer study.* Proc Natl Acad Sci U S A, 1997. **94**(24): p. 13134-9.

32. Lai, S.Y., W. Xu, S.L. Gaffen, K.D. Liu, G.D. Longmore, W.C. Greene, and M.A. Goldsmith, *The molecular role of the common gamma c subunit in signal transduction reveals functional asymmetry within multimeric cytokine receptor complexes.* Proc Natl Acad Sci U S A, 1996. **93**(1): p. 231-5.

33. Taga, T. and T. Kishimoto, *Gp130 and the interleukin-6 family of cytokines.* Annu Rev Immunol, 1997. **15**: p. 797-819.

34. Jostock, T., J. Mullberg, S. Ozbek, R. Atreya, G. Blinn, N. Voltz, M. Fischer, M.F. Neurath, and S. Rose-John, *Soluble gp130 is the natural inhibitor of soluble*

interleukin-6 receptor transsignaling responses. Eur J Biochem, 2001. **268**(1): p. 160-7.

35. Krause, C.D., E. Mei, J. Xie, Y. Jia, M.A. Bopp, R.M. Hochstrasser, and S. Pestka, *Seeing the Light: Preassembly and Ligand-Induced Changes of the Interferon gamma Receptor Complex in Cells.* Mol Cell Proteomics, 2002. **1**(10): p. 805-15.

36. Isaacs, A. and J. Lindenmann, *Virus interference. I. The interferon.* Proc R Soc Lond B Biol Sci, 1957. **147**(927): p. 258-67.

37. Pestka, S., C.D. Krause, and M.R. Walter, *Interferons, interferon-like cytokines, and their receptors.* Immunol Rev, 2004. **202**: p. 8-32.

38. Deonarain, R., D.C. Chan, L.C. Platanias, and E.N. Fish, *Interferon-alpha/beta-receptor interactions: a complex story unfolding.* Curr Pharm Des, 2002. **8**(24): p. 2131-7.

39. Runkel, L., L. Pfeffer, M. Lewerenz, D. Monneron, C.H. Yang, A. Murti, S. Pellegrini, S. Goelz, G. Uze, and K. Mogensen, *Differences in activity between alpha and beta type I interferons explored by mutational analysis.* J Biol Chem, 1998. **273**(14): p. 8003-8.

40. Stark, G.R., I.M. Kerr, B.R. Williams, R.H. Silverman, and R.D. Schreiber, *How cells respond to interferons.* Annu Rev Biochem, 1998. **67**: p. 227-64.

41. Platanias, L.C. and E.N. Fish, *Signaling pathways activated by interferons.* Exp Hematol, 1999. **27**(11): p. 1583-92.

42. Meurs, E., K. Chong, J. Galabru, N.S. Thomas, I.M. Kerr, B.R. Williams, and A.G. Hovanessian, *Molecular cloning and characterization of the human double-stranded RNA-activated protein kinase induced by interferon.* Cell, 1990. **62**(2): p. 379-90.

43. Carpick, B.W., V. Graziano, D. Schneider, R.K. Maitra, X. Lee, and B.R. Williams, *Characterization of the solution complex between the interferon-induced, double-stranded RNA-activated protein kinase and HIV-I trans-activating region RNA.* J Biol Chem, 1997. **272**(14): p. 9510-6.

44. Wreschner, D.H., T.C. James, R.H. Silverman, and I.M. Kerr, *Ribosomal RNA cleavage, nuclease activation and 2-5A(ppp(A2'p)nA) in interferon-treated cells.* Nucleic Acids Res, 1981. **9**(7): p. 1571-81.

45. Dong, B. and R.H. Silverman, *2-5A-dependent RNase molecules dimerize during activation by 2-5A.* J Biol Chem, 1995. **270**(8): p. 4133-7.

References

46.   Schneider-Schaulies, S., J. Schneider-Schaulies, A. Schuster, M. Bayer, J. Pavlovic, and V. ter Meulen, *Cell type-specific MxA-mediated inhibition of measles virus transcription in human brain cells.* J Virol, 1994. **68**(11): p. 6910-7.

47.   Schwemmle, M., K.C. Weining, M.F. Richter, B. Schumacher, and P. Staeheli, *Vesicular stomatitis virus transcription inhibited by purified MxA protein.* Virology, 1995. **206**(1): p. 545-54.

48.   Parganas, E., D. Wang, D. Stravopodis, D.J. Topham, J.C. Marine, S. Teglund, E.F. Vanin, S. Bodner, O.R. Colamonici, J.M. van Deursen, G. Grosveld, and J.N. Ihle, *Jak2 is essential for signaling through a variety of cytokine receptors.* Cell, 1998. **93**(3): p. 385-95.

49.   Kirkwood, J.M., J.G. Ibrahim, V.K. Sondak, M.S. Ernstoff, and M. Ross, *Interferon alfa-2a for melanoma metastases.* Lancet, 2002. **359**(9310): p. 978-9.

50.   Talpaz, M., H. Kantarjian, K. McCredie, J. Trujillo, M. Keating, and J.U. Gutterman, *Therapy of chronic myelogenous leukemia.* Cancer, 1987. **59**(3 Suppl): p. 664-7.

51.   Mazzella, G., G. Saracco, D. Festi, F. Rosina, S. Marchetto, F. Jaboli, R. Sostegni, A. Pezzoli, F. Azzaroli, C. Cancellieri, M. Montagnani, E. Roda, and M. Rizzetto, *Long-term results with interferon therapy in chronic type B hepatitis: a prospective randomized trial.* Am J Gastroenterol, 1999. **94**(8): p. 2246-50.

52.   Pianko, S. and J.G. McHutchison, *Treatment of hepatitis C with interferon and ribavirin.* J Gastroenterol Hepatol, 2000. **15**(6): p. 581-6.

53.   Sen, G.C., R. Herz, V. Davatelis, and S. Pestka, *Antiviral and protein-inducing activities of recombinant human leukocyte interferons and their hybrids.* J Virol, 1984. **50**(2): p. 445-50.

54.   Silberberg, D.H., *Specific treatment of multiple sclerosis.* Clin Neurosci, 1994. **2**(3-4): p. 271-4.

55.   Leppert, D., E. Waubant, M.R. Burk, J.R. Oksenberg, and S.L. Hauser, *Interferon beta-1b inhibits gelatinase secretion and in vitro migration of human T cells: a possible mechanism for treatment efficacy in multiple sclerosis.* Ann Neurol, 1996. **40**(6): p. 846-52.

56.   Antonelli, G., G. Giannelli, M. Currenti, E. Simeoni, S. Del Vecchio, F. Maggi, M. Pistello, L. Roffi, G. Pastore, L. Chemello, and F. Dianzani, *Antibodies to interferon (IFN) in hepatitis C patients relapsing while continuing recombinant IFN-alpha2 therapy.* Clin Exp Immunol, 1996. **104**(3): p. 384-7.

57.   Borden, E.C., D. Lindner, R. Dreicer, M. Hussein, and D. Peereboom, *Second-generation interferons for cancer: clinical targets.* Semin Cancer Biol, 2000. **10**(2): p. 125-44.

58.   Novick, D., B. Cohen, and M. Rubinstein, *The human interferon alpha/beta receptor: characterization and molecular cloning.* Cell, 1994. **77**(3): p. 391-400.

59.   Uze, G., G. Lutfalla, and K.E. Mogensen, *Alpha and beta interferons and their receptor and their friends and relations.* J Interferon Cytokine Res, 1995. **15**(1): p. 3-26.

60.   Bazan, J.F., *Structural design and molecular evolution of a cytokine receptor superfamily.* Proc Natl Acad Sci U S A, 1990. **87**(18): p. 6934-8.

61.   Mogensen, K.E., M. Lewerenz, J. Reboul, G. Lutfalla, and G. Uze, *The type I interferon receptor: structure, function, and evolution of a family business.* J Interferon Cytokine Res, 1999. **19**(10): p. 1069-98.

62.   Chill, J.H., S.R. Quadt, R. Levy, G. Schreiber, and J. Anglister, *The human type I interferon receptor. NMR structure reveals the molecular basis of ligand binding.* Structure (Camb), 2003. **11**(7): p. 791-802.

63.   Arduini, R.M., K.L. Strauch, L.A. Runkel, M.M. Carlson, X. Hronowski, S.F. Foley, C.N. Young, W. Cheng, P.S. Hochman, and D.P. Baker, *Characterization of a soluble ternary complex formed between human interferon-beta-1a and its receptor chains.* Protein Sci, 1999. **8**(9): p. 1867-77.

64.   Prejean, C. and O.R. Colamonici, *Role of the cytoplasmic domains of the type I interferon receptor subunits in signaling.* Semin Cancer Biol, 2000. **10**(2): p. 83-92.

65.   Uddin, S., E.N. Fish, D. Sher, C. Gardziola, O.R. Colamonici, M. Kellum, P.M. Pitha, M.F. White, and L.C. Platanias, *The IRS-pathway operates distinctively from the Stat-pathway in hematopoietic cells and transduces common and distinct signals during engagement of the insulin or interferon-alpha receptors.* Blood, 1997. **90**(7): p. 2574-82.

66.   Rani, M.R., A.R. Asthagiri, A. Singh, N. Sizemore, S.S. Sathe, X. Li, J.D. DiDonato, G.R. Stark, and R.M. Ransohoff, *A role for NF-kappa B in the induction of beta-R1 by interferon-beta.* J Biol Chem, 2001. **276**(48): p. 44365-8.

67.   Takaoka, A., S. Hayakawa, H. Yanai, D. Stoiber, H. Negishi, H. Kikuchi, S. Sasaki, K. Imai, T. Shibue, K. Honda, and T. Taniguchi, *Integration of interferon-alpha/beta signalling to p53 responses in tumour suppression and antiviral defence.* Nature, 2003. **424**(6948): p. 516-23.

References

68. Abramovich, C., L.M. Shulman, E. Ratovitski, S. Harroch, M. Tovey, P. Eid, and M. Revel, *Differential tyrosine phosphorylation of the IFNAR chain of the type I interferon receptor and of an associated surface protein in response to IFN-alpha and IFN-beta.* Embo J, 1994. **13**(24): p. 5871-7.

69. Domanski, P., O.W. Nadeau, L.C. Platanias, E. Fish, M. Kellum, P. Pitha, and O.R. Colamonici, *Differential use of the betaL subunit of the type I interferon (IFN) receptor determines signaling specificity for IFNalpha2 and IFNbeta.* J Biol Chem, 1998. **273**(6): p. 3144-7.

70. Platanias, L.C., S. Uddin, P. Domanski, and O.R. Colamonici, *Differences in interferon alpha and beta signaling. Interferon beta selectively induces the interaction of the alpha and betaL subunits of the type I interferon receptor.* J Biol Chem, 1996. **271**(39): p. 23630-3.

71. Croze, E., D. Russell-Harde, T.C. Wagner, H. Pu, L.M. Pfeffer, and H.D. Perez, *The human type I interferon receptor. Identification of the interferon beta-specific receptor-associated phosphoprotein.* J Biol Chem, 1996. **271**(52): p. 33165-8.

72. Mintzer, R.J., E. Croze, G.M. Rubanyi, and A. Johns, *Differential effects of IFN-beta1b on the proliferation of human vascular smooth muscle and endothelial cells.* J Interferon Cytokine Res, 1998. **18**(11): p. 939-45.

73. Russell-Harde, D., T.C. Wagner, H.D. Perez, and E. Croze, *Formation of a uniquely stable type I interferon receptor complex by interferon beta is dependent upon particular interactions between interferon beta and its receptor and independent of tyrosine phosphorylation.* Biochem Biophys Res Commun, 1999. **255**(2): p. 539-44.

74. Grumbach, I.M., E.N. Fish, S. Uddin, B. Majchrzak, O.R. Colamonici, H.R. Figulla, A. Heim, and L.C. Platanias, *Activation of the Jak-Stat pathway in cells that exhibit selective sensitivity to the antiviral effects of IFN-beta compared with IFN- alpha.* J Interferon Cytokine Res, 1999. **19**(7): p. 797-801.

75. da Silva, A.J., M. Brickelmaier, G.R. Majeau, A.V. Lukashin, J. Peyman, A. Whitty, and P.S. Hochman, *Comparison of gene expression patterns induced by treatment of human umbilical vein endothelial cells with IFN-alpha 2b vs. IFN-beta 1a: understanding the functional relationship between distinct type I interferons that act through a common receptor.* J Interferon Cytokine Res, 2002. **22**(2): p. 173-88.

76. Piehler, J. and G. Schreiber, *Mutational and structural analysis of the binding interface between type I interferons and their receptor ifnar2.* Journal of Molecular Biology, 1999. **294**(1): p. 223-237.

77. Roisman, L.C., J. Piehler, J.Y. Trosset, H.A. Scheraga, and G. Schreiber, *Structure of the interferon-receptor complex determined by distance constraints from double-mutant cycles and flexible docking.* Proc Natl Acad Sci U S A, 2001. **98**(23): p. 13231-6.

78. Radhakrishnan, R., L.J. Walter, A. Hruza, P. Reichert, P.P. Trotta, T.L. Nagabhushan, and M.R. Walter, *Zinc mediated dimer of human interferon-alpha 2b revealed by X-ray crystallography.* Structure, 1996. **4**(12): p. 1453-63.

79. Karpusas, M., A. Whitty, L. Runkel, and P. Hochman, *The structure of human interferon-beta: implications for activity.* Cell Mol Life Sci, 1998. **54**(11): p. 1203-16.

80. Piehler, J., L.C. Roisman, and G. Schreiber, *New structural and functional aspects of the type I interferon-receptor interaction revealed by comprehensive mutational analysis of the binding interface.* J Biol Chem, 2000. **275**(51): p. 40425-33.

81. Lewerenz, M., K.E. Mogensen, and G. Uze, *Shared receptor components but distinct complexes for alpha and beta interferons.* J Mol Biol, 1998. **282**(3): p. 585-99.

82. Lu, J., A. Chuntharapai, J. Beck, S. Bass, A. Ow, A.M. De Vos, V. Gibbs, and K.J. Kim, *Structure-function study of the extracellular domain of the human IFN-alpha receptor (hIFNAR1) using blocking monoclonal antibodies: the role of domains 1 and 2.* J Immunol, 1998. **160**(4): p. 1782-8.

83. Goldman, L.A., E.C. Cutrone, A. Dang, X. Hao, J.K. Lim, and J.A. Langer, *Mapping human interferon-alpha (IFN-alpha 2) binding determinants of the type I interferon receptor subunit IFNAR-1 with human/bovine IFNAR- 1 chimeras.* Biochemistry, 1998. **37**(37): p. 13003-10.

84. Cutrone, E.C. and J.A. Langer, *Identification of critical residues in bovine IFNAR-1 responsible for interferon binding.* J Biol Chem, 2001. **276**(20): p. 17140-8.

85. Cajean-Feroldi, C., F. Nosal, P.C. Nardeux, X. Gallet, J. Guymarho, F. Baychelier, P. Sempe, M.G. Tovey, J.L. Escary, and P. Eid, *Identification of residues of the IFNAR1 chain of the type I human interferon receptor critical for ligand binding and biological activity.* Biochemistry, 2004. **43**(39): p. 12498-512.

86. Piehler, J. and G. Schreiber, *Biophysical analysis of the interaction of human ifnar2 expressed in E. coli with IFNalpha2.* J Mol Biol, 1999. **289**(1): p. 57-67.

87. Piehler, J. and G. Schreiber, *Biophysical analysis of the interaction of human ifnar2 expressed in E-coli with IFN alpha 2.* Journal of Molecular Biology, 1999. **289**(1): p. 57-67.

88.   Baneyx, F., *Recombinant protein expression in Escherichia coli.* Curr Opin Biotechnol, 1999. **10**(5): p. 411-21.

89.   Kapust, R.B. and D.S. Waugh, *Escherichia coli maltose-binding protein is uncommonly effective at promoting the solubility of polypeptides to which it is fused.* Protein Sci, 1999. **8**(8): p. 1668-74.

90.   Venturi, M., C. Seifert, and C. Hunte, *High level production of functional antibody Fab fragments in an oxidizing bacterial cytoplasm.* J Mol Biol, 2002. **315**(1): p. 1-8.

91.   Skerra, A. and T.G. Schmidt, *Applications of a peptide ligand for streptavidin: the Strep-tag.* Biomol Eng, 1999. **16**(1-4): p. 79-86.

92.   Kidd, I.M. and V.C. Emery, *The use of baculoviruses as expression vectors.* Appl Biochem Biotechnol, 1993. **42**(2-3): p. 137-59.

93.   Piehler, J. and G. Schreiber, *Fast transient cytokine-receptor interactions monitored in real time by reflectometric interference spectroscopy.* Analytical Biochemistry, 2001. **289**(2): p. 173-186.

94.   Gavutis, M., S. Lata, P. Lamken, P. Muller, and J. Piehler, *Lateral ligand-receptor interactions on membranes probed by simultaneous fluorescence-interference detection.* Biophys J, 2005.

95.   Lata, S. and J. Piehler, *Stable and functional immobilization of histidine-tagged proteins via multivalent chelator headgroups on a molecular poly(ethylene glycol) brush.* Anal Chem, 2005. **77**(4): p. 1096-105.

96.   Schmitt, H.M., A. Brecht, J. Piehler, and G. Gauglitz, *An integrated system for optical biomolecular interaction analysis.* Biosensors & Bioelectronics, 1997. **12**(8): p. 809-816.

97.   Piehler, J., A. Brecht, T. Giersch, K. Kramer, B. Hock, and G. Gauglitz, *Affinity characterization of monoclonal and recombinant antibodies for multianalyte detection with an optical transducer.* Sensors and Actuators B-Chemical, 1997. **39**(1-3): p. 432-437.

98.   Ho, A.S., Y. Liu, T.A. Khan, D.H. Hsu, J.F. Bazan, and K.W. Moore, *A receptor for interleukin 10 is related to interferon receptors.* Proc Natl Acad Sci U S A, 1993. **90**(23): p. 11267-71.

99.   Gavutis, M., S. Lata, P. Lamken, P. Müller, and J. Piehler, *Lateral ligand-receptor interactions on membranes probed by simultaneous fluorescence-interference detection.* Biophysical Journal, 2005: p. in press.

100. Gavutis, M., S. Lata, P. Lamken, P. Müller, and J. Piehler, *Lateral ligand-receptor interactions on membranes probed by simultaneous fluorescence-interference detection.* Biophysical Journal, 2004: p. submitted.

101. Poo, H., J.C. Krauss, L. Mayo-Bond, R.F. Todd, 3rd, and H.R. Petty, *Interaction of Fc gamma receptor type IIIB with complement receptor type 3 in fibroblast transfectants: evidence from lateral diffusion and resonance energy transfer studies.* J Mol Biol, 1995. **247**(4): p. 597-603.

102. Cutrone, E.C. and J.A. Langer, *Contributions of cloned type I interferon receptor subunits to differential ligand binding.* FEBS Lett, 1997. **404**(2-3): p. 197-202.

103. Bernat, B., G. Pal, M. Sun, and A.A. Kossiakoff, *Determination of the energetics governing the regulatory step in growth hormone-induced receptor homodimerization.* Proc Natl Acad Sci U S A, 2003. **100**(3): p. 952-7.

104. Letzelter, F., Y. Wang, and W. Sebald, *The interleukin-4 site-2 epitope determining binding of the common receptor gamma chain.* Eur J Biochem, 1998. **257**(1): p. 11-20.

105. Ozbek, S., J. Grotzinger, B. Krebs, M. Fischer, A. Wollmer, T. Jostock, J. Mullberg, and S. Rose-John, *The membrane proximal cytokine receptor domain of the human interleukin- 6 receptor is sufficient for ligand binding but not for gp130 association.* J Biol Chem, 1998. **273**(33): p. 21374-9.

106. Grotzinger, J., *Molecular mechanisms of cytokine receptor activation.* Biochim Biophys Acta, 2002. **1592**(3): p. 215-23.

107. Takaoka, A., Y. Mitani, H. Suemori, M. Sato, T. Yokochi, S. Noguchi, N. Tanaka, and T. Taniguchi, *Cross talk between interferon-gamma and -alpha/beta signaling components in caveolar membrane domains.* Science, 2000. **288**(5475): p. 2357-60.

108. Constantinescu, S.N., E. Croze, A. Murti, C. Wang, L. Basu, D. Hollander, D. Russell-Harde, M. Betts, V. Garcia-Martinez, J.E. Mullersman, and et al., *Expression and signaling specificity of the IFNAR chain of the type I interferon receptor complex.* Proc Natl Acad Sci U S A, 1995. **92**(23): p. 10487-91.

10 Publications

Results of this work were published in these articles:

Peter Lamken, Suman Lata, Martynas Gavutis and Jacob Piehler
Ligand-induced Assembling of the Type I Interferon Receptor on Supported Lipid Bilayers
Journal of Molecular Biology, JMB (2004), No. 341, p. 303-318

Martynas Gavutis, Suman Lata, Peter Lamken, Pia Müller and Jacob Piehler
Lateral ligand-receptor interactions on membranes probed by simultaneous fluorescence-interference detection
Biophysical Journal, Volume 88, June 2005, p. 4289-4302

Peter Lamken, Martynas Gavutis, José Van der Heyden, Gilles Uzé, Jacob Piehler
Functional cartography of the ectodomain of the type I interferon receptor subunit ifnar1
Journal of Molecular Biology, JMB, 2005, in press

Danksagung

Peter Lamken, Diplom-Biochemiker, Karlsbader Strasse 3, 65451 Kelsterbach
Telefon: 06107-301795, Mobil: 0173-6937233, Email: lamken@em.uni-frankfurt.de

Lebenslauf

Persönliche Informationen

Geburtsdatum:	16. Juni 1976
Geburtsort:	Groß-Gerau
Familienstand:	Verheiratet
Nationalität:	Deutsch

Naturwissenschaftliche Ausbildung

Promotion

seit 07/2001	**Promotion** am Institut für Biochemie des Biozentrums der J.W. Goethe-Universität Frankfurt am Main
	Projekt: Biophysikalische Charakterisierung der Ligand-Rezeptor-Interaktion des humanen Typ I Interferon Rezeptors
	Doktorvater: Dr. Jacob Piehler; Institutsleiter: Prof. Dr. Robert Tampé

Studium

04/2001	Abschluss: Diplom-Biochemiker an der der J.W. Goethe-Universität Frankfurt am Main
09/2000 – 04/2001	Diplomarbeit am Institut für Physiologische Chemie an der Philipps-Universität Marburg im Arbeitskreis Zelluläre Biochemie
	Projekt: Heterologe Expression und Aufreinigung der extrazellulären Domäne des humanen Typ I Interferon Rezeptors Ifnar1
	Betreuer: Prof. Dr. Robert Tampé und Prof. Dr. Heinz Rüterjans
08/1998	Vordiplom in Biochemie
10/1996 – 08/2000	Studium der Biochemie an der J.W. Goethe-Universität Frankfurt am Main

Wirtschaftswissenschaftliche Zusatzausbildung

04/2004	Vordiplom Wirtschaftswissenschaft
seit 09/2001	Aufbaustudium „Wirtschaftswissenschaft für Naturwissenschaftler und Ingenieure" an der Fernuniversität Hagen

Schule und Zivildienst

08/1995 – 08/1996	Zivildienst in einer psychosozialen Beratungsstelle des Caritasverbandes Rüsselsheim
07/1995	Abitur, Note 1.7
08/1988 – 07/1995	Gymnasium (Max-Planck-Schule in Rüsselsheim)

Peter Lamken, Diplom-Biochemiker, Karlsbader Strasse 3, 65451 Kelsterbach
Telefon: 06107-301795, Mobil: 0173-6937233, Email: lamken@em.uni-frankfurt.de

Industriepraktika

07/1999 – 09/1999   Merck KGaA, Darmstadt (10 Wochen)
Industriepraktikum in der Sparte Wissenschaftliche Laborprodukte,
Projekt: Entwicklung eines nicht-radioaktiven Nachweis-Verfahrens für
Nukleinsäure-Silikat-Interaktionen

09/1998 – 10/1998   Gesellschaft für biotechnologische Forschung mbH (GBF),
Braunschweig (6 Wochen)
Praktikum in der Abteilung Biochemical engineering
Projekt: Fermentation von anaeroben Bakterien für die Synthese
organischer Verbindungen

Publikationen

Peter Lamken, Suman Lata, Martynas Gavutis and Jacob Piehler
Ligand-induced Assembling of the Type I Interferon Receptor on Supported Lipid Bilayers
Journal of Molecular Biology, JMB (2004), No. 341, p. 303-318

Martynas Gavutis, Suman Lata, **Peter Lamken**, Pia Müller and Jacob Piehler
Lateral ligand-receptor interactions on membranes probed by simultaneous fluorescence-interference detection
Biophysical Journal, 2005, Volume 88, June 2005, p. 4289-4302

Peter Lamken, Martynas Gavutis, José Van der Heyden, Gilles Uzé, Jacob Piehler
Functional cartography of the ectodomain of the type I interferon receptor subunit ifnar1
Journal of Molecular Biology, JMB (2005), in press

Peter Lamken   Kelsterbach, 28. Juni 2005